Characterization of *Plasmodium falciparum* CTP:phosphocholine cytidylyltransferase, a prospective antimalarial drug target

PhD Thesis

Lívia Marton PharmD

Genome Metabolism and Repair Research Group

Institute of Enzymology

Research Centre for Natural Sciences

Hungarian Academy of Sciences

Doctoral School of Multidisciplinary Medical Science

Faculty of Medicine

University of Szeged

Supervisor: Beáta G. Vértessy PhD, DSc

Szeged

2017

LIST OF PUBLICATIONS

List of full papers directly related to the subject of the thesis:

I. Nagy GN, Marton L, Contet A, Ozohanics O, Ardelean L-M, Révész Á, *et al.* Composite Aromatic Boxes for Enzymatic Transformations of Quaternary Ammonium Substrates. Angew Chemie Int Ed. 2014;53: 13471–13476. doi:10.1002/anie.201408246b **IF: 11.261**

II. Marton L, Nagy GN, Ozohanics O, Lábas A, Krámos B, Oláh J, *et al.* Molecular Mechanism for the Thermo-Sensitive Phenotype of CHO-MT58 Cell Line Harbouring a Mutant CTP:Phosphocholine Cytidylyltransferase. PLoS One. 2015;10: e0129632. doi:10.1371/journal.pone.0129632 **IF: 3.057**

Cumulative impact factor of papers directly related to the thesis: 14.318

List of full papers indirectly related to the subject of the thesis:

III. Nagy GN, Marton L, Krámos B, Oláh J, Révész Á, Vékey K, *et al.* Evolutionary and mechanistic insights into substrate and product accommodation of CTP:phosphocholine cytidylyltransferase from Plasmodium falciparum. FEBS J. 2013;280: 3132–48. doi:10.1111/febs.12282 **IF: 3.986**

Cumulative impact factor of papers indirectly related to the thesis: 3.986

THE AUTHOR'S CONTRIBUTION

My PhD thesis is based on the publications listed on page 1 and on a manuscript in preparation. The presented measurements were designed, performed and evaluated by me, although some experiments closely related to the subject of the thesis were conducted by the co-authors of the publications. Below I enlist the co-authors and their contribution for the thesis and gratefully thank for their significant input.

Statement of contribution of co-authors for the thesis:

Contributor	**Statement of contribution**
Gergely Nándor Nagy PhD	isothermal titration calorimetry ligand binding measurements of *Pf*CCT$_{(528\text{-}795)}$ wild type and point mutant constructs
Olivér Ozohanics PhD Károly Vékey PhD DSc	mass spectrometric analysis of *Pf*CCT$_{(528\text{-}795)}$ wild type and point mutant constructs
Anikó Lábas (Krezinger) Balázs Krámos PhD Julianna Oláh PhD	homology modelling of the second catalytic domain *Pf*CCT constructs molecular dynamics simulations of *Pf*CCT$_{(528\text{-}795)}$ WT and R681H protein constructs
Fanni Hajdú	kinetic measurements of *Pf*CCT$_{(528\text{-}795)}$ H630N
Nóra Kucsma Gergely Szakács PhD	fluorescence activated cell sorting experiments of CHO-K1 and CHO-MT58 cells

TABLE OF CONTENTS

ABBREVIATIONS

ACT	artemisinin-based combination therapies
AI	auto-inhibitory
ATF	activating transcription factor
*Bs*GCT	*Bacillus subtilis* CTP:glycerol-3-phosphate cytidylyltransferase
C1/C2	catalytic domain 1/ catalytic domain 2
CCT	CTP:phosphocholine cytidylyltransferase
CDPCho	cytidine 5'-diphosphocholine
CEPT	choline/ethanolamine phosphotransferase
Cho	choline
CHO-K1	Chinese hamster ovarian cell line K1 subclone
CHO-MT58	Chinese hamster ovarian cell line mutant 58
ChoP	choline-phosphate
CHOP	CCAAT/enhancer-binding protein-homologous protein
CK	choline-kinase
CM domain	catalytic and membrane binding domain
CMAP	cross term map of φ, ψ (backbone dihedral angles in proteins)
CRISPR	clustered regularly interspaced short palindromic repeat
CT	cytidylyltransferase
CTP	cytidine 5'-triphosphate
dbSNP	single nucleotide polymorphism database
DIC	differential interference contrast
E. coli	*Escherichia coli*
EC	enzyme commission number
ECT	CTP:ethanolamine phosphate cytidylyltransferase
EGFP	enhanced green fluorescent protein
eIF2α	eukaryotic initiation factor 2α
ER	endoplasmic reticulum
ESI-MS	electrospray ionization mass spectrometry
FACS	fluorescence activated cell sorting
FBS	fetal bovine serum
FSC	forward scatter, the scatter measured along the path of the laser in flow cytometry.
GBSW	generalized Born model with a simple switching function
GCT	CTP:glycerol-3-phosphate cytidylyltransferase
IPTG	isopropyl β-D-1-thiogalactopyranoside
IRE1	inositol-requiring protein 1
IRES	internal ribosome entry site
ITC	isothermal titration calorimetry
JNK	Jun N-terminal kinase

M domain	membrane-binding domain
M1/M2	membrane binding domain 1/membrane binding domain 2
MD	molecular dynamics
MESG	7-methyl-6-thioguanosine
mito	mitochondrial
MS	mass spectrometry
Ni-NTA	nickel-nitrilotriacetic acid
NLS	nuclear localization signal
OD_{600nm}	optical density measured at 600 nm
P domain	phosphorylation domain
PB radii	ionic radii calculated by the Poisson-Boltzmann equation
PBS	phosphate buffered saline
PC	phosphatidylcholine
PDB	protein data bank
PE	phosphatidylethanolamine
PERK	protein kinase RNA-like ER kinase
*Pf*CCT	*Plasmodium falciparum* CTP:phosphocholine cytidylyltransferase
PI	propidium iodide
PL	phospholipid
PMDB	protein model database
PNP	purine nucleoside phosphorylase
PPase	pyrophosphatase
PPi	inorganic pyrophosphate
RBC	red blood cell
*Rn*CCT	*Rattus norvegicus* CTP:phosphocholine cytidylyltransferase
SSC	side scatter, the scatter measured at a ninety degree angle relative to the path of the laser in flow cytometry
TALEN	transcription activator-like effector nuclease
TCEP	tris(2-carboxyethyl)phosphine
TE	trypsin-EDTA
UPR	unfolded protein response
UPR^{ER}	endoplasmic reticulum unfolded protein response
UPR^{mito}	mitochondrial unfolded protein response
WT	wild type
XBP1	X-box binding protein 1
ZFN	zinc finger nuclease

1. INTRODUCTION

1.1. Malaria and the life cycle of Plasmodium parasites

Malaria is still one of the most serious vector-borne infectious diseases threatening approximately 2.75 billion people worldwide[1]. The bites of Anopheles mosquito vectors transmit the causative agents of malaria that are Apicomplexan protozoan parasites belonging to the Plasmodium genus. Among the parasite species infecting humans (*P. falciparum, P. vivax, P. malariae, P. ovale, and P. knowlesi*) *Plasmodium falciparum* is the deadliest causing the majority of mortality related to malaria. The recent antimalarial efforts that yielded a marked decrease in malaria incidence are featured by the use of insecticide-impregnated bed nets and the artemisinin-based combination therapies (ACT). Besides, attempts are made recently to produce malaria vaccine with high efficiency[2]. Nevertheless, further progress in roll back of malaria is at risk due to the rapidly emerging artemisinin resistance of parasites[3,4] which urges the development of antimalarials with an alternative mechanism of action.

Plasmodium parasites have a complex life cycle involving two hosts (Figure 1). At the beginning of the cycle, a malaria-infected female Anopheles mosquito inoculates parasites in form of sporozoites into the human host. Sporozoites infect liver cells (hepatocytes) and develop in 6-10 days into schizonts, which rupture and release merozoites. After this initial replication in the liver, referred as exo-erythrocytic stage or liver cycle, the parasites undergo asexual multiplication in the erythrocytes known as erythrocytic stage or blood cycle. The newly escaped merozoites invade red blood cells (RBC), then the ring stage trophozoites mature into schizonts, which rupture releasing merozoites continuing this vicious circle. Blood stage parasites are responsible for the clinical symptoms of the disease, e.g. intermittent fever. Some parasites differentiate into gametocyte sexual erythrocytic stages, which will be transmitted to the mosquito to begin a sexual multiplication cycle in the vector yielding a new generation of merozoites ready to infect another human host (mosquito stage)[5].

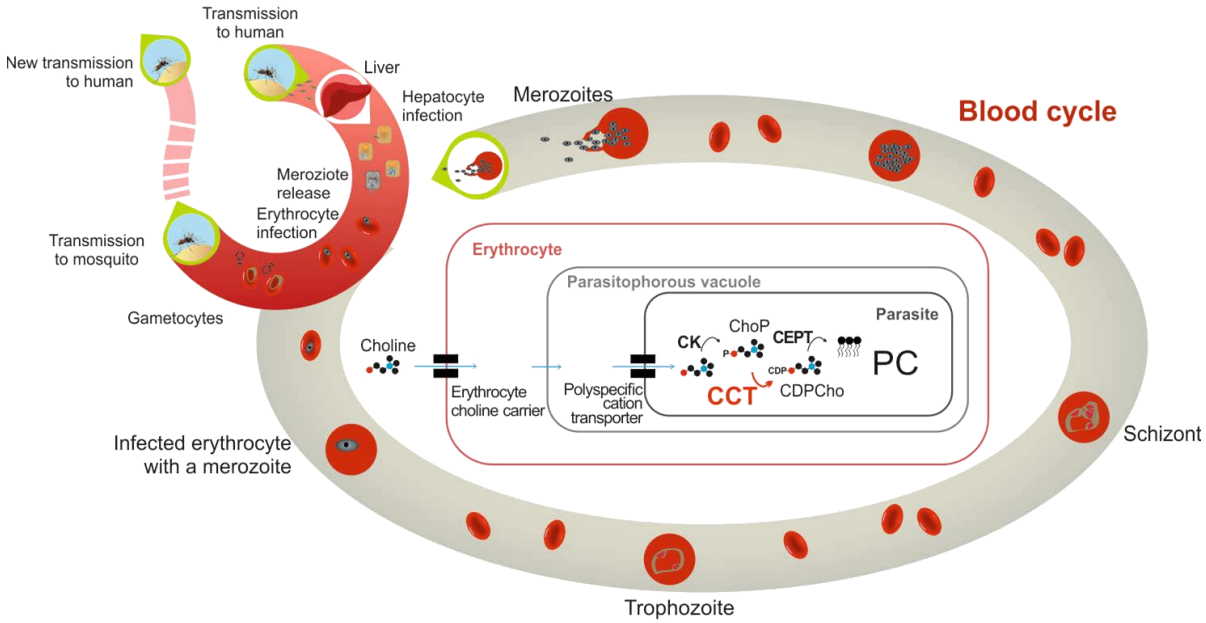

Figure 1. Life cycle of Plasmodium parasites and *de novo* phosphatidylcholine biosynthesis performed in their erythrocytic stage. In the middle of the circle a scheme of choline transport and Kennedy PC biosynthesis pathway is shown for parasite infected red blood cells.

1.2. Phosphatidylcholine biosynthesis as an antimalarial drug target

Plasmodium parasites upon invasion of red blood cells produce large amount of membranes consisting mainly of phospholipids, neutral lipids and fatty acids, while the cholesterol and sphingomyelin content of the infected red blood cell membrane is negligible[6]. In the membrane fraction of the infected red blood cells phosphatidylcholine (PC) and phosphatidyl-ethanolamine (PE) are present in the largest quantity. The choline precursor molecules required for *de novo* PC biosynthesis are transported from the RBC cytoplasm *via* active transport (Figure 1)[7]. In Plasmodium the most abundant way of PC synthesis is the Kennedy pathway[8] consisting of three consecutive steps catalyzed by the enzymes choline kinase (CK), CTP:phosphocholine cytidylyltransferase (CCT) and choline/ethanolamine phosphotransferase (CEPT) (Figure 1). *In vitro* and *in vivo* antimalarial effects of bis-quaterner ammonium choline analogue compounds appointed the parasites' Kennedy pathway as a potential target[9]. Albitiazolium, as the lead compound, was found to inhibit active choline transport and also to partially inhibit the three enzymes of the Kennedy pathway (CK, CCT and CEPT)[10]. The aim of further drug development approaches is to increase the bioavailability of this compound[11]. Recently phase II clinical studies of parenterally administered albitiazolium bromide (SAR97276) were discontinued due to the lack of sufficient efficacy among young patients[12].

Plasmodium falciparum CCT (*Pf*CCT) may be considered as an additional potential target of choline analogue antimalarial compounds[13]. Further assessment of *Pf*CCT as an antimalarial target necessitates the characterization of the enzyme structure and function on molecular and cellular levels.

1.3. Structure and mechanism of CCT

CCT (EC number: 2.7.7.15) is a key enzyme of the *de novo* PC biosynthesis as it catalyzes the second, rate-limiting step of the pathway[14] (Figure 1). In this enzymatic reaction choline-phosphate (ChoP) and cytidine 5'-triphosphate (CTP) are converted to cytidine 5'-diphosphocholine (CDPCho) metabolic intermediate and pyrophosphate (PP_i). CCT is a member of the HxGH nucleotidyltransferase enzyme superfamily named after the conserved motif of the nucleotide binding loop[15]. The catalytic domain of the enzyme adopts an α/β Rossmann-fold consisting of five β-strands surrounded by six α-helices (Figure 2).

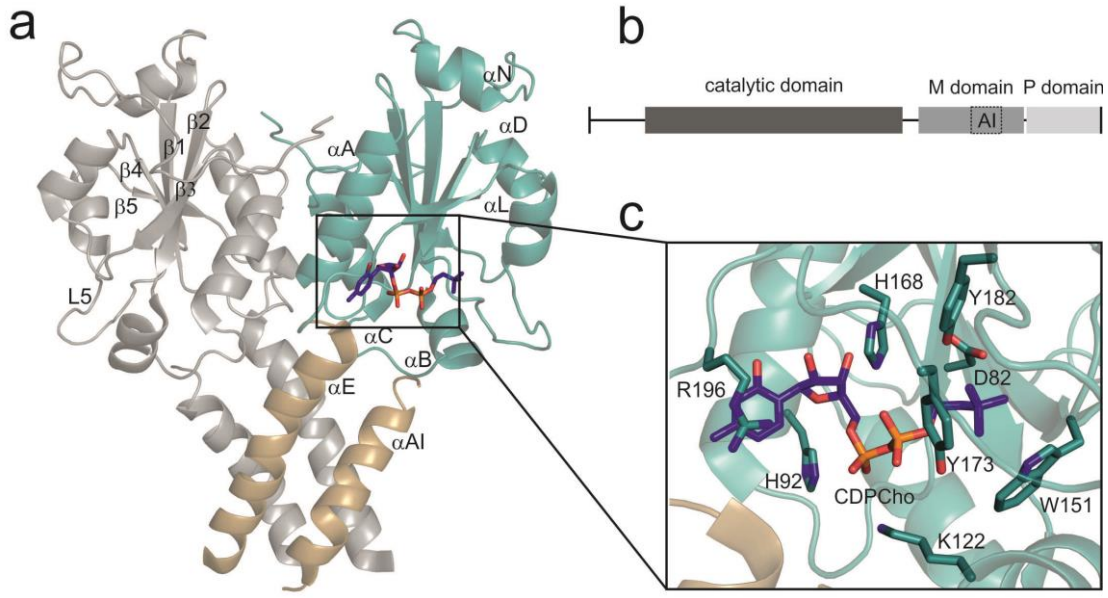

Figure 2. Structural build-up of CCT. a) Crystal structure of rat CCT (PDB: 4MVC) featuring a dimer of catalytic domains (grey and dark cyan with yellow helix αE) and αAI auto-inhibitory segments from membrane binding domains (grey and yellow). b) Domain organization of mammalian CCT. c) Close-up to the active site with CDPCho ligand and residues forming key contacts to that shown as sticks.

Most CCT enzymes form dimers in solution[16,17] stabilized by the conserved RYVD dimerization motif[18]. In case of the extensively studied rat CCT nuclear isoform (CCTα, referred as *Rattus norvegicus* CCT, *Rn*CCT), it was shown by cross-linking mass spectrometric

experiments that a pre-catalytic region contributes also to the dimer cohesion[17]. The C-terminal end of the protein comprises regulatory sequences including a membrane binding segment (M domain) and a phosphorylation region (P domain) (Figure 2). As a key regulator of the lipid composition of membranes CCT plays a decisive role in numerous physiological processes such as vesicular transport[19], adiposome size control[20], plasma lipoprotein balance[21], and lung surfactant production[22]. These are made possible by the reversible membrane binding regulatory mechanism of the enzyme, which fine tunes the transition between the inactive cytosolic and the active membrane bound forms (Figure 3).

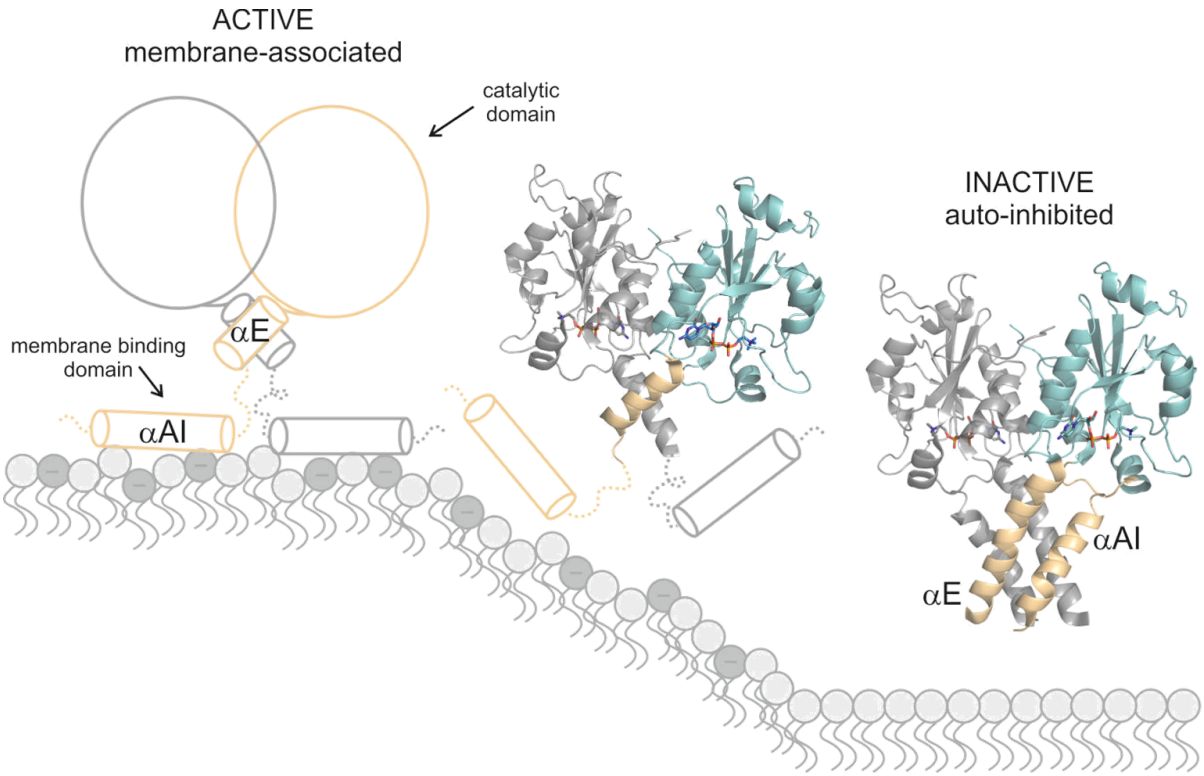

Figure 3. Reversible membrane binding regulatory mechanism of CCT. The αAI helix of CCT contributes to upregulation of enzymatic activity by selectively associating with membranes rich in anionic lipids (shown with dark grey headgroup) but not with PC-rich membranes (light grey lipid headgroup). This segment forms auto-inhibitory interactions with the catalytic domain in absence of membranes deprived of PC.

The membrane binding segment has a dual role in enzyme activity regulation[23]. On the one hand in absence of lipid vesicles the so called silencing interaction between the catalytic and membrane binding domains leads to an activity decrease. Interaction of two helices, the amphipathic αAI helix of M domain and the C-terminal αE helix of the catalytic domain serves as the structural basis of this phenomenon (Figure 3), which modifies the conformational

dynamics at the active site[24,25]. On the other hand membrane-association boosts catalytic efficiency by increasing enzyme activity and decreasing the Michaelis-Menten constant of CTP[26]. The αAI helix of M domain selectively associates to membranes deprived of PC and rich in other neutral or anionic lipids (Figure3) whereupon it adopts a helical structure instead of its partially disordered state in solution[27]. This regulatory mechanism of CCT enables a feedback regulation of PC producing capacity through the Kennedy pathway. The complex regulatory mechanism of mammalian CCTs has two more participants; the N-terminal positively charged nuclear localisation signal (NLS) and the C-terminal phosphorylation region[27,28]. The removal of the membrane binding domain results in a lipid independent, constitutive enzyme activity[16].

1.4. *Plasmodium falciparum* CCT

De novo PC biosynthesis is essential for Plasmodium parasites based on a gene disruption experiment in *P. berghei*, a Plasmodium strain infecting rodents[7]. CCT is rate limiting in the biosynthetic pathway[8]. Plasmodium genomes contain only a single annotated *cct* gene copy. Suprisingly, these genes encode two, duplicated CM segments in one open reading frame, consisting of a cytidylyltransferase catalytic domain (C1/C2 domain) and a membrane binding domain (M1/M2 domain) (cf. Figure 2). The duplicated CM segments are linked with a Plasmodium specific segment comprising ca. 300 residues which together add up to a total length of 896 residues in case of *Pf*CCT (Figure 4). In contrast, CCTs from other organisms except some Apicomplexan parasites contain only one catalytic and membrane binding domain and form homodimers in solution. According to this an intramolecular dimer (pseudoheterodimer) structure of the full length *Pf*CCT enzyme can be assumed in its soluble form, although this has not been demonstrated yet.

Beyond the presence of this unprecedently long linker that has emerged concomitantly to the CM segment duplication of Plasmodial CCTs[29] there are further structural differences between the Plasmodium and mammalian CCTs which may make *Pf*CCT a suitable antimalarial drug target. The first and second catalytic domains of *Pf*CCT display high identity to each other and both were shown to be active[30]. It is worth to note that a recombinantly expressed *Pf*CCT construct comprising the second catalytic and membrane binding domain was less active and less lipid inducible than its rat homologue[31]. In the catalytic domains of *Pf*CCT a Plasmodium specific lysine rich segment of unknown function is inserted in loop L5. Previous experimental

results and bioinformatic analyses demonstrated that the overall regulatory mechanisms of Plasmodium CCT enzymes may differ somewhat from the general rat CCT auto-inhibitory scheme[23,31,32]. *Pf*CCT does not have a NLS segment, excluding the nuclear import-export cycle from the regulatory possibilities[33] and the existence of a phosphorylation region is also not yet verified. The putative membrane binding domain consists of two helices separated by a proline instead of a single long alpha helical segment and it also shows moderate similarity to the corresponding sequences in rat CCT. In case of *Pf*CCT the exact sequences described as polybasic and autoinhibitory segments[25] are not yet identified.

1.5. CHO-MT58, an inducible CCT knock-down cell line

Due to *cct* gene duplication in Plasmodia, the respective full length enzyme is challenging to express and study *in vitro*. However cellular studies may be facilitated in the CHO-MT58 cell model. CHO-MT58, a Chinese Hamster Ovarian (CHO) cell line generated by chemical mutagenesis from CHO-K1, was described as a tool for the functional investigation of CCT[34,35]. In CHO-MT58, the endogenous *cct* gene contains a point mutation resulting in an amino acid change (R96H) that is responsible for the thermosensitive phenotype of the cell line[36]. While at 37°C (permissive temperature) functional protein is formed albeit in smaller amount, at 40°C (non-permissive temperature) an accelerated rate of CCT degradation is observed as a result of the point mutation. This temperature induced deficiency causes drastically decreased PC levels, morphological changes such as endoplasmic reticulum (ER) dilation[37] and eventually leads to apoptosis within 30-48 hours[38]. Although the point mutation in the *cct* gene was already described in 1994[36], and this cellular model has been extensively used to study the relation of CCT deficiency and apoptosis[37,39–42], still there are no direct *in vitro* enzyme studies to describe the molecular mechanism causing this thermosensitive phenotype.

As CHO-MT58 can be rescued either *via* exogenous PC supply, reverting the temperature to 37°C or through heterologous CCT expression, this cell line has the potential for functional characterization of CCT orthologues in a cellular environment. Considering that at the non-permissive temperature (40°C) the hamster CCT is not functional, heterologously expressed CCT constructs can be studied with conditional exclusion of the effect of the endogenous thermosensitive CCT. Thus a cellular test system may be created employing the thermosensitive CHO-MT58 cell line as a platform for functional analysis of *Pf*CCT and screening antimalarial compounds targeting plasmodial CCT.

2. AIMS

In the present PhD thesis I aimed to characterize the potent antimalarial drug target *Plasmodium falciparum* CTP:phosphocholine cytidylyltransferase *in vitro* and also in a cellular environment. The dual purpose of the study was to biochemically characterize the active site of this rate-limiting biosynthetic enzyme and to establish a cellular model system for further characterization of the full length protein and its enzyme variants.

Specifically, I focused to resolve the following questions:

1. What is the role of residues constituting the choline binding site of *Pf*CCT in ligand binding and catalysis?
2. What is the exact molecular mechanism underlying the thermal instability of CCT from the thermosensitive CHO-MT58 cell line?
3. Can the heterologous expression of *Pf*CCT rescue the mammalian CHO-MT58 cell line at the non-permissive temperature?
4. How can a well applicable test system be established for studying the structural differences of *Pf*CCT and mammalian orthologues in a cellular environment?

3. MATERIALS AND METHODS

3.1. Cloning of *Pf*CCT constructs

The *Pf*CCT 3D7 cDNA sequence (PlasmoDB: PF3D7_1316600) was codon-optimized for expression in *E. coli* (GenScript, Piscataway, NJ, USA). The *Pf*CCT$_{(528-795)}$ constructs and mutants used for *in vitro* studies were obtained using the previously described *Pf*CCT$_{(528-795)}$ (pET15b) catalytic domain construct lacking the lysine-rich Plasmodium specific loop (720-737)[43]. For site-directed mutagenesis the QuikChange method (Agilent) was applied. Primer synthesis and verification of the mutagenesis were performed by Eurofins MWG GmbH (Table 1).

Table 1. Primer sequences used to create the different protein constructs and vectors.

Primer name	5'-3' sequence
D623N for	CGTGGTGATTTACGCCAATGGTGTTTACGACATGC
D623N rev	GCATGTCGTAAACACCATTGGCGTAAATCACCACG
H45N for	GTGTATGATCTGCTGAATCTGGGCCATATG
H45N rev	CATATGGCCCAGATTCAGCAGATCATACAC
H630N for	GGTGTTTACGACATGCTGAACCTGGGT
H630N rev	GTTTCATGTGACCCAGGTTCAGCATGT
pBs MCS1 for	CGACTCACTATGCTAGCAATTGGGTACCGGGCCCCCCGTCGAGGTCGAC
pBs MCS1 rev	GTCGACCTCGACGGGGGGCCCGGTACCCAATTGCTAGCATAGTGAGTCG
pBs MCS2 for	GTTCTAGAGCGAGCTCCACCGCGGTGCTCGAGCAGCTTTTGTTC
pBs MCS2 rev	GAACAAAAGCTGCTCGAGCACCGCGGTGGAGCTCGCTCTAGAAC
R681H for	GAAACACATCCATTGGGTTGA
R681H rev	GTCAACCCAATGGATGTGTTTC
R96H for	CCCTGAAACATATTCACTGGGTGGATGAAATC
R96H rev	GATTTCATCCACCCAGTGAATATGTTTCAGGG
W692A for	CATTTCTCCGTGTCCGGCGGTGGTGACGCCG
W692A rev	CGGCGTCACCACCGCCGGACACGGAGAAATG
W692F for	CATTTCTCCGTGTCCGTTCGTGGTGACGCCGG
W692F rev	CCGGCGTCACCACGAACGGACACGGAGAAATG
Y714F for	CATGATGACATCCCGTTTGCTAACAATCAGAAAGAAG
Y714F rev	CTTCTTTCTGATTGTTAGCAAACGGGATGTCATCATG
Y741F for	CAATCAGAAAGAAGATATTTTTGCTTGGCTGAAAC
Y741F rev	GTTTCAGCCAAGCAAAAATATCTTCTTTCTGATTG

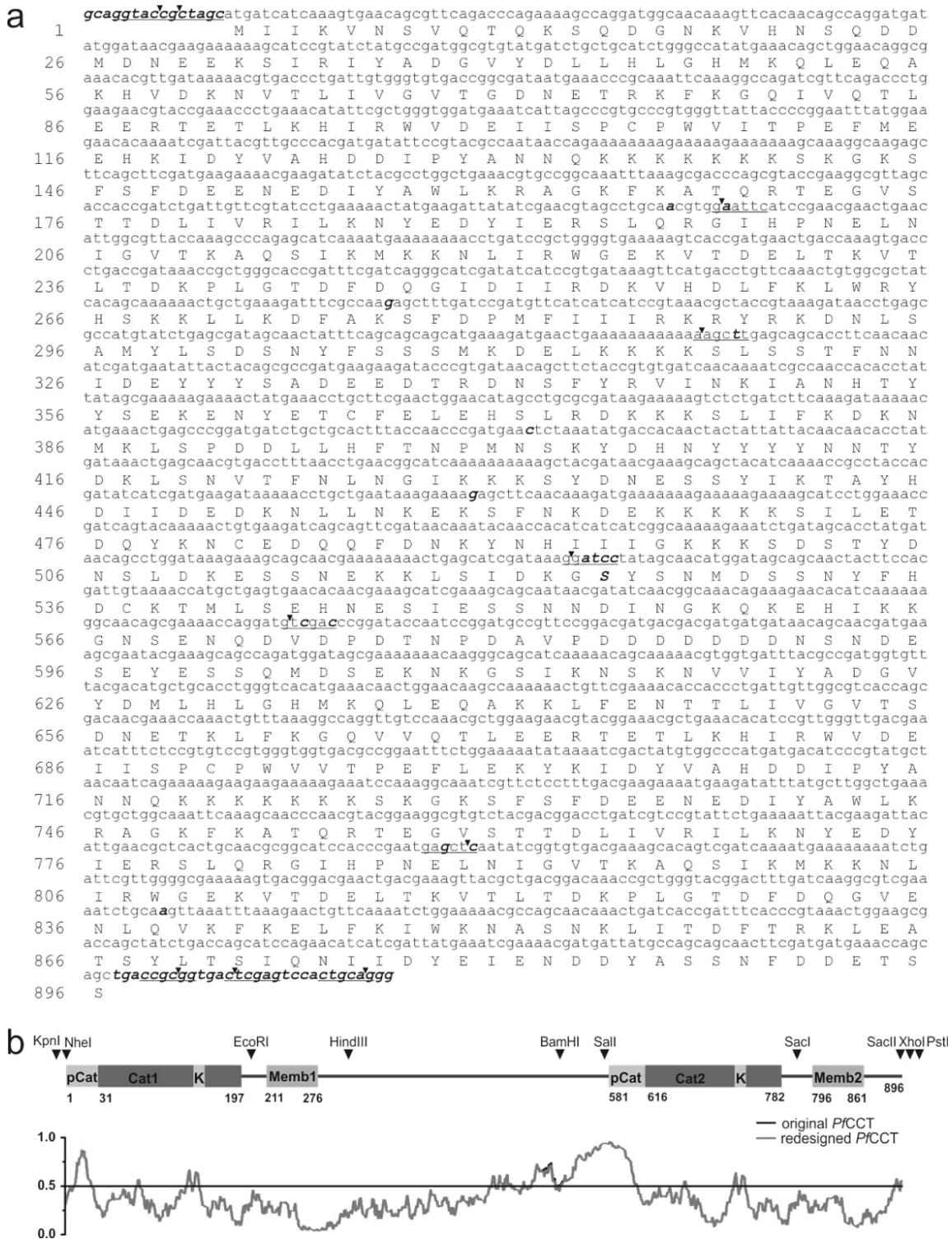

Figure 4. Sequence and domain organization of the redesigned *Pf*CCT. a) Nucleotide sequence of resynthesized *Pf*CCT enzyme. Every change compared to the original sequence is indicated by bold and italic format. Restriction sites are underlined. b) Predicted domain organization of full length enzyme with the engineered restriction sites shown as arrowheads. Note that the redesigned *Pf*CCT has an almost identical disorder profile[44] as the original.

For cellular experiments constructs containing the full length *Pf*CCT sequence were obtained. Due to the high sequence identity of the two catalytic domains of *Pf*CCT, resynthesis of the previously codon-optimized cDNA sequence was necessary (GenScript) to install unique restriction sites for cloning and mutagenesis (Figure 4). *Pf*CCT$_{(1\text{-}896)}$ was constructed in two sequential copy paste cloning steps by subcloning the full length sequence from pUC57-Kan to pBluescript SK (+)* using NheI/SacII restriction sites and from the cloning vector to pIRES-EGFP-puro using the NheI/XhoI restriction endonucleases. A modified pBluescript SK (+)* plasmid was created from the commercially available pBluescript SK (+) using the QuikChange method (for primers see Table 1) to serve the restriction site needs of the redesigned construct (Figure 5).

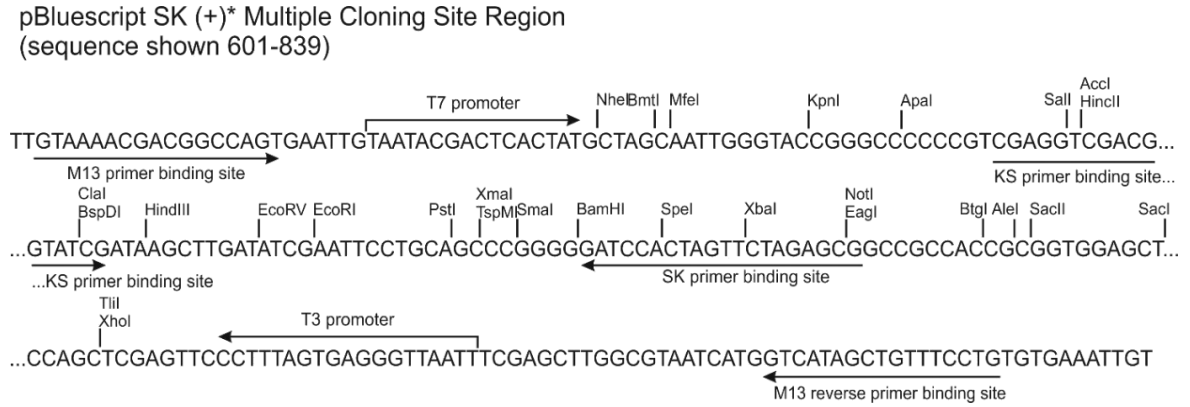

Figure 5. Multiple cloning site of the modified pBluescript SK (+)* vector.

*Pf*CCT$_{(1\text{-}522)}$ and *Pf*CCT$_{(523\text{-}896)}$ were engineered by subcloning from the *Pf*CCT (pUC57-Kan) plasmid to pBluescript SK (+)* using the restriction enzyme pairs NheI/BamHI and BamHI/SacII, respectively. The inactivating (H/N) and thermosensitizing (R/H) mutations were introduced into constructs harboring only one of the active sites by QuikChange mutagenesis using the forward and reverse primers H45N, H630N, R96H and R681H. The constructs *Pf*CCT$_{(1\text{-}896)}$ H45N H630N and *Pf*CCT$_{(1\text{-}896)}$ R96H R681H were cloned in pBluescript SK (+)* using restriction enzymes NheI/BamHI/SacII and subcloned to the mammalian expression vector pIRES-EGFP-puro with NheI/XhoI restriction sites. DNA sequences of the different constructs were verified by sequencing at Eurofins MWG GmbH or Microsynth AG.

3.2. Protein expression and purification

The His-tagged *Pf*CCT$_{(528-795)}$ catalytic domain construct used as a wild type (WT) reference in *in vitro* studies and its mutants were expressed using the BL21 (DE3) Rosetta *E. coli* expression system. Expression was induced at OD_{600nm} OD_{600nm}=0.4-0.6 with 0.5 mM IPTG for 18 h at 16°C followed by cell lysis and nickel-nitrilotriacetic acid (Ni-NTA) affinity chromatography performed at ambient temperature with 250 mM imidazole elution, except in case of *Pf*CCT$_{(528-795)}$ R681H where purification was performed at 18°C to maintain protein stability. Protein eluted from Ni-NTA column was dialyzed into 20 mM HEPES, pH 7.5 buffer, containing 100 mM NaCl and 2 mM β-mercaptoethanol. Samples for MS analysis were further purified by size-exclusion chromatography (gel filtration) using a GE Healthcare ÄKTA system with a Superose12 10/300 GL column. Protein concentrations were determined spectrophotometrically from the absorbance at 280 nm using a Nanodrop 2000c spectrophotometer (Thermo Scientific). Approximate extinction coefficients were calculated on the basis of amino acid composition by using ProtParam server[45].

3.3. Steady-state enzyme activity measurements

Steady-state activity measurements were performed in 20 mM HEPES, pH 7.5 buffer, containing 100 mM NaCl using a continuous coupled pyrophosphatase enzyme assay, which employs pyrophosphatase (PPase) and purine nucleoside phosphorylase (PNP) auxiliary enzymes and 7-methyl-6-thioguanosine (MESG) substrate for colorimetric phosphate detection at 360 nm[43]. The reaction was performed at 20°C in a Specord 200 spectrophotometer. Coupling enzyme and substrate concentrations were adjusted to keep the enzymatic conversion catalysed by CCT as the rate limiting step. The reaction was started by adding *Pf*CCT to the reaction mixture (final concentration: 1-3 μM). Initial velocity was determined from the slope of the first 10% of the progress curve. For CTP substrate titrations, CTP concentration was varied while ChoP concentration was kept at 5 mM. For ChoP substrate titrations, ChoP concentration was varied while CTP concentration was kept at 1 mM. In the heat inactivation assay, protein samples were incubated for 15 min at various temperatures (10-60°C) followed by the immediate use in enzyme activity assay at 20°C. In case of constructs with deteriorated activity the enzyme was used in 10 μM concentration and the slope of the absorbance change was determined after monitoring the reaction for 20 minutes. Kinetic data were fitted with Michaelis–Menten equation and competitive substrate inhibition equation using OriginPro 8.6.

3.4. Isothermal titration calorimetry

Calorimetric measurements were performed on a MicroCal-ITC 200 titration calorimeter (Malvern) at 20°C. The protein samples were dialyzed against buffer containing 20 mM HEPES, pH 7.5, 100 mM NaCl, 1 mM TCEP. Ligands were freshly dissolved in the dialysis buffer of protein samples followed by pH adjustment. In the experimental setup, the cell of the instrument was filled with protein and the syringe with the respective ligand. Each titration typically included 27 steps of injection with 1.5 µl of ligand per injection spaced 180 s apart from each other, with the injection syringe rotating at 500 rpm. The data were analyzed using MICROCAL ORIGIN software, following the directions of the manufacturer. Integrated heat data were normalized by subtracting heat data of ligand-to-buffer titration, performed under identical conditions.

3.5. Mass spectrometry

In the mass spectrometric study of protein complexes, a commercial Waters QTOF Premier instrument (Waters, Milford, MA, USA) equipped with electrospray ionization source (Waters, Milford, MA, USA) was used in the positive ion mode. Mass spectra were obtained under native conditions: namely, the ions were generated from aqueous 10 mM NH_4HCO_3 buffer solution (pH 7.15) containing the gel filtered *Pf*CCT$_{(528-795)}$ protein constructs at a 0.4 µM monomer concentration. These conditions allow transfer of the native protein complex present in the solution into the gas phase. The capillary voltage was 3600 V, the sampling cone voltage was 125 V and the temperature of the source was kept at 80°C, collision cell pressure was $3.38 \cdot 10^{-3}$ mbar and ion guide gas flow was 35.00 ml/min. Mass spectra were recorded using the software MassLynx 4.1 (Waters, Milford, MA, USA) in the mass range 1000-5000 m/z as no signals could be detected above 5000 m/z.

3.6. Molecular dynamics

The catalytic domain structure of *Rn*CCT (PDB: 4MVC)[25] was used to construct the homodimer homology models of *Pf*CCT$_{(528-795)}$ WT and its point mutant *Pf*CCT$_{(528-795)}$ R681H. The aligned sequences were 44.6 % and 44.0 % identical in the case of wild type and R681H mutant CCT, respectively[46]. MODELLER 9.14[47] software was used to create 80 homology models in both cases using the same alignment. The models with the lowest value of the MODELLER objective function were selected and visually inspected using VMD program[48]. The selected

models were evaluated using PROCHECK, WHAT_CHECK[49] and ERRAT[50] programs. Model data are made available in the Protein Model Database (PMDB) under the accession numbers PM0079950 (*Pf*CCT$_{(528\text{-}795)}$ WT) and PM0079951 (*Pf*CCT$_{(528\text{-}795)}$ R681H).

Molecular dynamics (MD) simulations were carried out for both enzyme variant models using the same computational protocol. The protonation state of the ionisable amino acid side chains was verified by H++ webserver version 3.1[51] and PROPKA[52]. CHARMM program[53] and CHARMM27 force field[54] was applied using the self-consistent GBSW implicit solvent model[55] to carry out the MD simulations. The calculations were carried out with the optimized PB radii[56], and the CMAP correction optimized for GBSW[57]. The nonpolar surface tension coefficient was 0.005 kcal/(mol·Å^2), the number of angular integration points was 50 and the grid spacing for lookup table was 1.5 Å. Structures were heated up from 10 K to 310 K over 60 ps. At this temperature MD equilibration was carried out over 100 ps, which was followed by the final 5 ns long productive MD simulation. Interaction energies between the two chains of enzyme variants were calculated over the whole trajectory for all frames (i):

$$W(R^M)^i_{\text{int}} = W(R^M)^i_{dimer} - W(R^M)^i_{chainA} - W(R^M)^i_{chainB}$$

where W(R^M) is the effective energy of the protein with coordinates R^M in solution:

$$W(R^M) = H_{intra}(R^M) + \Delta G_{solv}(R^M)$$

where H_{intra} is the intramacromolecular energy consisting of bonded and non-bonded energy terms, and ΔG_{solv} is the solvation free energy[58].

The volume and the surface of the proteins were calculated by 3V website[59] using a high resolution grid and 1.4 Å probe radius. The number of hydrogen bonds were measured by CHARMM using the default 2.4 Å distance and 999.0 angle cut-offs.

3.7. Cell culture conditions

The CHO-K1 and CHO-MT58 cell lines were maintained in F-12 medium supplemented with 10% FBS and 1% Penicillin-Streptomycin at 37°C or 40°C in a humidified 5% CO_2 atmosphere. Cell lines were regularly screened and the measurements were carried out on Mycoplasma-negative cells.

3.8. Microscopy

CHO-K1 and CHO-MT58 cells grown in 6-well plates at 37°C and 5% CO_2 were transiently transfected with FuGene HD transfection reagent according to the manufacturer's instructions at a confluency of 80% with 2 μg purified plasmid DNA (*Pf*CCT$_{(1-896)}$ in pIRES-EGFP-puro). After 24 h the incubation temperature was shifted to 40°C. After 10 days the transfected and non-transfected cells serving as controls were inspected by fluorescence microscopy. Differential interference contrast (DIC) and green fluorescent (EGFP) images were captured by a Leica DM IL LED 500 system using a Leica HCX PL Fluotar 40x/0.75 objective.

3.9. Fluorescence activated cell sorting

Transfection of *Pf*CCT$_{(1-896)}$, *Pf*CCT$_{(1-896)}$ H45N H630N and *Pf*CCT$_{(1-896)}$ R96H R681H in pIRES-EGFP-puro into CHO-K1 and CHO-MT58 cells were performed as described in 3.8. After 24 h the cells were treated with Trypsin-EDTA (TE) and the cell suspension was split 1:1 equally to two new plates, which were cultured at 40°C and 37°C, respectively. CHO-K1 and CHO-MT58 cells were collected for fluorescence activated cell sorting (FACS) analysis 72 hours post-transfection. After centrifugation at 1,100 rpm for 5 min (Eppendorf MiniSpin) the cells were resuspended in 600 μl PBS and were treated with propidium iodide (PI) in a 1 μg/ml final concentration. The GFP positivity (%) was detected by FACS Attune® Acoustic Focusing Cytometer, Blue/Violet (excitation wavelength: 488 nm solid state laser; emission filters: 530/15 nm). Intact cells were gated based on the forward scatter (FSC) and side scatter (SSC) parameters. Dead cells were excluded based on propidium iodide positivity.

4. RESULTS

4.1. *In vitro* analysis of the different amino acid residues building up the *Pf*CCT choline binding site

4.1.1. Charged and cation-π interactions at the choline binding cleft of *Pf*CCT

Exploration of druggability of *Pf*CCT using virtual screening of compound libraries and subsequent rational drug design ultimately requires an in-depth knowledge on the architecture and interactions of the active site. Analysis of *Pf*CCT catalytic domain homology model structure (PMDB: PM0078719) created using rat CCT crystal structure (PDB: 3HL4) as template indicated that the choline binding subsite of *Pf*CCT is a partially hydrophobic pocket that accommodates the quaternary ammonium moiety of the substrate CDPCho (Figure 6).

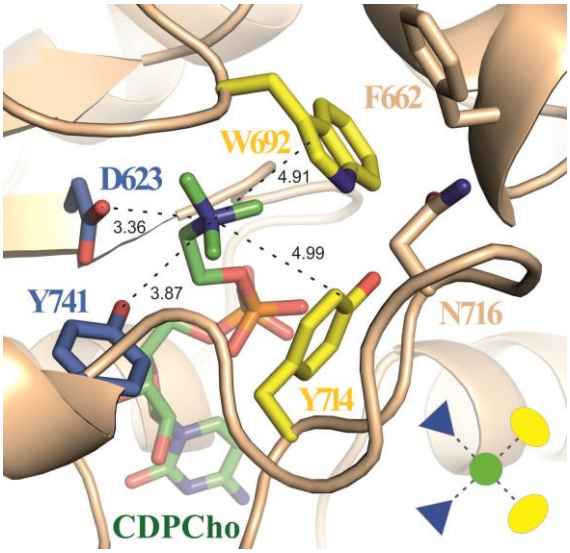

Figure 6. Coordination of CDPCho at the active site of *Pf*CCT. *Pf*CCT homology model structure is shown as wheat cartoon model with CDPCho (green carbon). Side chains of residues providing charged (blue carbon) and cation-π (yellow carbon) interactions are depicted as sticks. The scheme of composite aromatic box is shown at the bottom right corner.

This subsite is built up of strictly conserved residues of either charged or aromatic character (termed here as composite aromatic box). These include D623 and Y741 that provide electrostatic interactions; Y714 providing both cation-π interaction to the trimethyl ammonium group and coordinating the β phosphate oxygen of CDPCho; and W692, a cation-π interactor for the choline moiety of CDPCho[43]. The indole ring of W692 also assists the local structural integrity of the enzyme by forming π-π interaction with the conserved F662 of helix αB and coordinating N716 of loop L5.

4.1.2. Role of charged and cation-π interactors in *Pf*CCT catalysis and ligand binding

To investigate the role of these residues in catalysis and in the structural integrity of the choline subsite, a series of point mutants were designed in the *Pf*CCT$_{(528\text{-}795)}$ catalytic domain construct[43] by modulating the character of charged (D623N, Y741F) and aromatic (W692F, W692Y and Y714F) residues or fully abolishing the aromatic character (W692A). To assess any indirect effects of the designed residue alterations on the quaternary enzyme structure, oligomerisation state of the different protein constructs was studied by electrospray ionization mass spectrometry (ESI-MS). Mass spectra of the mutants did not differ significantly from that of the wild type *Pf*CCT$_{(528\text{-}795)}$. Dimer:monomer abundance ratios were found to be approximately 1:1 and no higher oligomeric forms were observed (Figure 7), except in case of *Pf*CCT$_{(528\text{-}795)}$ Y741F where the low resolution of monomer and dimer peaks might correlate with the decreased protein stability under the experimental conditions. These results indicate that the mutants specifically form dimers so the engineered mutations do not induce major conformational changes affecting dimer stability.

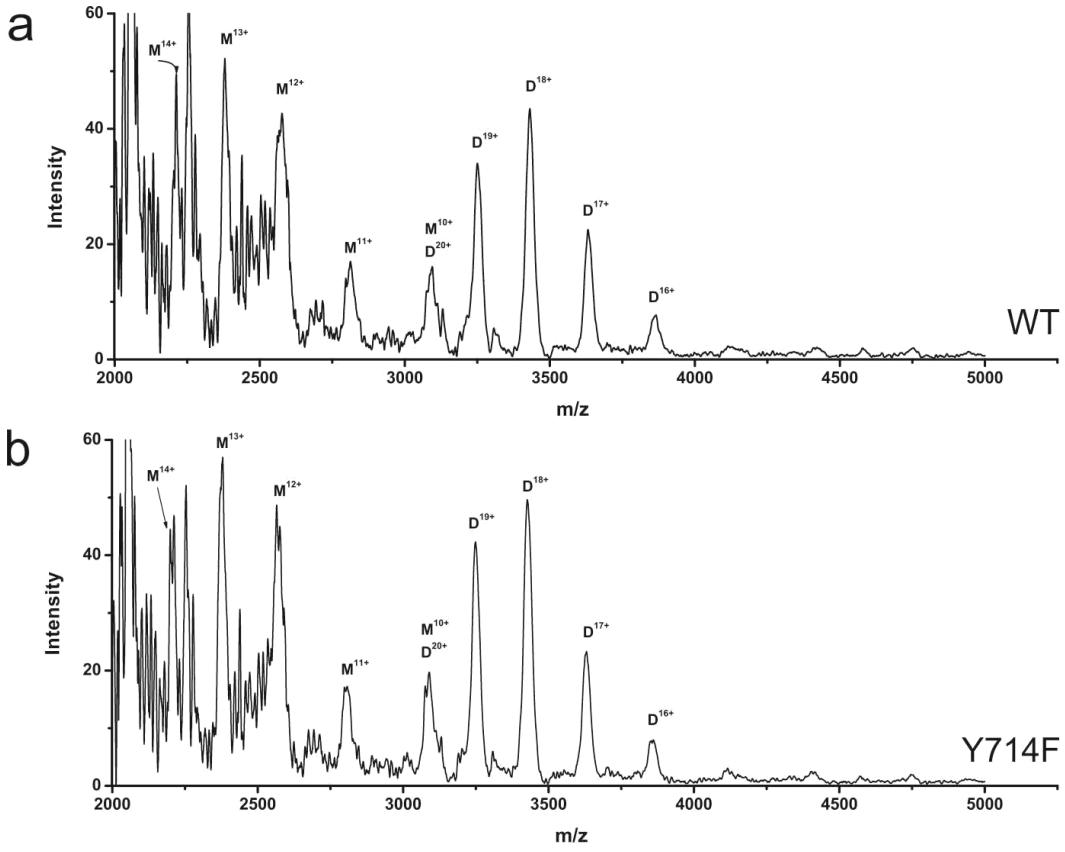

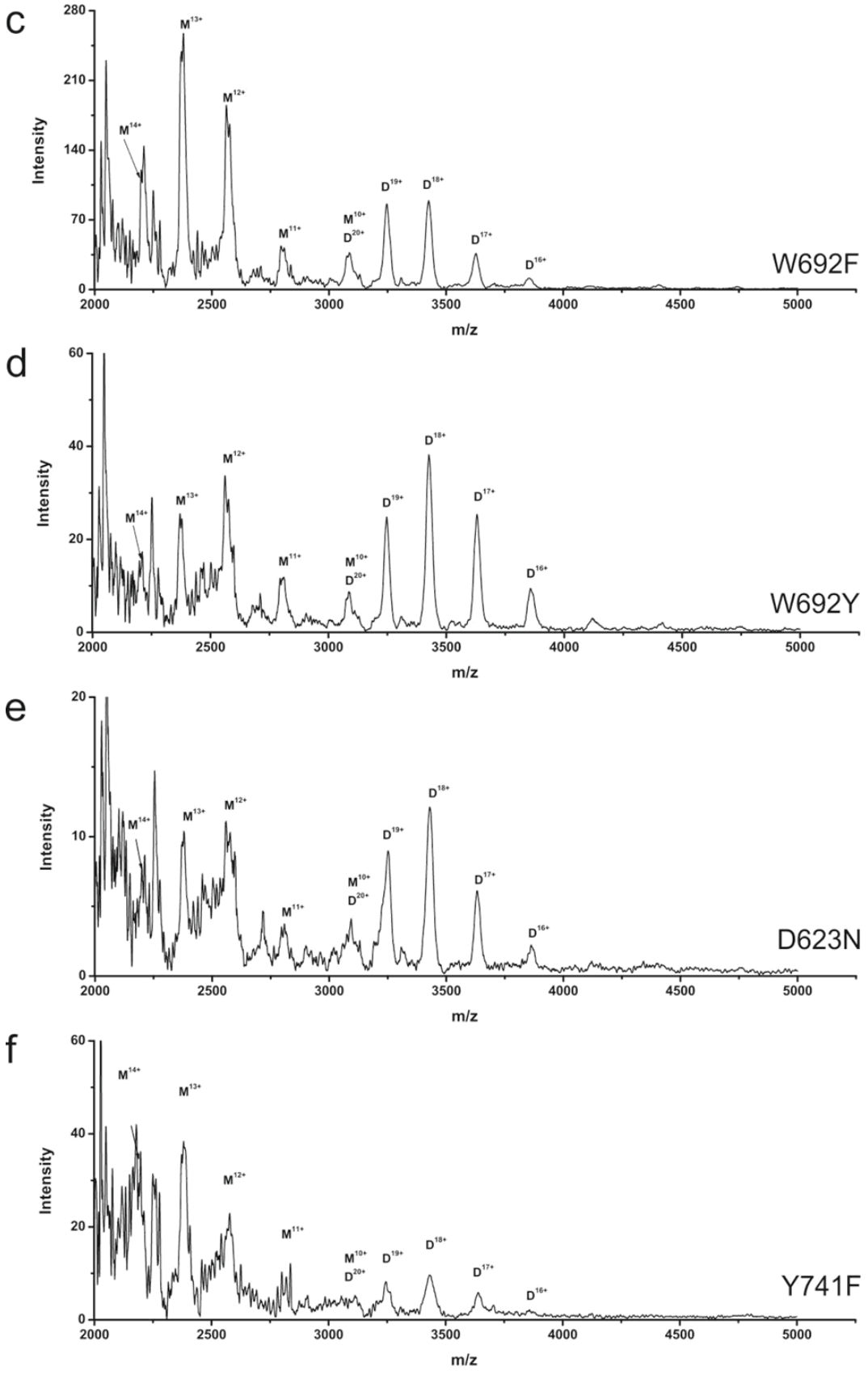
c
Intensity
m/z
M14+
M13+
M12+
M11+
M10+
D20+
D19+
D18+
D17+
D16+
W692F
d
W692Y
e
D623N
f
Y741F

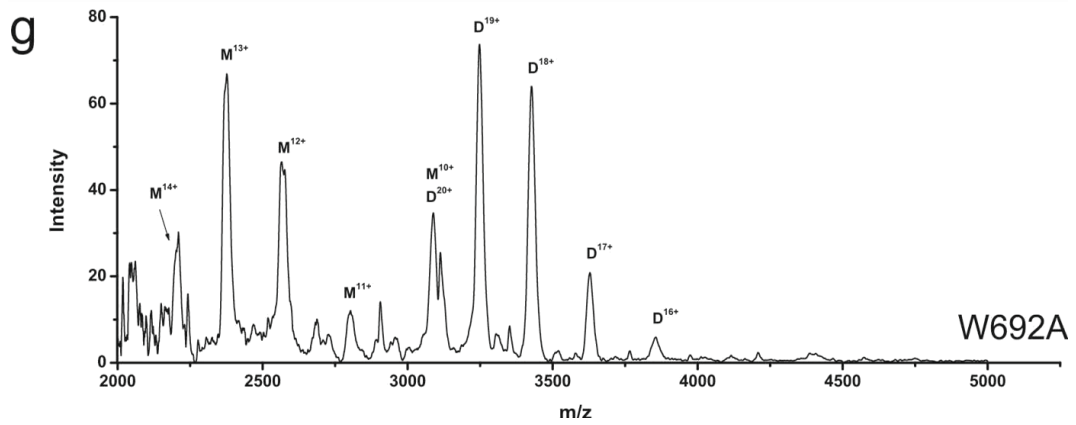

Figure 7. Mass spectra of *Pf*CCT$_{(528-795)}$ mutant proteins under native electrospray conditions. a-g) M and D denote monomer and dimer signals, respectively with upper case numbers indicating the charged state of particles. No signals were detected above 5000 m/z.

To evaluate the consequences of the different modulations at the active site enzyme kinetic investigations as well as CDPCho ligand binding measurments were performed. Results indicate that the substitution of charged to non-charged residues yielded drastic perturbation effects on catalytic efficiency (Figure 8, Table 2). The reason for that is mainly the altered choline coordination coordination as judged by the substantially altered $K_{M,ChoP}$ values and the impaired CDPCho binding (Figure 9, Table 3 and Figure 10).

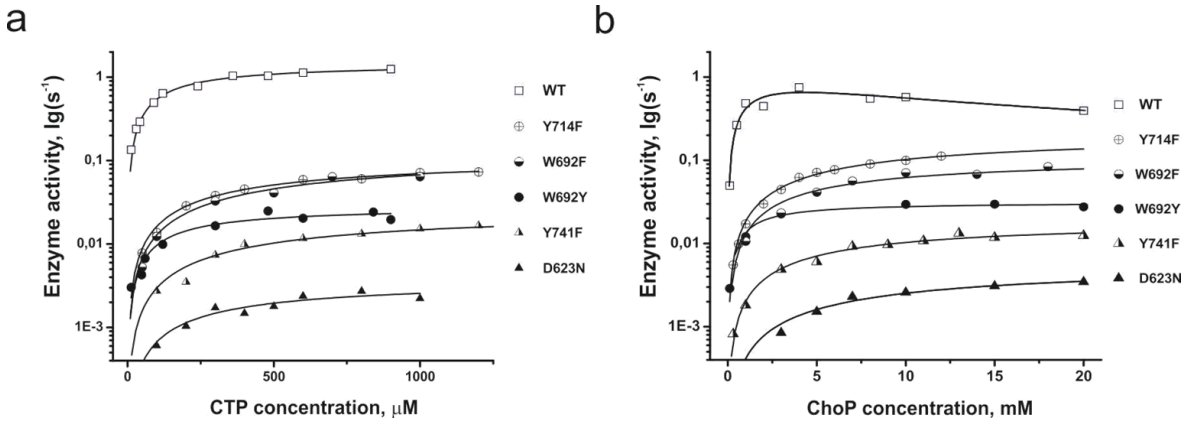

Figure 8. Steady-state kinetics of *Pf*CCT$_{(528-795)}$ point mutants. Michaelis-Menten titrations are shown with a) CTP b)ChoP variable substrates. Data points corresponding to mutants of charged interactors are indicated as triangles whereas mutants of cation-π interactors are depicted as circles. Note the logarithmic scale of enzyme activity.

Table 2. Kinetic parameters of *Pf*CCT$_{(528-795)}$ and its point mutants perturbing either cation-π or charged interactions. ND: not determined due to low enzymatic activity.

Enzyme	k_{cat} s^{-1}	$K_{M,CTP}$ μM	$K_{M,ChoP}$ mM	rel. $k_{cat}/K_{M,CTP}$	rel. $k_{cat}/K_{M,ChoP}$
WT	1.45 ± 0.05	168 ± 17	1.8 ± 1.1	1	1
Y714F	0.21 ± 0.01	575 ± 60	10.2 ±1.1	0.042	0.026
W692F	0.13 ± 0.03	890 ± 380	7.5 ± 2.4	0.018	0.022
W692Y	0.03 ± 0.003	191 ± 64	1.3 ± 0.2	0.017	0.029
D623N	0.006 ± 0.001	457± 191	13.1 ±3.1	0.0015	0.00057
Y741F	0.019 ± 0.002	786 ±175	8.5 ± 2.0	0.0028	0.0028
W692A	$6 \cdot 10^{-4}$	ND	ND	ND	ND

In contrast, when the aromatic character of residues involved in cation-π interactions was partially retained, i.e. only the electrostatics, ring size and quadrupole moment of the aromatic ring was modulated, the mutation was found to be somewhat compatible with catalysis and ligand binding. CDPCho binding affinity of the aromatic substituted W692 point mutants (W692Y and W692F) was attenuated with binding enthalpy also being decreased 2-3-fold (Table 3). These results are well explained with the perturbation of an important contact to the quaternary ammonium moiety, while preserving the binding enthalpy of the nucleotide moiety. It seems that aromatic substitutions can only partially complement the structural or electronic role of the W692 residue, in the functionality order W>Y>F, which is in agreement with the π donor character order of their sidechains[60]. Kinetic and ligand binding analysis of the mutants indicate their charged or cation-π type interactions with charged interactors having a pronounced role in the binding of the choline moiety.

Table 3. Thermodynamic parameters of CDPCho binding to *Pf*CCT$_{(528-795)}$ and its point mutants perturbing either cation-π or charged interactions.

Enzyme	K_d μM	ΔH kcal·mol^{-1}	ΔS cal·mol^{-1}·K^{-1}
WT	44.4 ± 3.3	−22.9 ± 1.0	−58.1 ± 5.0
Y714F	140 ± 50	−19.6 ± 6.0	−49.1 ± 22.3
W692F	680 ± 60	−6.8 ± 0.8	−8.9 ± 1.3
W692Y	220 ± 50	−9.8 ± 4.5	−16.8 ± 8.6
D623N	790 ± 60	−2.7 ± 0.1	5.1 ± 0.5
Y741F	1000 ± 80	−9.3 ± 1.9	-17.8 ± 3.9
W692A	460 ± 100	−1.7 ± 0.3	9.6 ± 2.6

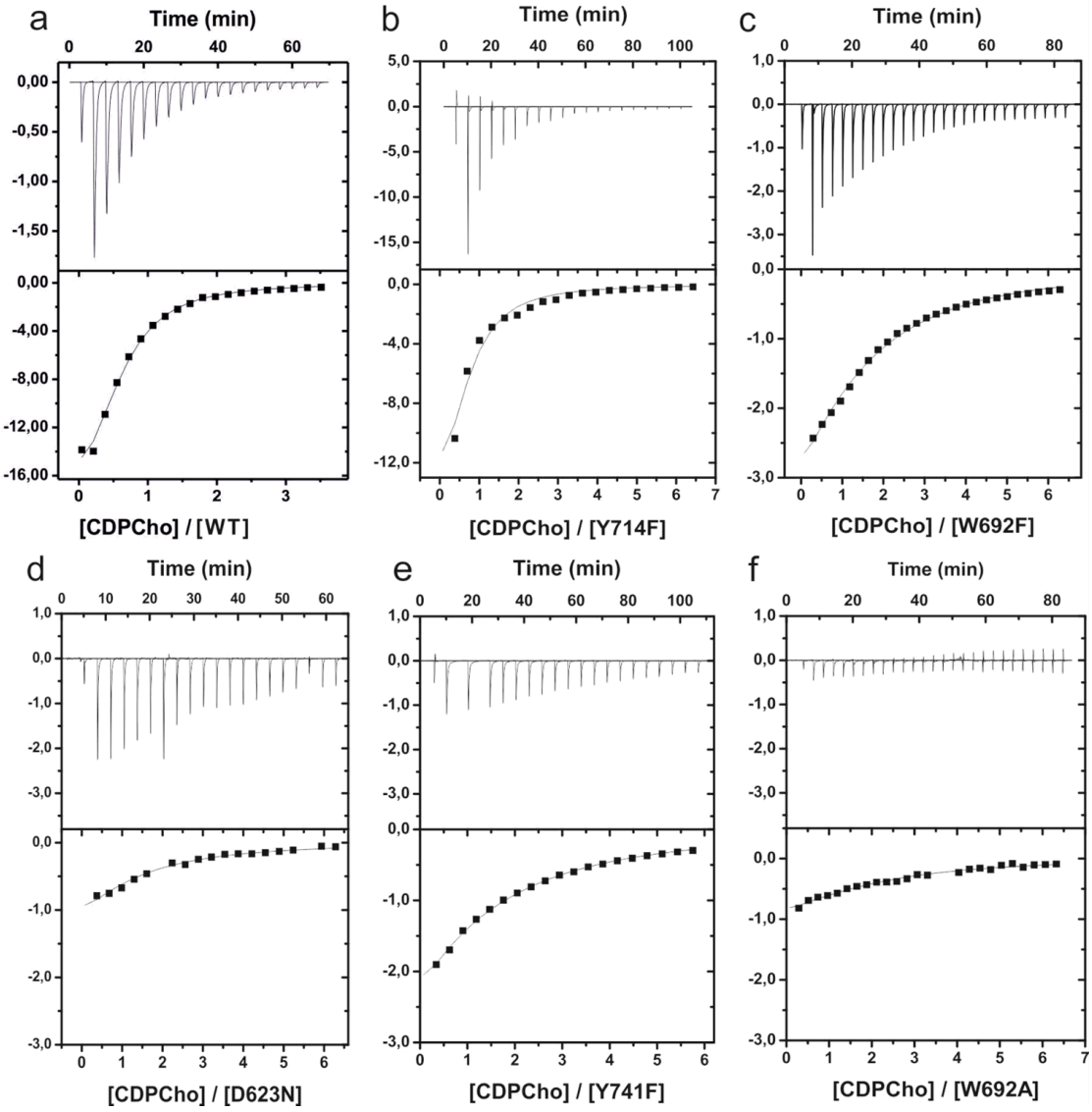

Figure 9. Isothermal titration calorimetry (ITC) analysis of CDPCho binding to *Pf*CCT and mutant enzymes. Top parts of each sub-panels show raw ITC thermograms, whereas bottom parts depict integrated heat values. Data gave best fit with the one set of binding sites model.

To assess the full contribution of the tryptophan 692 to the enzymatic function and structural stability, alanine mutagenesis was used as an alternative investigation approach. Elimination of the aromatic character of W692 abolished the catalytic function and heavily impaired the thermodynamics of the substrate binding. It seems that CDPCho binding of *Pf*CCT$_{(528\text{-}795)}$ W692A is now entropy-, rather than enthalpy governed indicating a much less directed and tight binding.

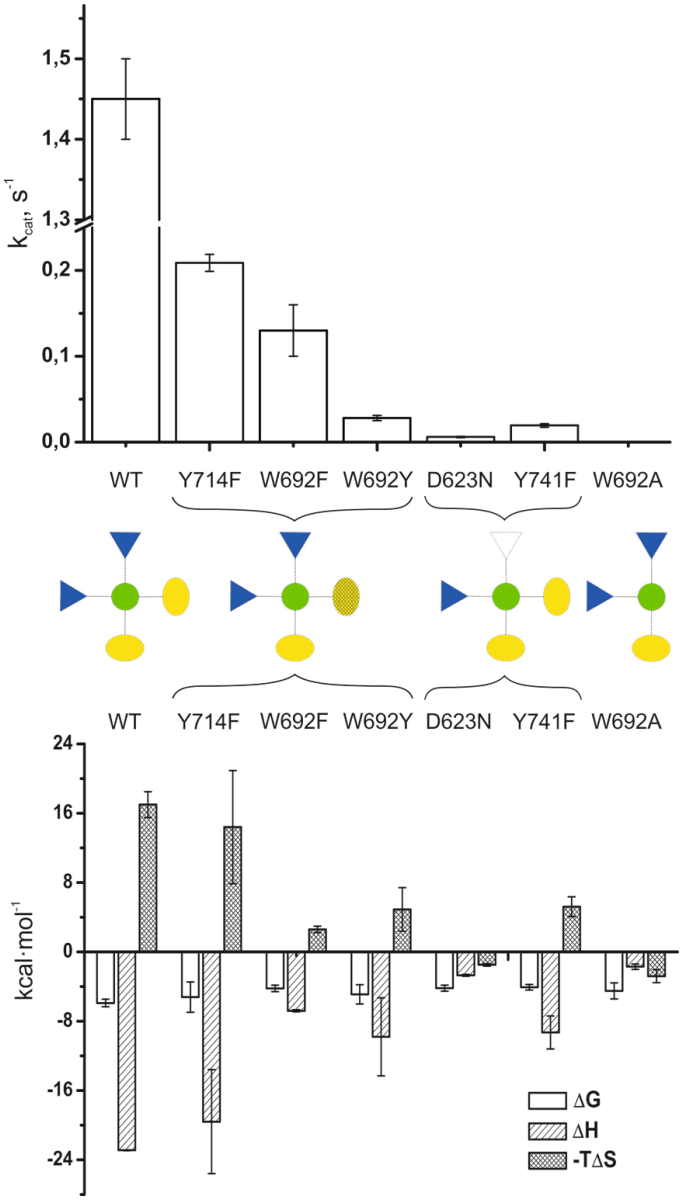

Figure 10. Consequences of *Pf*CCT mutations on enzyme catalytic turnover (k_{cat}) (top) and CDPCho ligand binding energetics (ΔG: binding free enthalpy, ΔH: enthalpy, ΔS: entropy) (bottom). Colored schematic representation shows the engineered modification of residues providing cation-π interactions (yellow ellipse) and charged interactions (blue triangle) to the quaternary ammonium ligand moiety (green circle).

4.2. Molecular mechanism underlying the thermosensitive phenotype of CHO-MT58 cell line harboring a mutant CCT

4.2.1. *In silico* analysis of the role of *P. falciparum* CCT R681 corresponding R140 in dimerization

The inducible CCT knock-down cell line CHO-MT58 contains a single point mutation at amino acid position 140 (R140H) causing the thermosensitive phenotype. As this amino acid is part of the ^{140}RYVD^{143} motif, which was shown to have prime importance in dimer stabilization in *Rn*CCT[18], I decided to analyze the conservation pattern of these amino acids in CCT enzymes. Two hundred CCT sequences from different evolutionary clusters were compared by the PipeAlign webserver[61]. The previously proposed high degree of conservation[62] was verified; the first amino acid of the motif has a conserved basic character (R/K), while the second position featured aromatic residues (Y/W). The last two positions are exclusively occupied by V and D. RYVD was apparent in ca. 50% of the investigated sequences being the most frequently occurring combination. Adjacent histidine and cysteine residues also contributing to the dimer stabilization interaction network of *Rn*CCT[18] were also conserved. Remarkably, neither of the investigated sequences contained a histidine instead of the arginine. In addition, no amino acid variation was documented at the dbSNP database at this sequence position for the *pcyt1a* gene corresponding to the human CCTα orthologue. The importance of the integrity of the RYVD motif is further underlined by the V142M mutation of human CCT described by Payne et al.[63]. The exchange of this valine, the main interaction partner of R140, to a methionine was responsible for causing congenital lipodystrophy and fatty liver disease marked by a reduced expression of CCT. The herein discussed *Plasmodium falciparum* CCT includes ^{681}RWVD^{684} corresponding to the cognate motif of ^{140}RYVD^{143} in the rat sequence. The *Pf*CCT$_{(528\text{-}795)}$ second catalytic domain construct expedient for *in vitro* studies was shown to exist in dimer oligomerization state (cf. Figure 7 panel a and [43]). To visualize inter-chain interaction of formed dimers, a homology model was built based on the *Rn*CCT crystal structure as a template[25]. Due to the considerably high sequence identity of the Plasmodium and rat catalytic domains, the *Pf*CCT model displayed similar fold as the rat CCT. Inter-subunit polar interactions of the ^{681}RWVD^{684} motif and R681 are listed in Table 4 and shown in Figure 11.

Table 4. Inter-chain interaction distances at the dimerization surface in homology models of WT and R681H enzyme variant of *Pf*CCT$_{(528-795)}$.

***Pf*CCT$_{(528-795)}$ WT**			***Pf*CCT$_{(528-795)}$ R681H**		
L3	**L3'**	**d (Å)**	**L3**	**L3'**	**d (Å)**
H679, O	R681, N	2.98	H679, O	H681, N	3.00
R681, NH2	I680, O	2.96	H681, ND1	I680, O	3.50
R681, NH1	I680, O	3.54			
R681, NH2	R681, O	2.79	H681, ND1	H681, O	3.40
R681, NH2	V683, O	2.65			
R681, N	H679, O	2.96	H681, N	H679, O	2.81
L3	**αA'**	**d (Å)**	**L3**	**αA'**	**d (Å)**
H679, NE2	K635, NZ	3.31			
L3	**Nterm'***	**d (Å)**	**L3**	**Nterm'***	**d (Å)**
R681, NH2	D584, OD1	2.69			
R681, NH1	D584, OD1	3.28			
R681, NH2	D584, OD2	3.53			
W682, NE1	A581, O	2.58	W682, NE1	A581, O	2.58
Nterm*	**L3'**	**d (Å)**	**Nterm***	**L3'**	**d (Å)**
A581, O	W682, NE1	2.77	A581, O	W682, NE1	2.69
V582, O	R681, NH2	2.98			

*the N-terminal region consists of residues 581-620

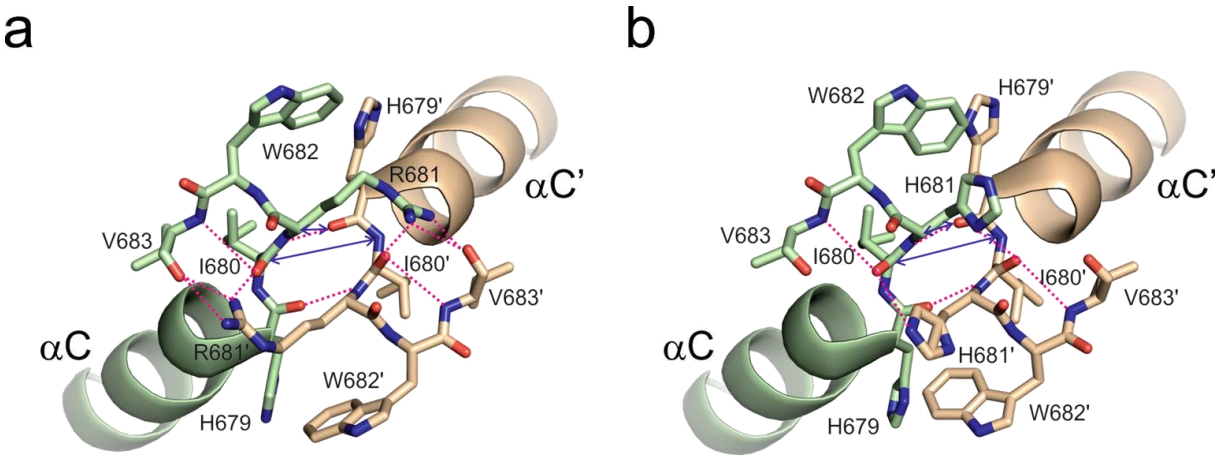

Figure 11. Inter-chain interactions of RYVD motifs of the *Pf*CCT$_{(528-795)}$ WT and *Pf*CCT$_{(528-795)}$ R681H. The residues involved in polar inter-chain interactions are shown in stick representation and interactions are indicated by pink dashed lines. Characteristic dimer interface distances d(R/H681, CA - H679', O) and d(I680, CA - I680', N) are denoted by blue double-headed arrows.

R681 provides two direct inter-chain interactions to the main chain carbonyl of V683' and one polar main chain interaction indirectly through I680 to V683'. Another polar main chain interaction is present between I680 and R681' bringing the two chains the closest at this specific point (d(R/H681, CA - H679', O=3.7 Å) (Figure 11 panel a). Interactions between H679 and W682 (corresponding the H138 and Y141 in rat, part of dimer stabilization interactions) are missing (Table 4, Figure 11 panel a). In total, thirteen polar inter-subunit interactions identified in the *Pf*CCT second catalytic domain structural model contribute to dimer stability. *In silico* modelling of the R681H mutation corresponding to the R140H mutation in the endogenous CCT of CHO-MT58 showed that interactions R681, NH1-I680', O and R681, NH2-V683', O are lost (Table 4, Figure 11 panel b), which indicated a possibility for decreased stability of the dimer oligomerization state[64]. Contacts between the N-terminal helix αA and loop L3 are also effected by the R681H mutation (Table 4), which could further contribute to destabilization of the dimer state.

4.2.2. Kinetic and heat inactivation studies of the R681H mutant enzyme

For *in vitro* experiments the R681H variant of the *Pf*CCT$_{(528\text{-}795)}$ construct was generated. Overexpression of *Pf*CCT$_{(528\text{-}795)}$ R681H in *E. coli* provided a significantly lower yield than that of *Pf*CCT$_{(528\text{-}795)}$ WT, an observation not unusual in case of protein mutants with decreased structural stability. Nevertheless, the functionality of the mutant enzyme was not altered substantially as proved by k_{cat} and K_M values originating from Michaelis-Menten curves of enzyme activity measurements performed at 20°C (Table 5 and Figure 12). These results are in good agreement with findings on the CHO-MT58 cell line, which was shown to have a WT phenotype when cultured at the permissive temperature[36].

Table 5. Kinetic parameters of WT and thermosensitive *Pf*CCT constructs at 20°C.

	CTP titration		**ChoP titration**		
	k_{cat} (s^{-1})	**$K_{M,CTP}$ (mM)**	**k_{cat} (s^{-1})**	**$K_{M,ChoP}$ (mM)**	**$K_{i,ChoP}$ (mM)**
***Pf*CCT$_{(528\text{-}795)}$ WT**	1.45±0.05	0.17±0.02	1.2±0.4	1.8±1.1	10.5±7.5
***Pf*CCT$_{(528\text{-}795)}$ R681H**	0.59±0.02	0.19±0.03	1.2±0.2	1.6±0.4	3.8±1.0

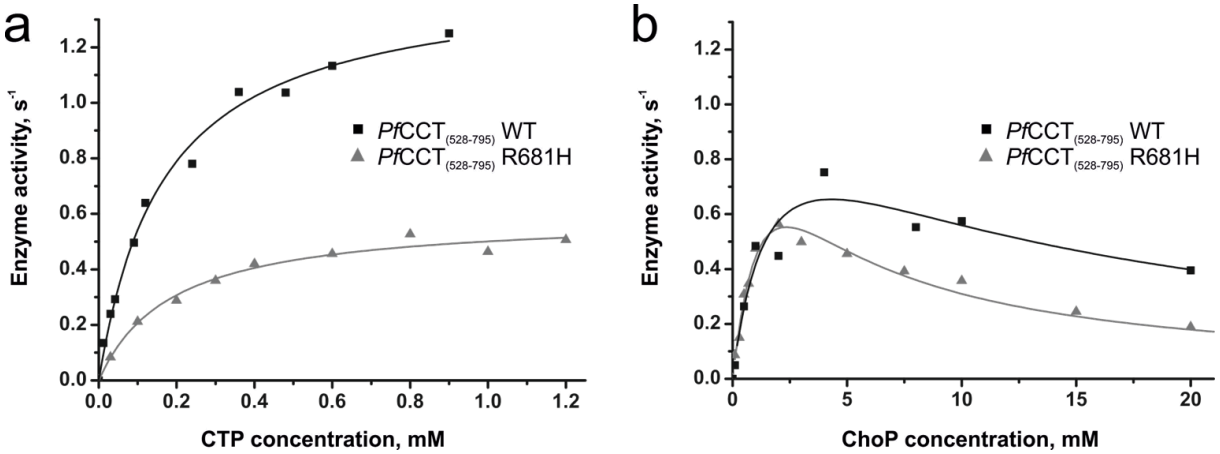

Figure 12. CTP and ChoP titration kinetic analysis of WT and thermosensitive *Pf*CCT constructs at 20°C.

To elucidate the mechanism of temperature-induced inactivation of the endogenous CCT in CHO-MT58, I investigated the thermal stability of cytidylyltransferase activity of *Pf*CCT$_{(528-795)}$ R681H by adopting the experimental method described by Belužić et al.[65]. For assessment of the temperature dependence of protein stability and functionality enzyme samples were incubated at different temperatures form 4°C to 60°C for 15 minutes then their enzyme activity was measured at 20°C. The R681H variant has lost 50% of its activity around 25°C and was completely inactivated at 30°C, while similar thermal inactivation of the wild type enzyme could be observed at 45°C and 55°C, respectively (Figure 13). This marked difference occurred in kinetic stability at the physiological temperature range, which can be paralleled with the temperature sensitivity of the CHO-MT58 cell line.

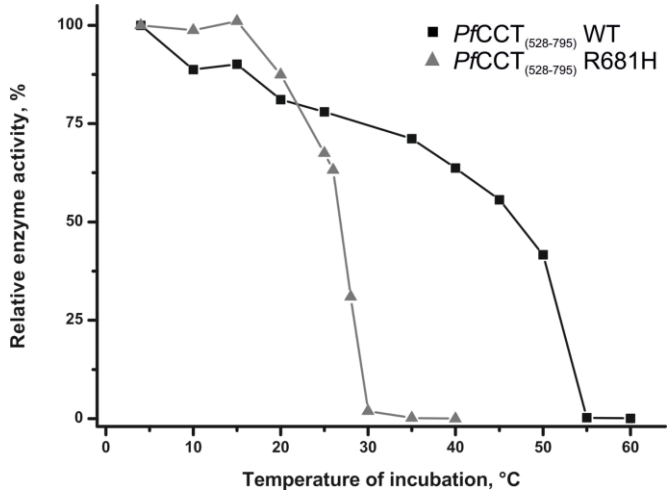

Figure 13. Thermal inactivation analysis of *Pf*CCT$_{(528-795)}$ WT and R681H constructs.

4.2.3. ESI-MS and molecular dynamics analysis of *Pf*CCT$_{(528\text{-}795)}$ R681H

The proposed role of R681 in dimerization and the drastically impaired thermal stability of the R681H enzyme variant (cf. Figure 13) suggested that the mutation might perturb the oligomerization of *Pf*CCT$_{(528\text{-}795)}$ R681H. Potential alterations in dimer formation can be studied by mass spectrometry under native electrospray conditions (ESI-MS), as it was shown to be an appropriate method to study protein oligomerization states (cf. Figure 7 and [66]). In case of *Pf*CCT$_{(528\text{-}795)}$ WT and *Pf*CCT$_{(528\text{-}795)}$ R681H mass spectrometric analysis provided different dimer:monomer abundance ratios reproducible within 20%. While reasonable amount of dimer was present in the wild type enzyme (Figure 14 panel a), dimer:monomer ratios were ca. 20 times lower in case of the mutant enzyme (Figure 14 panel b) indicating a perturbed dimer formation.

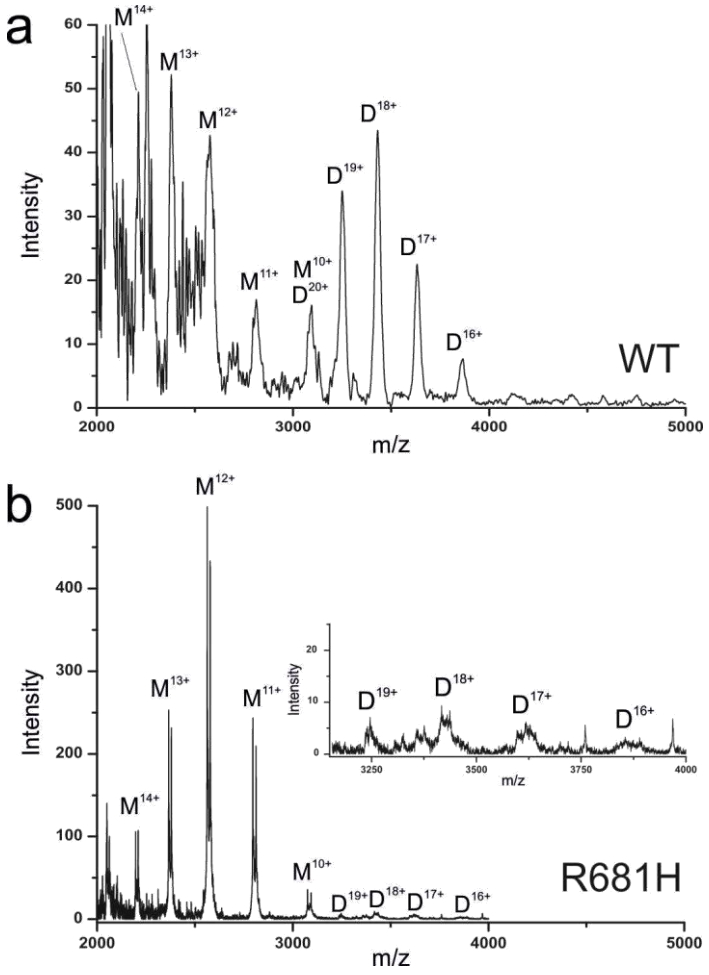

Figure 14. ESI-MS spectra of *Pf*CCT constructs display altered dimerization capacity for *Pf*CCT$_{(528\text{-}795)}$ R681H.

To provide further experimental evidence for the underlying mechanism of the thermosensitivity of *Pf*CCT$_{(528\text{-}795)}$ R681H, molecular dynamics simulations (MD) were performed on the homology models of the WT and mutant enzymes. The effect of the mutation on binding energetics and dimer stability was analysed by productive MD simulations using an implicit solvent model at 310 K for 5 ns. The average inter-chain interaction energy of the mutant enzyme decreased by 25% compared to the WT (Table 6). This is a result of the contribution of multiple energy constituents involving a less favourable solvation energy (ΔG_{solv}^{eq}), smaller contribution of van der Waals-type hydrophobic interactions (E_{vdW}^{eq}) and reduced interacting surface area of the homodimers (A_{int}^{lf}) leading to a loosened overall structure and a less compact volume (V^{lf}) (Table 6).

Table 6. Calculated energetic contributions of inter-chain interactions in case of *Pf*CCT$_{(528\text{-}795)}$ WT and R681H.

	W_{int}^{eq}	ΔG_{solv}^{eq}	E_{vdW}^{eq}	E_{Cou}^{eq}	N_{H-b}^{eq}	V^{lf}	A^{lf}	A_{int}^{lf}
	kcal·mol^{-1}	kcal·mol^{-1}	kcal·mol^{-1}	kcal·mol^{-1}		Å^3	Å^2	Å^2
***Pf*CCT$_{(528\text{-}795)}$ WT**	-2315±266	-2777±275	-188±8	654±54	4.0	61064	17057	1814
***Pf*CCT$_{(528\text{-}795)}$ R681H**	-1729±233	-1973±244	-141±7	383±58	3.0	61428	17339	1383

To illustrate that the impaired interaction of the R681H variant monomers can be observed particularly at the ^{681}RWVD^{684} conserved motif two representative inter-chain distances were followed during the MD simulations. The distance d(R/H681, CA - H679', O) is the shortest inter-monomer distance of the *Pf*CCT homology model as well as the rat CCT structure[18], while d(I680, CA - I680', N) is an atomic distance not directly affected by the mutation, which was chosen as a control (cf. Figure 11). The characteristic deviation of d(R/H681, CA - H679', O) between *Pf*CCT$_{(528\text{-}795)}$ R681H and *Pf*CCT$_{(528\text{-}795)}$ WT argues for severely perturbed local contacts that could contribute to the previously observed reduced dimer interacting surface area in case of the mutant enzyme (Figure 15).

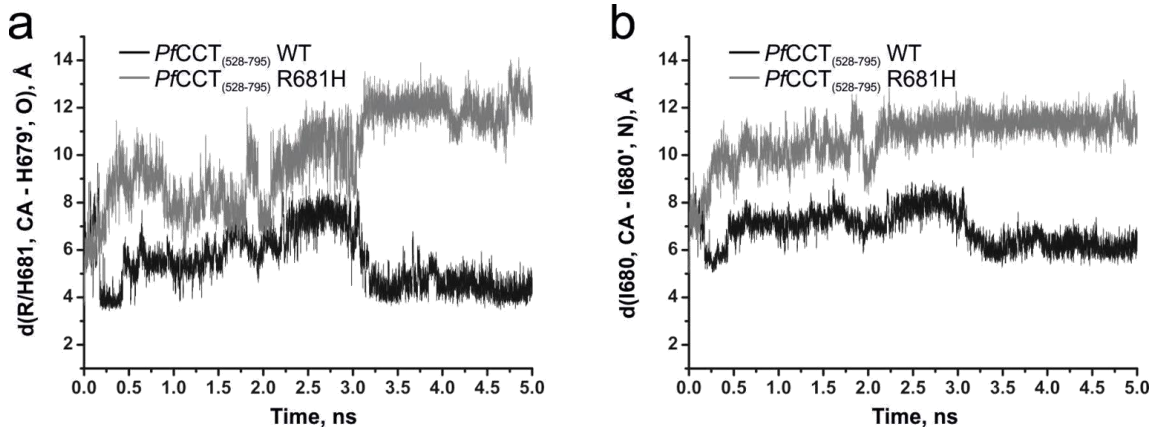

Figure 15. Variation of characteristic inter-chain interaction distances during the course of MD simulations of *Pf*CCT$_{(528\text{-}795)}$ WT and R681H.

In silico results showing perturbed local contacts and reduced inter-subunit interaction energies thus indicate the adverse effect of the arginine histidine exchange on dimer stability. Supposedly, these perturbed inter-domain interactions might affect the overall structural stability of the full length protein as well leading to the observed thermosensitive phenotype of the CHO-MT58 strain.

4.3. Heterologous expression of *Pf*CCT rescues CHO cells deficient in PC biosynthesis Kennedy pathway

4.3.1. Transient transfection studies for analyzing the rescue capabilities of *Pf*CCT in CHO-MT58 cells at the non-permissive temperature

Previously it has been shown that CHO-MT58 cells cultured at 40°C undergo apoptosis due to PC defieciency[38], which was reported to be restored by heterologous expression of *Rn*CCT[36] reducing the onset of apoptosis. My aim was to test whether heterologous expression of CCT from *P. falciparum* can also rescue CHO-MT58 at the non-permissive temperature (40°C) despite the structural and functional differences compared to rat CCT[23,31,32]. First, transient transfection of the full length *Pf*CCT was performed in the not thermosensitive wild type CHO-K1 and the CHO-MT58 cell line harboring a thermolabile endogenous CCT. The culturing temperature (37°C) was shifted to the non-permissive temperature (40°C) 24 hours post-transfection. Apoptosis of non-transfected (control) CHO-MT58 could be observed after 48 hours while CHO-K1 cells proliferated at an accelerated rate, as expected due to shortened doubling times at higher temperature also reported in the literature[67]. After 10 days, differential interference contrast (DIC) images were taken of the cells and GFP fluorescence related to the expression of *Pf*CCT was investigated (Figure 16).

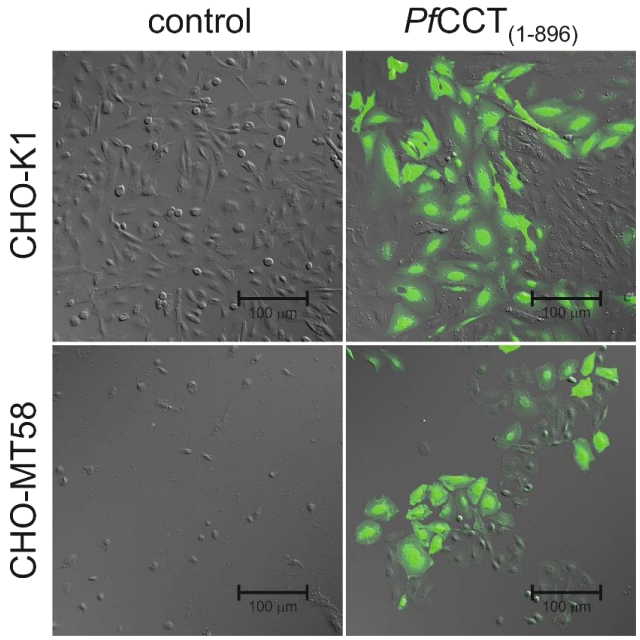

Figure 16. Overexpression of *Pf*CCT$_{(1-896)}$ in CHO cells. DIC and fluorescence images without transfection (left) or after transfection with *Pf*CCT$_{(1-896)}$ and EGFP (right).

Hardly any live non-transfected (control) CHO-MT58 cells were observable, while the WT cell line reached 100% confluency. Heterologous expression of *Pf*CCT$_{(1-896)}$, the full length functional enzyme could rescue CHO-MT58 cells as shown on the lower right panel of Figure 16. In case of CHO-K1 cells expressing and lacking *Pf*CCT both could grow while in CHO-MT58 there was a selective pressure in favor of the full length *Pf*CCT expressing cells.

4.3.2. *In vitro* characterization of an inactive *Pf*CCT mutant

To design a relatively simple model system for testing the efficiency of the rescue appropriate controls are needed. To verify that cytidylyltransferase activity is responsible for the rescue modified *Pf*CCT constructs were chosen as the basis for comparison. For a full length *Pf*CCT construct harboring thermosensitizing point mutations corresponding to the R140H mutation in the endogenous CCT of CHO-MT58[36] the R/H mutation was introduced in both catalytic segments at the positions 96 and 681. *In vitro* characterization of this R/H point mutation in the second catalytic domain construct (*Pf*CCT$_{(528-795)}$ R681H) demonstrated that the function of the protein is not effected although it is thermolabile and its dimer formation ability is heavily impaired (cf. Figure 13 and Figure 14). Another point mutant construct targeting the conserved HxGH motif of the cytidylyltransferase enzyme family was created to gain a presumably catalytically deficient *Pf*CCT[68]. It was shown in case of *Bacillus subtilis* CTP:glycerol-3-phosphate cytidylyltransferase (*Bs*GCT) and *Rn*CCT that the alanine mutagenesis of the first histidine destroyed the activity[69,70]. In *Rn*CCT the substitution of the same histidine (H89) to asparagine had a drastic effect on the catalytic turnover without perturbing CTP substrate binding. To investigate the effect of the mutation H630N corresponding to H89N in *Rn*CCT *in vitro*, the point mutant construct *Pf*CCT$_{(528-795)}$ H630N was generated. Kinetic analysis of the mutant revealed a severe, three orders of magnitude activity decrease (0.002±0.00002 s^{-1}) as compared to the original constitutively active *Pf*CCT$_{(528-795)}$ used as control (1.45±0.05 s^{-1})[43] (Figure 17 panel a). Remarkably, the increased $K_{M,CTP}$ of *Pf*CCT$_{(528-795)}$ H630N (1.28±0.04 mM, cf. 0.17±0.02 mM in case of the wild type enzyme) further contributed to the pronounced loss in the catalytic efficiency ($k_{cat}/K_{M,CTP}$) (Figure 17 panel b). Thus, it is apparent that the asparagine replacement of the first histidine in HxGH signature sequence in both catalytic domains at positions H45 and H630 will yield a catalytically deficient form of *Pf*CCT that corresponds to an inactive enzyme phenotype.

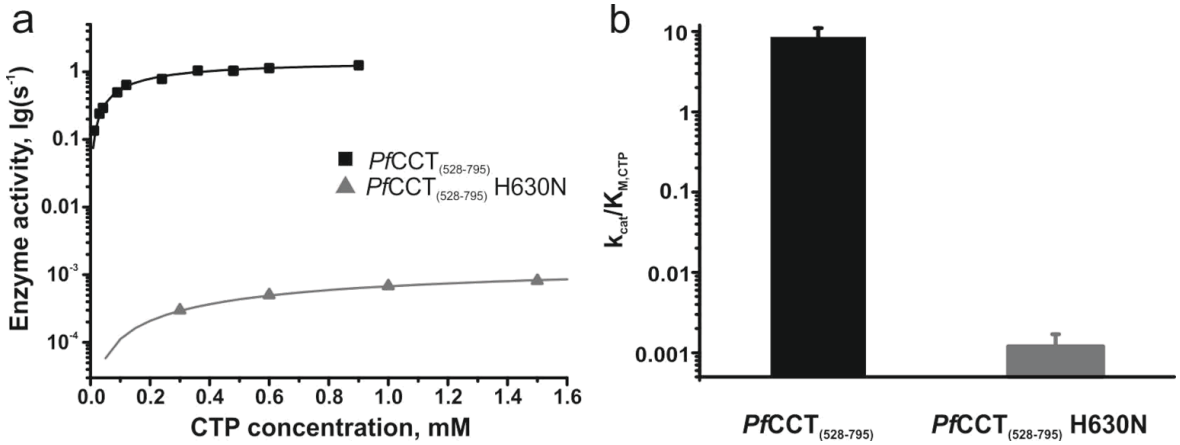

Figure 17. Kinetic analysis *Pf*CCT catalytic domain constructs. Data is fitted with the Michaelis-Menten kinetic model assuming no cooperativity. Note the logarithmic scale representation of the enzyme activity (panel a) and catalytic efficiency (panel b). Error bars represent standard deviation from regression analysis.

4.3.3. Analysis of *Pf*CCT rescue potential in CHO cells

For the quantitative characterization of the rescue potential of *Pf*CCT in the mammalian cell line CHO-MT58 I aimed to design a well applicable test system. Fluorescence activated cell corting (FACS) is a suitable technique for the characterization of heterogenous cell populations based on differences in the fluorescence as well as cell size and volume of cell subpopulations. The full length *Pf*CCT$_{(1\text{-}896)}$ and both controls (the inactive *Pf*CCT$_{(1\text{-}896)}$ H45N H630N and the thermosensitive *Pf*CCT$_{(1\text{-}896)}$ R96H R681H) were all transiently transfected and heterologously expressed in CHO-K1 and CHO-MT58 cell lines using an internal ribosomal entry site (IRES) system to ensure the co-expression of EGFP and the *Pf*CCT excluding any disturbing effect of the fusion. Transiently transfected cells were incubated at the permissive temperature (37°C) for 24 h then the culturing temperature was shifted to 40°C. Samples were prepared for FACS analysis 72 h post-transfection. The rescue potential of the different *Pf*CCT constructs was calculated based on the proportion of propidium iodide (PI) negative i.e. live cells referred to the corresponding control experiments.

$$Rescue\ potential\ (\%): \frac{live}{all}\%\ of\ control = \frac{[(all - PI\ positive)/all]\ at\ 40°C}{[(all - PI\ positive)/all]\ at\ 37°C} \cdot 100$$

As reported by the results, transfection of the inactive *Pf*CCT construct (*Pf*CCT$_{(1\text{-}896)}$ H45N H630N) provided only 1.6% rescue potential to CHO-MT58 cells. A somewhat higher percentage of cells (4.7%) was rescued by the transfection of the

thermosensitive *Pf*CCT$_{(1-896)}$ R98H R681H while 13.6% of cells expressing the fully functional *Pf*CCT$_{(1-896)}$ were able to escape apoptosis (Table 7, Figure 18). Although the percentage of rescued cells is compromised due to low transfection efficiency (typically 5-15%), the almost 9-fold increase in the rescue potential is remarkable and demonstrates that catalytically functional and structurally intact form of the additional *Pf*CCT is required to rescue CHO-MT58 cells lacking a functional endogenous CCT at 40°C.

Table 7. Effect of *Pf*CCT variant overexpression on live cell fraction and rescue potential. Live fraction of cells was detected based on PI staining and intact cell detection.

	CHO-MT58			CHO-K1		
***Pf*CCT**	**inactive**	**thermo-sensitive**	**WT**	**inactive**	**thermo-sensitive**	**WT**
Live cell fraction (%) at 37°C	76.0	69.5	68.5	73.0	74.0	77.6
Live cell fraction (%) at 40°C	1.2	3.3	9.3	56.0	58.0	56.0
Rescue potential (%)	1.6	4.7	13.6	76.7	78.4	72.2

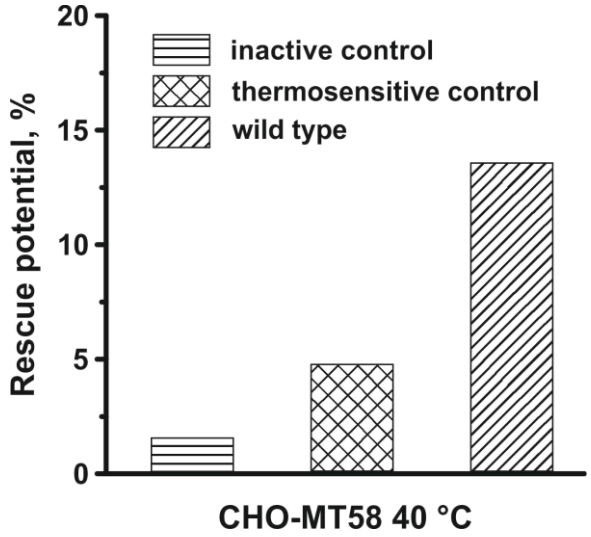

Figure 18. Rescue potential of different *Pf*CCT constructs in CHO-MT58 cells at 40°C. The inactive and thermosensitive controls are the *Pf*CCT$_{(1-896)}$ H45N H630N and *Pf*CCT$_{(1-896)}$ R98H R681H double point mutant constructs of the full length *Pf*CCT enzyme, respectively.

5. DISCUSSION

*Pf*CCT as the rate-limiting enzyme of the validated antimalarial target PC biosynthesis pathway is subjected to several *in vitro* studies[30,32,43,71,72]. Kinetic and ligand binding characterization performed here uncover novel insights into the involvement of key active site residues in CCT mechanism of action. The present study showed that during the CCT catalytic mechanism enzymatic function at the choline binding site is governed by a combination of cation-π and charged interactions forming a composite aromatic box. Generally, structural solutions for binding of quaternary ammonium ligands in proteins might be accomplished to a hydrophobic pocket instead of to an anionic site, as suggested first in 1990[73]. In acetylcholinesterases, it was shown that aromatic rings facing the positively charged quaternary ammonium moiety of acetylcholine can provide a suitable environment by means of cation-π interactions[74]. The energetic contribution of such an interaction to ligand binding was shown to be comparable to that of an H–bond or an ion-pair[75]. The acetylcholinesterase active site also contains dominant charged residues binding to the choline moiety, similarly to that of CCT. However, in many examples, the quaternary ammonium ion is recognized by the so called aromatic box, where three or four aromatic rings are positioned to face the bound charged moiety of the ligand and thus provide an ideal geometric fit[76]. The additive interactions from multiple aromatic rings ensure exceptionally strong ligand binding due to the chelate or multivalence effect[77]. Importantly, in an aromatic box, charged residues provide less pronounced, if any, binding contribution to the ligand. By contrast in composite aromatic boxes besides cation-π interactions provided by aromatic rings electrostatic or charged interactions have also a prominent role in ligand binding and catalysis. The dissimilar behavior of the point mutant catalytic domain constructs proves the different aromatic or electrostatic character of the active site residue interactions. A decisive role of the residue W692 was found as exchanging this residue to alanine lead to a disruptive effect on CCT catalytic efficiency that appears comparable to that of the alanine mutagenesis of strictly conserved histidines within the CCT signature motif HxGH[70]. The 3D structural model of the *Pf*CCT catalytic domain in complex with CDPCho provides a plausible explanation for the critical importance of W692 as this residue has central role in maintaining local structural integrity. Involved in a π-π interaction with F662 and coordinating N716 residue, W692 holds together three structural elements that participate in assembly of the choline binding cavity (Figure 6).

Upon investigation of the molecular mechanism underlying the thermosensitive phenotype of CHO-MT58 I found that formation of an intact dimer is essential for the enzymatic function of *Pf*CCT. This finding is in good agreement with the preferential dimer assembly of the evolutionarily related cytidylyltransferases involving CCT, GCT and CTP:ethanolamine phosphate cytidylyltransferase (ECT). This is underlined by a gene disruption experiment affecting *Plasmodium berghei cct* gene where remnant *P. berghei* CCT truncated part comprising only the first catalytic domain could not restore the function of the wild type enzyme[7]. This effect may be attributed to the disruption of the dimer interaction surface. Biochemical and structural analyses of *Bs*GCT and *Rn*CCT showed homodimer formation[18,27,62] for these structurally related cytidylyltransferases possessing only a single CT domain. The equivalent of the herein studied RYVD motif is a generally occurring signature sequence in cytidylyltransferases[69,70] found at dimer interface of crystal structures of *Rn*CCT (PDB ID: 3HL4), *Bs*GCT (PDB ID: 1COZ) and the human ECT (PDB ID: 3ELB)[18,62]. The role of the conserved arginine at the first position of this motif was also investigated in case of *Bs*GCT. The alanine mutation of the corresponding R63 residue decreased the enzymatic activity by 10-fold, while $K_{M,CTP}$ was not altered considerably[69]. Based on my experiments and the results described in the literature it is suggested that this conserved residue does not interfere with substrate binding. A recently identified splice variant of the murine ECT (Pcyt2γ) lacking the C-terminal CT domain and being completely inactive indicated also that both cytidylyltransferase domains are required for activity[78]. It is also not without precedent that a single point mutation has great impact on structural stability as e.g. an arginine to histidine exchange in crystallins was shown to be responsible for congenital cataract due to disrupted interactions at the inter-subunit interface[79].

While the most reliable description of protein function can be derived from studies of the entire protein so far it was challenging to investigate the full length *Pf*CCT due to its structural and functional differences compared to *Rn*CCT[23,31,32]. Noteworthy, to my best knowledge this is the first time that functional investigation of the full length *Pf*$CCT_{(1\text{-}896)}$ (PF3D7_1316600) subjected to domain duplication[43] is presented. It is demonstrated here that the heterologous expression of the full length *Pf*CCT can prevent apoptosis of CHO-MT58 cells under non-permissive hyperthermic conditions (40°C). I verified that the enzymatic activity of *Pf*CCT is

responsible for this effect as transfection with cDNA of the catalytically deficient *Pf*CCT H45N, H630N mutant yielded considerably lower population of live cells at 40°C than the wild type *Pf*CCT. After evidencing the rescue potential of *Pf*CCT, the possibility to establish a well applicable test system using the isogenic CHO-K1 and CHO-MT58 cell lines was analyzed. CHO cell lines have rapid doubling times and are also resilient to manipulation therefore they are compatible with large-scale studies[80]. Understanding the mechanism underlying the apoptosis induction and the detailed consequences of temperature-induced CCT decay is a necessary pre-requisite for further harnessing this system as a model platform.

Apoptosis due to PC deficiency is known to occur through the unfolded protein response (UPR) pathways[41,42] (Figure 19). Beyond the classical endoplasmic reticulum UPR (UPR^{ER}), a compartment-specific mitochondrial UPR (UPR^{mito}) is also responsible for cellular proteostasis[81]. In CHO-MT58 cells decreased PC levels upregulate both UPR pathways with a significant contribution of UPR^{mito} [82]. PC depletion activates the different branches of UPR by an indirect perturbation of protein-folding environment and of Ca^{2+} homeostasis. Trans-membrane regions of UPR sensor proteins additionally contribute to the proteostasis-independent upregulation of signaling by sensing biophysical properties of membranes[83]. Moderate stress initiates *inter alia* ER biogenesis *via* upregulation of lipid biosynthetic enzymes and ER associated degradation of mis- or unfolded proteins (adaptive response)[84]. As in CCT deficient CHO-MT58 cells misfolded dysfunctional CCT is expressed with an accelerated rate[36], upregulation of lipid biosynthesis and adaptation are rendered futile. Thus the stress prevails and cells enter the apoptosis phase. Increased levels of CCAAT/enhancer-binding protein-homologous protein (CHOP), also known as growth arrest and DNA damage-inducible protein 153 together with caspases are hallmarks for this phase in apoptotic CHO-MT58 cells[41,42]. Importantly, the primary ER and redox stress effects can be relieved by the heterologous expression of a functional CCT within ~30 hours when cells have not yet entered the early apoptotic phase. A transient transfection event within this period thus is expected to effectively revert the conditional CCT-knockout by efficiently restoring the phospholipid depletion and the ratio of cholesterol/phospholipid.

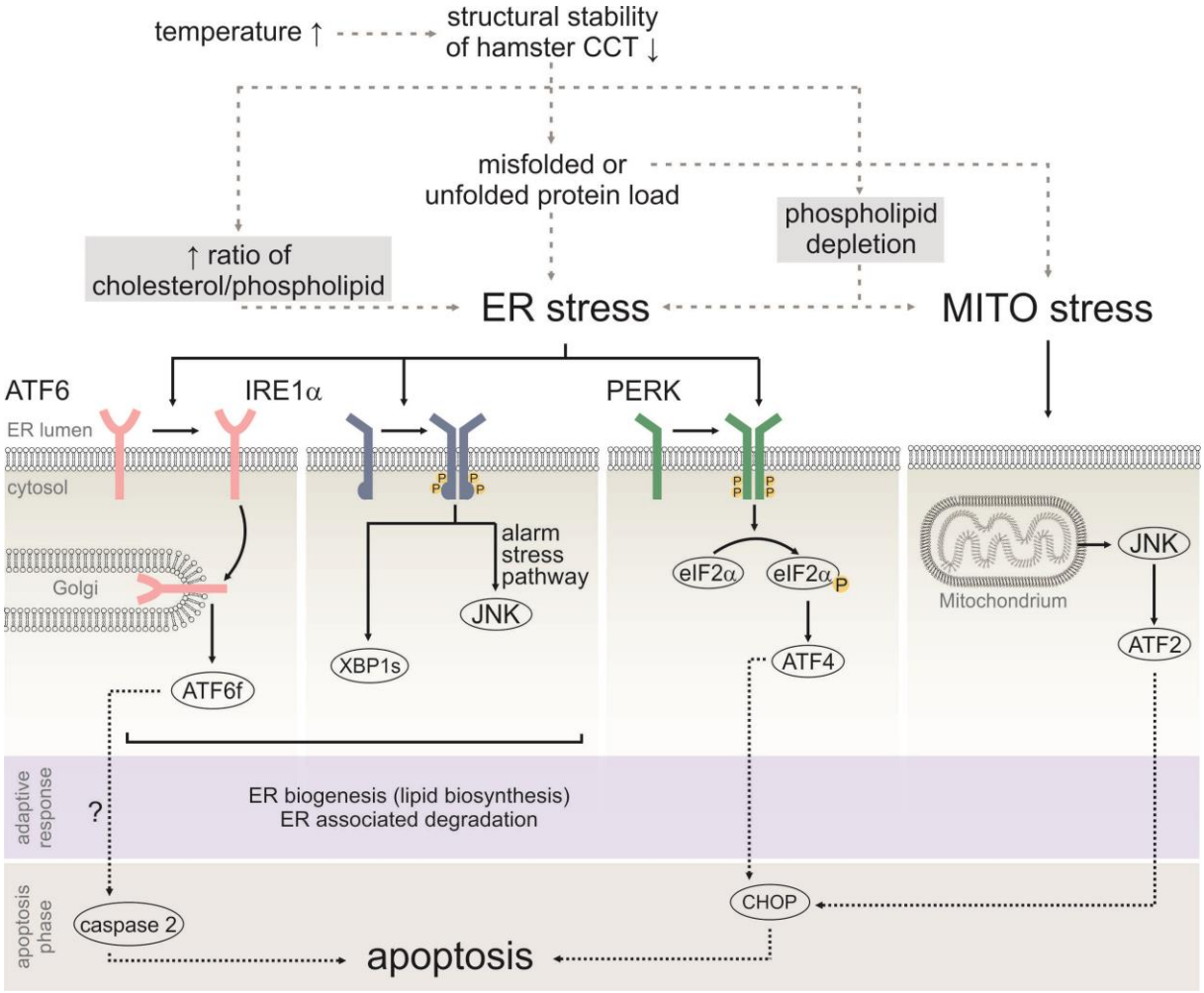

Figure 19. Downstream effects of CCT decay at the non-permissive temperature in CHO-MT58. At elevated temperatures (40°C) the structural stability of hamster CCT in CHO-MT58 decreases causing a massive misfolded protein load and phospholipid depletion simultaneously. This leads to ER and mitochondrial stress and activates the different branches of UPR^{ER} and UPR^{mito}. Activating transcription factor 6 (ATF6), inositol-requiring protein 1 (IRE1) and protein kinase RNA-like ER kinase (PERK) initiates an adaptive response including ER biogenesis and ER associated degradation. The excessive phospholipid depletion subsequently triggers apoptotic pathways through the activation of caspases, kinases, transcription factors and CHOP. Initiating factors with grey background can be reverted by heterologous expression of a functional CCT.

Considering the devastating effect of the absence of a functional CCT on several organisms and cell lines, the herein discussed inducible CCT deficient cell-based assay is an advantageous approach for studying CCT functionality with the conditional exclusion of the endogenous background compared to implementing knock-out of endogenous enzymes in the reporter cell line by recently emerged genome-editing techniques, such as CRISPR-Cas9, TALEN and

ZFN[85,86]. Further improvement and standardization of the methodology is also necessary e.g. to achieve higher transfection efficiencies. Nevertheless, our experimental data indicate that the herein described *in vitro* cell line model together with the redesigned modular *Pf*CCT cDNA presents a promising basis to establish a cell-based system for the functional analysis of *Pf*CCT. Moreover, as structural differences between the mammalian and protist CCT orthologs could enable development of *Plasmodium falciparum* specific CCT inhibitors, a cell-based test system with built-in comparison with the human CCT would not only be advantageous for structure-function studies but this model system may additionally be applied to screen effectiveness and toxicity of antimalarial therapeutic agents that target CCT within the PL biosynthesis pathway (Figure 20).

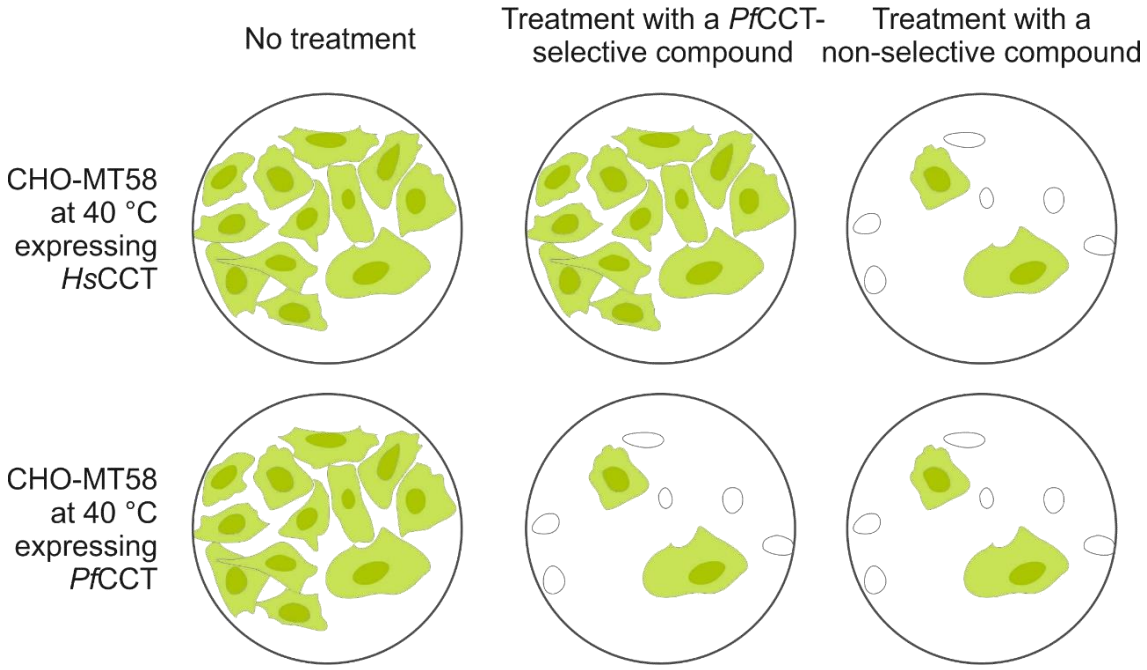

Figure 20. Principle of a proposed high-throughput screening system set up to assess the effectiveness and toxicity of antimalarial compounds targeting *Pf*CCT.

6. CONCLUSION

Conclusions drawn from the presented results provide specific replies to the questions asked in the Aims section. Below I summarize these results:

1. What is the role of residues constituting the choline binding site of *Pf*CCT in ligand binding and catalysis?

   Active site interactors identified based on the homology model of the CDPCho complexed *Pf*CCT$_{(528\text{-}795)}$ can be classified based on the nature of the interaction. D623 and Y741 provide charged interactions to the quaternary ammonium moiety of CDPCho which have decisive role in catalysis. The partial conservation of the aromatic character of cation-π interactors W692 and Y714 is more compatible with ligand binding and catalysis, while W692 has also a significant role in the structural stability of the active site.
2. What is the exact molecular mechanism underlying the thermal instability of CCT from the thermosensitive CHO-MT58 cell line?

   The R681H mutation of the conserved motif RWVD in *P. falciparum* does not directly compromise the enzyme activity. Instead, it induces reduced thermal stability which in turn leads to the inactivation of the enzyme. *In vitro* and *in silico* results together show attenuation of dimer interactions induced by the mutation, thus maintaining intact dimer interactions is critical for enzymatic activity of *Pf*CCT.
3. Can the heterologous expression of *Pf*CCT rescue the mammalian CHO-MT58 cell line at the non-permissive temperature?

   I demonstrated that the heterologous expression of *Pf*CCT can decrease the onset of apoptosis in CHO-MT58 at 40°C. The importance of the functionality of the expressed enzyme is verified by the lack of rescue of cells transfected with an inactive *Pf*CCT.
4. How can a well applicable test system be established for studying the structural differences of *Pf*CCT and mammalian orthologues in a cellular environment?

   By FACS analysis of the cells transfected with different *Pf*CCT constructs, a rescue potential can be defined as a quantitative measure of the functionality of the enzyme. Thus working with truncated and point mutant *Pf*CCT constructs the role of the different elements in functionality can be assessed. The designed test system can also be applied to study the selectivity of potential antimalarials targeting CCT.

ACKNOWLEDGEMENT

Firstly, I would like to express my sincere gratitude to my supervisor Beáta G. Vértessy for the continuous support of my PhD study and related research, for her patience, motivation, and immense knowledge. Her guidance helped me in research and writing.

Besides my advisor, I would like to thank László Buday, György Keserű, and György Pokol, who provided me the opportunity to join the Institute of Enzymology in the Research Centre for Natural Sciences Hungarian Academy of Sciences, and who gave access to the laboratory and research facilities. I also owe gratitude to László Dux the chair of the Doctoral School of Multidisciplinary Medical Science at the Faculty of Medicine University of Szeged. Without they precious support it would not be possible to conduct my research and doctoral studies.

I thank my fellow labmates for the stimulating discussions, for their sleepless interest, and for all the fun we have had in the last years. Also I thank my colleagues Olivér Ozohanics, Károly Vékey, Anikó Lábas, Balázs Krámos, Julianna Oláh, Nóra Kucsma and Gergely Szakács for their contribution to my research. In particular, I am grateful to Gergely Nagy, Fanni Hajdú and all of the members of the CCT group for the close and friendly cooperation.

Last but not the least, I would like to thank my family: my husband Sanyi, my parents and my sister for supporting me in following my dreams and throughout writing this thesis.

REFERENCES

1. WHO. *World Malaria Report 2016*. (World Health Organization, 2016).
2. Mordmüller, B. *et al.* Sterile protection against human malaria by chemoattenuated PfSPZ vaccine. *Nature* **542,** 445–449 (2017).
3. Enjalbal, C. *et al.* Automated monitoring of phosphatidylcholine biosyntheses in Plasmodium falciparum by electrospray ionization mass spectrometry through stable isotope labeling experiments. *Anal. Chem.* **76,** 4515–21 (2004).
4. Klein, E. Y. Antimalarial drug resistance: a review of the biology and strategies to delay emergence and spread. *Int. J. Antimicrob. Agents* **41,** 311–7 (2013).
5. Cowman, A. F., Healer, J., Marapana, D. & Marsh, K. Malaria: Biology and Disease. *Cell* **167,** 610–624 (2016).
6. Vial, H. J., Ancelin, M. L., Philippot, J. R. & Thuet, M. J. Biosynthesis and dynamics of lipids in Plasmodium-infected mature mammalian erythrocytes. *Blood Cells* **16,** 531-55-61 (1990).
7. Déchamps, S., Shastri, S., Wengelnik, K. & Vial, H. J. Glycerophospholipid acquisition in Plasmodium - a puzzling assembly of biosynthetic pathways. *Int. J. Parasitol.* **40,** 1347–65 (2010).
8. Sen, P., Vial, H. J. & Radulescu, O. Kinetic modelling of phospholipid synthesis in Plasmodium knowlesi unravels crucial steps and relative importance of multiple pathways. *BMC Syst. Biol.* **7,** 123 (2013).
9. Wengelnik, K. *et al.* A class of potent antimalarials and their specific accumulation in infected erythrocytes. *Science* **295,** 1311–4 (2002).
10. Wein, S. *et al.* Transport and pharmacodynamics of albitiazolium, an antimalarial drug candidate. *Br. J. Pharmacol.* **166,** 2263–76 (2012).
11. Peyrottes, S., Caldarelli, S., Wein, S., Perigaud, C. & Vial, H. Exploring prodrug approaches for albitiazolium and its analogues. *Curr. Top. Med. Chem.* **14,** 1653–67 (2014).
12. Held, J. *et al.* Safety and efficacy of the choline analogue SAR97276 for malaria treatment: results of two phase 2, open-label, multicenter trials in African patients. *Malar. J.* **16,** 188 (2017).
13. González-Bulnes, P. *et al.* PG12, a phospholipid analog with potent antimalarial activity, inhibits Plasmodium falciparum CTP:phosphocholine cytidylyltransferase activity. *J. Biol. Chem.* **286,** 28940–7 (2011).
14. Li, Z. & Vance, D. E. Phosphatidylcholine and choline homeostasis. *J. Lipid Res.* **49,** 1187–94 (2008).
15. Aravind, L., Anantharaman, V. & Koonin, E. V. Monophyly of class I aminoacyl tRNA synthetase, USPA, ETFP, photolyase, and PP-ATPase nucleotide-binding domains: implications for protein evolution in the RNA. *Proteins* **48,** 1–14 (2002).

16. Friesen, J., Campbell, H. & Kent, C. Enzymatic and cellular characterization of a catalytic fragment of CTP:phosphocholine cytidylyltransferase alpha. *J. Biol. Chem.* **274,** 13384–9 (1999).

17. Xie, M., Smith, J. L., Ding, Z., Zhang, D. & Cornell, R. B. Membrane binding modulates the quaternary structure of CTP:phosphocholine cytidylyltransferase. *J. Biol. Chem.* **279,** 28817–25 (2004).

18. Lee, J., Johnson, J., Ding, Z., Paetzel, M. & Cornell, R. B. Crystal structure of a mammalian CTP: phosphocholine cytidylyltransferase catalytic domain reveals novel active site residues within a highly conserved nucleotidyltransferase fold. *J. Biol. Chem.* **284,** 33535–48 (2009).

19. Sarri, E., Sicart, A., Lázaro-Diéguez, F. & Egea, G. Phospholipid synthesis participates in the regulation of diacylglycerol required for membrane trafficking at the Golgi complex. *J. Biol. Chem.* **286,** 28632–43 (2011).

20. Krahmer, N. *et al.* Phosphatidylcholine synthesis for lipid droplet expansion is mediated by localized activation of CTP:phosphocholine cytidylyltransferase. *Cell Metab.* **14,** 504–15 (2011).

21. Cole, L. K., Vance, J. E. & Vance, D. E. Phosphatidylcholine biosynthesis and lipoprotein metabolism. *Biochim. Biophys. Acta* **1821,** 754–61 (2012).

22. Tian, Y., Zhou, R., Rehg, J. E. & Jackowski, S. Role of phosphocholine cytidylyltransferase alpha in lung development. *Mol. Cell. Biol.* **27,** 975–82 (2007).

23. Ding, Z. *et al.* A 22-mer segment in the structurally pliable regulatory domain of metazoan CTP: phosphocholine cytidylyltransferase facilitates both silencing and activating functions. *J. Biol. Chem.* **287,** 38980–91 (2012).

24. Huang, H. K. *et al.* The membrane-binding domain of an amphitropic enzyme suppresses catalysis by contact with an amphipathic helix flanking its active site. *J. Mol. Biol.* **425,** 1546–64 (2013).

25. Lee, J., Taneva, S. G., Holland, B. W., Tieleman, D. P. & Cornell, R. B. Structural basis for autoinhibition of CTP:phosphocholine cytidylyltransferase (CCT), the regulatory enzyme in phosphatidylcholine synthesis, by its membrane-binding amphipathic helix. *J. Biol. Chem.* **289,** 1742–55 (2014).

26. Yang, W., Boggs, K. P. & Jackowski, S. The association of lipid activators with the amphipathic helical domain of CTP:phosphocholine cytidylyltransferase accelerates catalysis by increasing the affinity of the enzyme for CTP. *J. Biol. Chem.* **270,** 23951–7 (1995).

27. Taneva, S., Dennis, M. K., Ding, Z., Smith, J. L. & Cornell, R. B. Contribution of each membrane binding domain of the CTP:phosphocholine cytidylyltransferase-alpha dimer to its activation, membrane binding, and membrane cross-bridging. *J. Biol. Chem.* **283,** 28137–48 (2008).

28. Dennis, M. K., Taneva, S. G. & Cornell, R. B. The intrinsically disordered nuclear localization signal and phosphorylation segments distinguish the membrane affinity of

two cytidylyltransferase isoforms. *J. Biol. Chem.* **286,** 12349–60 (2011).

29. Chichili, V. P. R., Kumar, V. & Sivaraman, J. A method to trap transient and weak interacting protein complexes for structural studies. *Intrinsically Disord. proteins* **1,** e25464 (2013)

30. Contet, A. *et al.* Plasmodium falciparum CTP:phosphocholine cytidylyltransferase possesses two functional catalytic domains and is inhibited by a CDP-choline analog selected from a virtual screening. *FEBS Lett.* **589,** 992–1000 (2015).

31. Yeo, H. J., Larvor, M. P., Ancelin, M. L. & Vial, H. J. Plasmodium falciparum CTP:phosphocholine cytidylyltransferase expressed in Escherichia coli: purification, characterization and lipid regulation. *Biochem. J.* **324 (Pt 3,** 903–10 (1997).

32. Larvor, M. *et al.* Characterization of the lipid-binding domain of the Plasmodium falciparum CTP:phosphocholine cytidylyltransferase through synthetic-peptide studies. *Biochem. J.* **375,** 653–61 (2003).

33. Gehrig, K., Morton, C. C. & Ridgway, N. D. Nuclear export of the rate-limiting enzyme in phosphatidylcholine synthesis is mediated by its membrane binding domain. *J. Lipid Res.* **50,** 966–76 (2009).

34. Esko, J. D. & Raetz, C. R. Autoradiographic detection of animal cell membrane mutants altered in phosphatidylcholine synthesis. *Proc. Natl. Acad. Sci. U. S. A.* **77,** 5192–6 (1980).

35. Esko, J. D., Wermuth, M. M. & Raetz, C. R. Thermolabile CDP-choline synthetase in an animal cell mutant defective in lecithin formation. *J. Biol. Chem.* **256,** 7388–93 (1981).

36. Sweitzer, T. D. & Kent, C. Expression of wild-type and mutant rat liver CTP: phosphocholine cytidylyltransferase in a cytidylyltransferase-deficient Chinese hamster ovary cell line. *Arch. Biochem. Biophys.* **311,** 107–16 (1994).

37. Testerink, N., van der Sanden, M. H. M., Houweling, M., Helms, J. B. & Vaandrager, A. B. Depletion of phosphatidylcholine affects endoplasmic reticulum morphology and protein traffic at the Golgi complex. *J. Lipid Res.* **50,** 2182–92 (2009).

38. Cui, Z. *et al.* A genetic defect in phosphatidylcholine biosynthesis triggers apoptosis in Chinese hamster ovary cells. *J. Biol. Chem.* **271,** 14668–71 (1996).

39. Niebergall, L. J. & Vance, D. E. The ratio of phosphatidylcholine to phosphatidylethanolamine does not predict integrity of growing MT58 Chinese hamster ovary cells. *Biochim. Biophys. Acta* **1821,** 324–34 (2012).

40. Morton, C. C., Aitchison, A. J., Gehrig, K. & Ridgway, N. D. A mechanism for suppression of the CDP-choline pathway during apoptosis. *J. Lipid Res.* **54,** 3373–84 (2013).

41. van der Sanden, M. H. M., Houweling, M., van Golde, L. M. G. & Vaandrager, A. B. Inhibition of phosphatidylcholine synthesis induces expression of the endoplasmic reticulum stress and apoptosis-related protein CCAAT/enhancer-binding protein-

homologous protein (CHOP/GADD153). *Biochem. J.* **369,** 643–50 (2003).

42. Van Der Sanden, M. H. M., Meems, H., Houweling, M., Helms, J. B. & Vaandrager, A. B. Induction of CCAAT/enhancer-binding protein (C/EBP)-homologous protein/growth arrest and DNA damage-inducible protein 153 expression during inhibition of phosphatidylcholine synthesis is mediated via activation of a C/EBP-activating transcription factor-r. *J. Biol. Chem.* **279,** 52007–52015 (2004).

43. Nagy, G. N. *et al.* Evolutionary and mechanistic insights into substrate and product accommodation of CTP:phosphocholine cytidylyltransferase from Plasmodium falciparum. *FEBS J.* **280,** 3132–48 (2013).

44. Dosztányi, Z., Csizmok, V., Tompa, P. & Simon, I. IUPred: web server for the prediction of intrinsically unstructured regions of proteins based on estimated energy content. *Bioinformatics* **21,** 3433–4 (2005).

45. Artimo, P. *et al.* ExPASy: SIB bioinformatics resource portal. *Nucleic Acids Res.* **40,** W597-603 (2012).

46. SIAS: Sequence Identity and Similarity. (2008). at <http://imed.med.ucm.es/Tools/sias.html>

47. Eswar, N. *et al.* Comparative protein structure modeling using Modeller. *Curr. Protoc. Bioinforma.* **Chapter 5,** Unit 5.6 (2006).

48. Humphrey, W., Dalke, A. & Schulten, K. VMD: visual molecular dynamics. *J. Mol. Graph.* **14,** 33–8, 27–8 (1996).

49. Laskowski, R. A., Rullmannn, J. A., MacArthur, M. W., Kaptein, R. & Thornton, J. M. AQUA and PROCHECK-NMR: programs for checking the quality of protein structures solved by NMR. *J. Biomol. NMR* **8,** 477–86 (1996).

50. Colovos, C. & Yeates, T. O. Verification of protein structures: patterns of nonbonded atomic interactions. *Protein Sci.* **2,** 1511–9 (1993).

51. Anandakrishnan, R., Aguilar, B. & Onufriev, A. V. H++ 3.0: automating pK prediction and the preparation of biomolecular structures for atomistic molecular modeling and simulations. *Nucleic Acids Res.* **40,** W537-41 (2012).

52. Olsson, M. H. M., Søndergaard, C. R., Rostkowski, M. & Jensen, J. H. PROPKA3 : Consistent Treatment of Internal and Surface Residues in Empirical p K a Predictions. *J. Chem. Theory Comput.* **7,** 525–537 (2011).

53. Brooks, B. R. *et al.* CHARMM: the biomolecular simulation program. *J. Comput. Chem.* **30,** 1545–614 (2009).

54. MacKerell, A. D., Banavali, N. & Foloppe, N. Development and current status of the CHARMM force field for nucleic acids. *Biopolymers* **56,** 257–65 (2001).

55. Im, W., Lee, M. S. & Brooks, C. L. Generalized born model with a simple smoothing function. *J. Comput. Chem.* **24,** 1691–702 (2003).

56. Nina, M., Beglov, D. & Roux, B. Atomic Radii for Continuum Electrostatics

Calculations Based on Molecular Dynamics Free Energy Simulations. *J. Phys. Chem. B* **101,** 5239–5248 (1997).

57. Chen, J., Im, W. & Brooks, C. L. Balancing solvation and intramolecular interactions: toward a consistent generalized Born force field. *J. Am. Chem. Soc.* **128,** 3728–36 (2006).

58. Lazaridis, T. & Karplus, M. Effective Energy Function for Proteins in Solution. *Proteins* **35,** 133–52 (1999).

59. Voss, N. R. & Gerstein, M. 3V: cavity, channel and cleft volume calculator and extractor. *Nucleic Acids Res.* **38,** W555-62 (2010).

60. Mecozzi, S., West, A. P. & Dougherty, D. A. Cation-pi interactions in aromatics of biological and medicinal interest: electrostatic potential surfaces as a useful qualitative guide. *Proc. Natl. Acad. Sci. U. S. A.* **93,** 10566–71 (1996).

61. Plewniak, F. PipeAlign: a new toolkit for protein family analysis. *Nucleic Acids Res.* **31,** 3829–3832 (2003).

62. Weber, C. H., Park, Y. S., Sanker, S., Kent, C. & Ludwig, M. L. A prototypical cytidylyltransferase: CTP:glycerol-3-phosphate cytidylyltransferase from bacillus subtilis. *Structure* **7,** 1113–24 (1999).

63. Payne, F. *et al.* Mutations disrupting the Kennedy phosphatidylcholine pathway in humans with congenital lipodystrophy and fatty liver disease. *Proc. Natl. Acad. Sci. U. S. A.* **111,** 8901–6 (2014).

64. Takács, E., Grolmusz, V. K. & Vértessy, B. G. A tradeoff between protein stability and conformational mobility in homotrimeric dUTPases. *FEBS Lett.* **566,** 48–54 (2004).

65. Beluzić, R. *et al.* A single mutation at Tyr143 of human S-adenosylhomocysteine hydrolase renders the enzyme thermosensitive and affects the oxidation state of bound cofactor nicotinamide-adenine dinucleotide. *Biochem. J.* **400,** 245–53 (2006).

66. Loo, J. A. Electrospray ionization mass spectrometry: a technology for studying noncovalent macromolecular complexes. *Int. J. Mass Spectrom.* **200,** 175–186 (2000).

67. Esko, J. D., Nishijima, M. & Raetz, C. R. Animal cells dependent on exogenous phosphatidylcholine for membrane biogenesis. *Proc. Natl. Acad. Sci. U. S. A.* **79,** 1698–702 (1982).

68. Cornell, R. B. Membrane lipid compositional sensing by the inducible amphipathic helix of CCT. *Biochim. Biophys. Acta* **1861,** 847–61 (2016).

69. Park, Y. S. *et al.* Identification of functional conserved residues of CTP:glycerol-3-phosphate cytidylyltransferase. Role of histidines in the conserved HXGH in catalysis. *J. Biol. Chem.* **272,** 15161–6 (1997).

70. Veitch, D. P., Gilham, D. & Cornell, R. B. The role of histidine residues in the HXGH site of CTP:phosphocholine cytidylyltransferase in CTP binding and catalysis. *Eur. J. Biochem.* **255,** 227–34 (1998).

71. Guca, E., Contet, A., Vial, H. J., Wengelnik, K. & Cerdan, R. in *Comprehensive Analysis*

of Parasite Biology: From Metabolism to Drug Discovery (eds. Müller, S., Cerdan, R. & Radulescum, O.) 171–191 (Wiley-VCH Verlag GmbH & Co. KGaA, 2016).

72. Maheshwari, S. *et al.* Biochemical characterization of Plasmodium falciparum CTP:phosphoethanolamine cytidylyltransferase shows that only one of the two cytidylyltransferase domains is active. *Biochem. J.* **450,** 159–67 (2013).

73. Dougherty, D. A. & Stauffer, D. A. Acetylcholine binding by a synthetic receptor: implications for biological recognition. *Science* **250,** 1558–60 (1990).

74. Sussman, J. L. *et al.* Atomic structure of acetylcholinesterase from Torpedo californica: a prototypic acetylcholine-binding protein. *Science* **253,** 872–9 (1991).

75. Zacharias, N. & Dougherty, D. Cation-pi interactions in ligand recognition and catalysis. *Trends Pharmacol. Sci.* **23,** 281–7 (2002).

76. Schärer, K. *et al.* Quantification of cation-pi interactions in protein-ligand complexes: crystal-structure analysis of Factor Xa bound to a quaternary ammonium ion ligand. *Angew. Chem. Int. Ed. Engl.* **44,** 4400–4 (2005).

77. Schneider, H.-J. Binding mechanisms in supramolecular complexes. *Angew. Chem. Int. Ed. Engl.* **48,** 3924–77 (2009).

78. Pavlovic, Z., Singh, R. K. & Bakovic, M. A novel murine CTP:phosphoethanolamine cytidylyltransferase splice variant is a post-translational repressor and an indicator that both cytidylyltransferase domains are required for activity. *Gene* **543,** 58–68 (2014).

79. Basak, A. *et al.* High-resolution X-ray Crystal Structures of Human γD Crystallin (1.25Å) and the R58H Mutant (1.15Å) Associated with Aculeiform Cataract. *J. Mol. Biol.* **328,** 1137–1147 (2003).

80. Hampton, S. L. & Kinnaird, A. I. Genetic interventions in mammalian cells; applications and uses in high-throughput screening and drug discovery. *Cell Biol. Toxicol.* **26,** 43–55 (2010).

81. Quirós, P. M., Mottis, A. & Auwerx, J. Mitonuclear communication in homeostasis and stress. *Nat. Rev. Mol. Cell Biol.* **17,** 213–26 (2016).

82. Hou, N. S. *et al.* Activation of the endoplasmic reticulum unfolded protein response by lipid disequilibrium without disturbed proteostasis in vivo. *Proc. Natl. Acad. Sci. U. S. A.* **111,** E2271-80 (2014).

83. Volmer, R. & Ron, D. Lipid-dependent regulation of the unfolded protein response. *Curr. Opin. Cell Biol.* **33,** 67–73 (2015).

84. Hetz, C. The unfolded protein response: controlling cell fate decisions under ER stress and beyond. *Nat. Rev. Mol. Cell Biol.* **13,** 89–102 (2012).

85. Pattanayak, V., Guilinger, J. P. & Liu, D. R. Determining the specificities of TALENs, Cas9, and other genome-editing enzymes. *Methods Enzymol.* **546,** 47–78 (2014).

86. Gaj, T., Gersbach, C. A. & Barbas, C. F. ZFN, TALEN, and CRISPR/Cas-based methods for genome engineering. *Trends Biotechnol.* **31,** 397–405 (2013).

ANNEX

I. Nagy GN, Marton L, Contet A, Ozohanics O, Ardelean L-M, Révész Á, *et al.* Composite Aromatic Boxes for Enzymatic Transformations of Quaternary Ammonium Substrates. Angew Chemie Int Ed. 2014;53: 13471–13476.

II. Marton L, Nagy GN, Ozohanics O, Lábas A, Krámos B, Oláh J, *et al.* Molecular Mechanism for the Thermo-Sensitive Phenotype of CHO-MT58 Cell Line Harbouring a Mutant CTP:Phosphocholine Cytidylyltransferase. PLoS One. 2015;10: e0129632.

I.

Enzyme Recognition

DOI: 10.1002/anie.201408246

Composite Aromatic Boxes for Enzymatic Transformations of Quaternary Ammonium Substrates**

Gergely N. Nagy, Lívia Marton, Alicia Contet, Olivér Ozohanics, Laura-Mihaela Ardelean, Ágnes Révész, Károly Vékey, Florin Dan Irimie, Henri Vial, Rachel Cerdan, and Beáta G. Vértessy**

Abstract: *Cation–π interactions to cognate ligands in enzymes have key roles in ligand binding and enzymatic catalysis. We have deciphered the key functional role of both charged and aromatic residues within the choline binding subsite of CTP:phosphocholine cytidylyltransferase and choline kinase from Plasmodium falciparum. Comparison of quaternary ammonium binding site structures revealed a general composite aromatic box pattern of enzyme recognition sites, well distinguished from the aromatic box recognition site of receptors.*

Cation–π interactions with electrostatic ion-quadrupol and ion-induced dipol character are frequent key elements of molecular recognition.[1] Trimethyl ammonium moieties are of peculiar interest as diffuse distribution of their charge renders them highly polarizable.[2] For their accommodation, a sterically restricted protein environment has evolved, in which desolvation of the charged moiety enables its efficient binding through cation–π interactions from aromatic residues (receptor function), as reviewed recently.[3] Beyond binding and transporting such ligands, numerous enzymes catalyze their chemical transformation, involved in key cellular functions. We introduce a clear general framework that governs the architecture of the active sites of these enzymes. Our experimental results together with a full range protein data bank query establish a novel common structural epitope for enzymes, termed as "composite aromatic box", distinct from the previously described aromatic box/cage of receptor proteins.

As a case study, we choose a model system to decipher key elements of ligand binding and mechanism of action of two enzymes, catalyzing consecutive steps in the phospholipid biosynthetic process of *Plasmodium falciparum*. Choline kinase (*Pf*CK, E.C. 2.7.1.32) phosphorylates Cho (choline) to ChoP (choline-phosphate) using ATP, CTP:phosphocholine cytidylyltransferase (PfCCT, E.C.2.7.7.15) catalyzes the CTP + ChoP (choline-phosphate)→CDPCho (CDP-choline) + PP_i (pyrophosphate) reaction. These enzymes are targets for recently developed highly potent choline analogue antimalarial agents;[4,5] however, current structural and mechanistic insights still fail to fully explain how the aromatic/hydrophobic interactions at the choline subsite contribute to ligand binding and catalysis.

The choline binding cleft of *Pf*CCT is a partially hydrophobic pocket that accommodates quaternary ammonium moieties of ChoP and CDPCho (Figure 1 A). This subsite consists of strictly conserved residues of either charged or aromatic character, the latter providing cation–π interaction to the choline moiety of cognate ligands.[6] To investigate the role of these residues in ligand binding and enzyme action, we designed a series of point mutants conservative for structure in a construct encompassing the catalytic domain of *Pf*CCT (*Pf*CCT MΔK[6]) by modulating the character of charged (D623N, Y741F) as well as aromatic (W692F, W692Y, Y714F) residues. The introduced mutations do not perturb the overall

[*] G. N. Nagy, B. G. Vértessy
Department of Applied Biotechnology and Food Science
Budapest University of Technology and Economics
1111 Budapest (Hungary)

L. Marton
Doctoral School of Multidisciplinary Medical Science
University of Szeged, 6720 Szeged, (Hungary)

G. N. Nagy, L. Marton, B. G. Vértessy
Institute of Enzymology, Research Centre of National Sciences, HAS
1117 Budapest (Hungary)
E-mail: nagy.gergely@ttk.mta.hu
vertessy@mail.bme.hu

L.-M. Ardelean, Prof. F. D. Irimie
Faculty of Chemistry and Chemical Engineering
Babes-Bolyai University
400028 Cluj-Napoca (Romania)

Dr. O. Ozohanics, Dr. Á. Révész, Prof. K. Vékey
Institute of Organic Chemistry
Research Centre of National Sciences, HAS
1117 Budapest (Hungary)

A. Contet, Dr. H. Vial, Dr. R. Cerdan
Laboratory Dynamique des Interactions Membranaires Normales et Pathologiques, UMR5235, CNRS, University Montpellier 2
34095 Montpellier (France)

[**] This work was supported the Hungarian Scientific Research Fund (OTKA NK 84008, OTKA K109486), the Baross program of the New Hungary Development Plan (3DSTRUCT, OMFB-00266/2010 REG-KM-09-1-2009-0050), the Hungarian Academy of Sciences (TTK IF-28/2012 and MedinProt) and the European Commission FP7 BioStruct-X project (contract No. 283570), to BGV, in addition, "Agence Nationale de la Recherche" (NKTH ADD-MAL, ANR-09-BLAN-0397), EU FP7/EviMalar NoE 242095). G.N.N. was supported by the Pro Progressio Foundation and Zsuzsa Szabo Foundation. M.L. is a fellow of the Multidisciplinary Medical Science PhD program, University of Szeged. This work was supported by a grant of the Romanian National Authority for Scientific Research, CNCS-UEFISCDI, project numberPN-II-ID-PCE-2011-3-0775.

Supporting information for this article is available on the WWW under http://dx.doi.org/10.1002/anie.201408246.

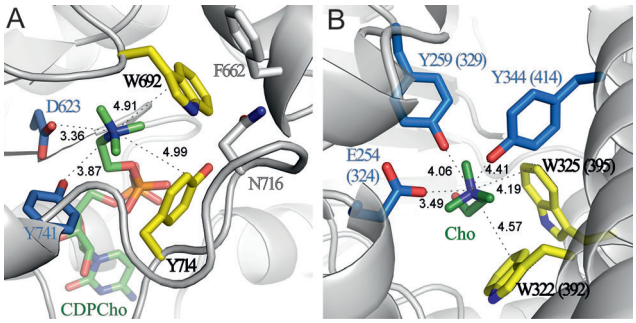

Figure 1. Coordination of the choline moiety at the active site of *Pf*CCT and *Pf*CK. A) Active site close-up of *Pf*CCT MΔK (PMDB ID: PM0078719). B) Active site close-up of choline kinase from *Plasmodium knowlesi*, a close homolog of *Pf*CK (PDB ID: 3C5I) Corresponding residue numbers of *Pf*CK are given in parenthesis. Structures are shown as a grey cartoon model, with the bound ligand shown as stick model, atomic coloring with green carbon. Side chains of charged and cation–π interactor residues within 5 Å and 6 Å of the quaternary nitrogen atom are displayed as sticks in atomic coloring with carbon is either blue or yellow for charged and aromatic interactions, respectively; O, red; N, blue; P, orange, with interaction distances indicated in Ångströms. Note the coordination partners of W692 in Figure 1 A, displayed as sticks, colored in atomic coloring, grey carbon.

quaternary structure of the enzyme (compare Figure S5 and Table S4 in the Supporting Information, SI). We performed enzyme kinetic investigations as well as a thermodynamic analysis of CDPCho binding by isothermal titration calorimetry as described in the SI.

Results indicate on one hand that the substitution of charged to noncharged residues yielded profound perturbation effects on catalytic efficiency (Figure 2, Table 1). This is mostly due to an altered choline coordination, as deduced from both $K_{M,ChoP}$ and the impaired CDPCho binding capability, characterized with diminished enthalpy of binding (Figure 2, Table 2, and Figure S7). On the other hand, partial conservation of the aromatic residues involved in cation–π interactions by tuning electrostatics, ring size, and quadrupole moment of the aromatic ring is still somewhat compatible with ligand binding and catalysis. The observed diverse performance of the mutants argue for the valid distinction of their charged versus cation–π interaction nature, and for

Table 1: Kinetic characterization of *Pf*CCT MΔK mutants.

Enzyme	k_{cat} [s^{-1}]	$K_{M,CTP}$ [μM]	$K_{M,ChoP}$ [mM]	rel. $k_{cat}/K_{M,CTP}$	rel. $k_{cat}/K_{M,ChoP}$
MΔK[a]	1.45 ± 0.05	168 ± 17	1.8 ± 1.1	1	1
$MΔK^{Y714F}$	0.21 ± 0.01	580 ± 60	10.2 ± 1.1	0.042	0.026
$MΔK^{W692F}$	0.13 ± 0.03	890 ± 380	7.5 ± 2.4	0.018	0.022
$MΔK^{W692Y}$	0.03 ± 0.003	191 ± 64	1.3 ± 0.2	0.017	0.029
$MΔK^{D623N}$	0.006 ± 0.001	460 ± 190	13.1 ± 3.1	0.0015	0.00057
$MΔK^{Y741F}$	0.019 ± 0.002	790 ± 180	8.5 ± 2.0	0.0028	0.0028
$MΔK^{W692A}$	6×10^{-4}	ND[b]	ND[b]	ND[b]	ND[b]

[a] Values reported previously.[6] [b] Values cannot be determined as seriously impaired ligand binding rendered results of Michaelis–Menten fit inaccurate.

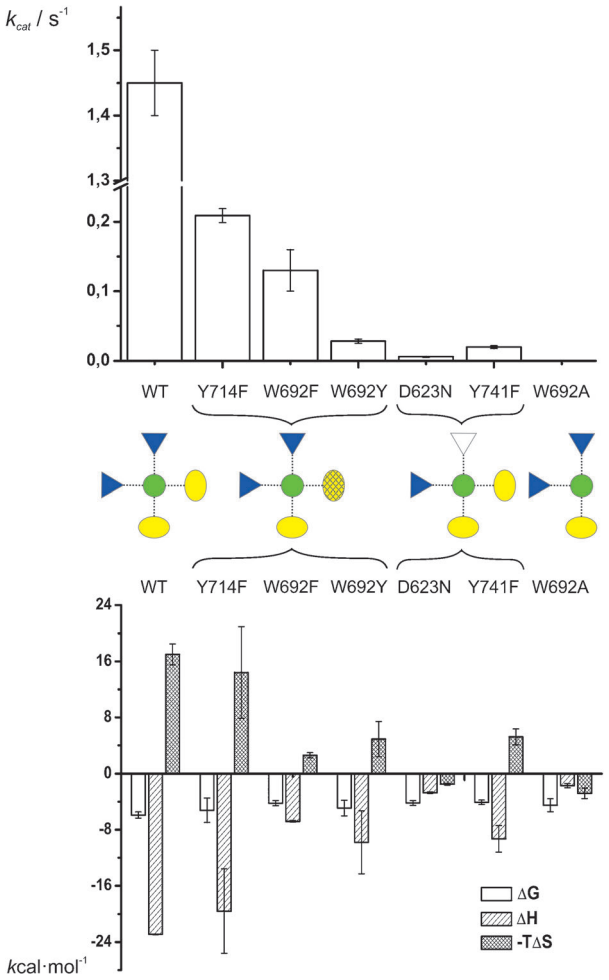

Figure 2. Effect of mutations on *Pf*CCT MΔK enzyme activity and ligand binding capability. Catalytic turnover and thermodynamic parameters of CDPCho binding (binding free enthalpy (Δ*G*), enthalpy (Δ*H*), and entropy (Δ*S*)) of *Pf*CCT MΔK and its point mutants are shown in top and bottom panels, respectively. The cartoon illustrates the quaternary ammonium binding site of *Pf*CCT with charged and aromatic interaction residues depicted as dark gray triangles and light gray ellipses, respectively. The functional effect of point mutation on a residue is indicated: altered aromatic character is depicted with a grid; exchange of charged to noncharged residue is marked by the empty triangle whereas alanine mutation of a given residue is depicted by deleting the respective symbol. Note the break on the *y* axis on the top panel.

Table 2: Thermodynamic analysis of CDPCho binding to *Pf*CCT MΔK mutants by ITC at 20 °C.

Enzyme	K_d [μM]	Δ*H* [kcal mol^{-1}]	Δ*S* [cal mol^{-1} K^{-1}]
MΔK[a]	44.4 ± 3.3	−22.9 ± 1.0	−58.1 ± 5.0
$MΔK^{Y714F}$	140 ± 50	−19.6 ± 6.0	−49.1 ± 22.3
$MΔK^{W692F}$	680 ± 60	−6.8 ± 0.8	−8.9 ± 1.3
$MΔK^{W692Y}$	220 ± 50	−9.8 ± 4.5	−16.8 ± 8.6
$MΔK^{D623N}$	790 ± 60	−2.7 ± 0.1	5.1 ± 0.5
$MΔK^{Y741F}$	1000 ± 80	−9.3 ± 1.9	−17.8 ± 3.9
$MΔK^{W692A}$	460 ± 100	−1.7 ± 0.3	9.6 ± 2.6

[a] Values reported previously.[6]

the key role of residues forming charged interactions with the choline moiety.

To assess the full contribution of interacting residues present at quaternary ammonium binding sites to enzyme action, we used alanine mutagenesis as an alternative investigation approach. Kinetic characterization was applied to the respective mutants of choline kinase from *Plasmodium falciparum*, a further example of an enzyme harboring a quaternary ammonium recognition site (Figure 1 B). Here, among the cognate charged interactors, as hypothesized based on the inspection of the CK crystal structure of *P. knowlesi*, a considerable role in enzyme action was only confirmed experimentally for E324, the equivalent of E254 of *P. knowlesi* CK (cf. Figure 3). In contrast, detrimental effects

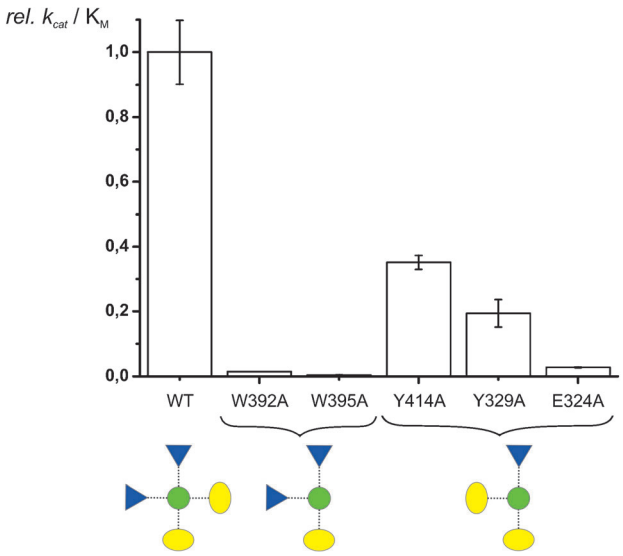

Figure 3. Kinetic parameters of wild-type *Pf*CK and its mutants. Relative catalytic efficiency of *Pf*CK mutants, compared to the wild type (WT) enzyme. The cartoon illustrates interaction types at the quaternary ammonium binding site of *Pf*CK; for the color code, see Figure 2. For the alanine mutation of a given residue, the respective symbol is deleted.

on enzyme action were also observed with the elimination of aromatic side chains (W392 and W395), which is mainly due to impaired ligand binding as indicated by K_M values. (Figure 3, Table 3, and Figure S8).

The significance of cation–π interactions to quaternary ammonium ligands, clearly demonstrated by these experiments with *Pf*CCT and *Pf*CK, is further underlined by the investigation of a *Pf*CCT MΔK mutant with fully abolished aromatic character, W692A. Elimination of the aromatic character at position 692 leads to a drastic disruption of catalytic function and also strongly perturbs the thermodynamics of CDPCho binding. Importantly, in this case the binding of CDPCho in the W692A mutant is now entropy-, rather than enthalpy-governed, which is in sharp contrast to its binding to other MΔK mutants, except for D623N (Figure 2, Table 2, and Figure S7). Such a thermodynamic pattern indicates that binding is accomplished in a much less directed and tight manner. Considering the 3D structural model of the CCT:CDPCho complex, we suggest that the W692 residue may have an additional role, beyond a catalytically competent accommodation of the substrate, in maintaining local structural integrity as well, by forming π–π interaction with the F662 and coordinating N716 (see Figure 1).

Table 3: Kinetic characterization of *Pf*CK mutants.[a]

Enzyme	k_{cat} [s^{-1}]	$K_{M,ChoP}$ [mM]	rel. $k_{cat}/K_{M,ChoP}$
*Pf*CK^{WT}	23.6 ± 1.0	0.24 ± 0.01	1.0 ± 0.1
*Pf*CK^{W392A}	7.0 ± 0.1	6.8 ± 0.2	0.01
*Pf*CK^{W395A}	ND[a]	ND[a]	ND[a]
*Pf*CK^{Y414A}	25.9 ± 1.1	0.94 ± 0.05	0.26
*Pf*CK^{Y329A}	58.1 ± 1.2	3.3 ± 0.1	0.18
*Pf*CK^{E324A}	35.5 ± 4.7	15.9 ± 2.3	0.028 ± 0.002

[a] Values cannot be determined precisely as seriously impaired ligand binding rendered results of Michaelis–Menten fit inaccurate.

Our study showed that during catalysis performed by *Pf*CK and *Pf*CCT, enzyme function is governed by a combination of cation–π and charged interactions to the quaternary ammonium moiety. We extended our investigations to all other enzymes harboring such site, by performing a comprehensive search in the protein data bank for structures containing quaternary ammonium ligands using Relibase[7] and analyzing the accommodation patterns in each case, as detailed in the SI. We found quaternary ammonium ligands in enzymes and also in receptors without enzymatic function (Table S5). In overwhelming majority of enzyme:ligand complex structures, the quaternary ammonium ligand was coordinated by both aromatic and charged or polar interactions (86 hits, i.e., 93 %).

In these structures, only one or two aromatic rings coordinated the respective substrate or product, whereas further coordination was accomplished by polar or negatively charged residues (Scheme 1, Figure 4, and Figure S9). The respective aromatic residues in several instances were shown to have key contribution to ligand binding[8] and catalysis.[9–15] Noteworthy, this general architecture appears in a great number of protein families, belonging to 15 protein family clans thus providing another spectacular example for the concept of convergent evolution. Importantly, these enzymes are involved in neurotransmission, epigenetics, and lipid metabolism. We propose here the term "composite aromatic box" for this universal enzyme binding geometry. The idea that the biological recognition of quaternary ammonium ligands is accomplished by the involvement of hydrophobic and cation–π interactions instead of a fully anionic site was proposed as early as 1990.[16] Later, this concept was confirmed for acetylcholinesterase, the most well-discussed representative enzyme in which the aromatic ring of a tryptophan facing the positively charged ligand moiety in the active site can provide a suitable environment by means of cation–π interactions.[17] The energetic contribution of such interactions to ligand binding was estimated to be comparable to a hydrogen bond or an ion pair.[18] Nevertheless, the herein defined universal composite aromatic box recognition pattern is clearly distinct from the well-known aromatic box or aromatic cage architecture, abundantly found at receptor

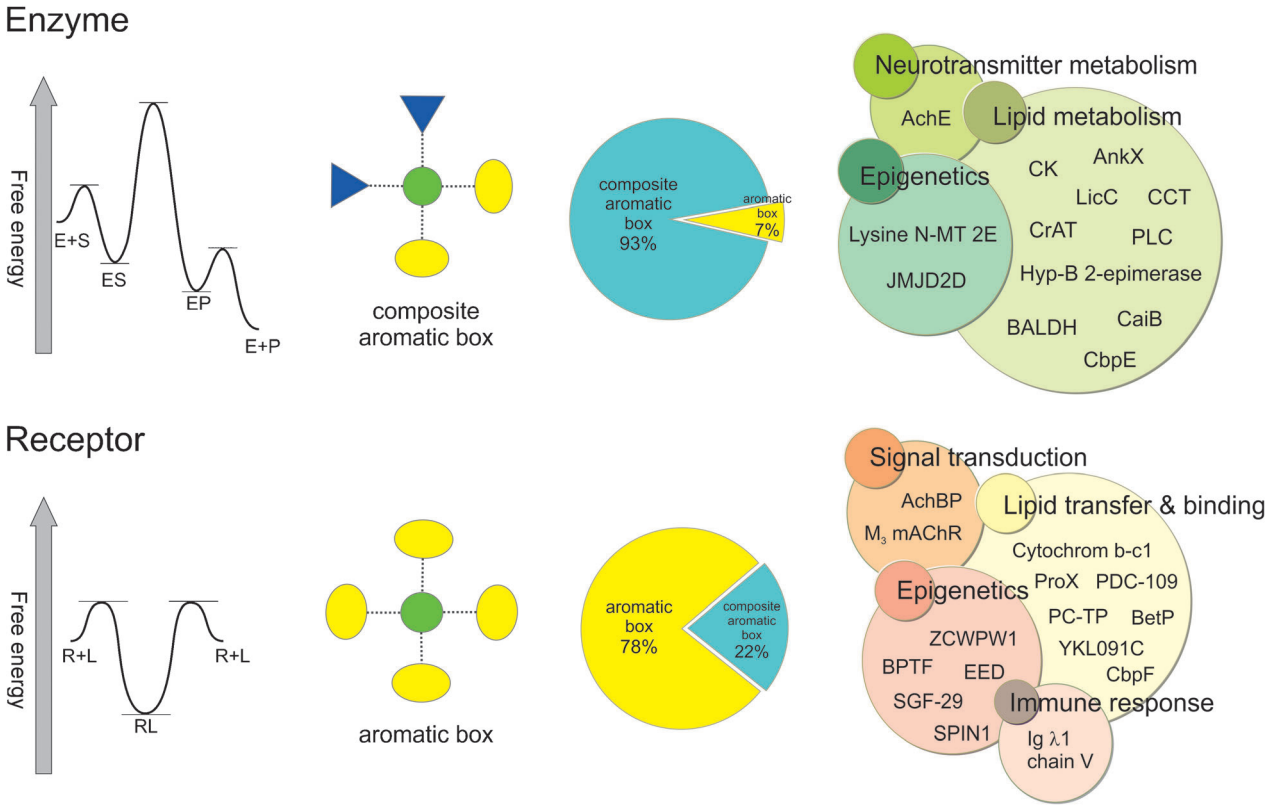

Scheme 1. Model of widespread structural solutions for quaternary ammonium binding sites in enzymes (composite aromatic box) and in receptors (aromatic box). General quaternary ammonium recognition site pattern of enzymes (E, left) differs from that of receptors (R, right). The different types of interactions are represented schematically; for the color code, see Figure 2. Representatives of enzymes and receptors with quaternary ammonium ligands are listed (for more detailed information see Tables S6 and S7 in the SI). Their distinct biological functions are illustrated by free energy profiles showing substrate (S) to product (P) interconversion, catalyzed by enzymes, and ligand (L) binding by receptors.

proteins (78% of relevant receptor hits; Figure S10) in which three or four aromatic rings are positioned to face the bound charged moiety of the quaternary ammonium ligand (Scheme 1), with an additional accompanying acidic residue for charge compensation (Figure 4, panel F).

The multiple aromatic rings in the aromatic box recognition site are positioned to face the bound charged moiety of the ligand and thus provide an optimal geometric fit.[19] This geometry can ensure a tight ligand binding due to the multivalence effect.[20] Accordingly, deletion of aromatic residues was shown to produce severe effects on ligand binding affinity as described in several studies.[21–24] Trimethyllysine recognition by histones is a peculiar event, which in some cases is accomplished by two aromatic side chains as well as charged residues, referred to as "half aromatic cage" site.[25] However, in this specific interaction type, found in 20 of 30 composite aromatic box-like receptor hits (see Table S5), the efficient ligand binding is further stabilized by additional peptide–peptide interactions.

Why are binding sites for quaternary ammonium ligand characteristically different in enzyme versus receptor proteins? We suggest that these differences are tuned to the different kinetic and thermodynamic requirements of enzymes and receptors. On the one hand, the physiological function of a receptor without enzymatic function is to provide specific high affinity binding in which both fast association and slow dissociation of the ligand is required. An aromatic box with its sterically restricted and in many cases rigid environment seems to be optimally suited to perform such a role.[26] Receptor proteins possessing aromatic boxes are associated with widespread physiological function from signaling to ligand binding or transfer and cellular defense mechanisms (Scheme 1). On the other hand, enzymatic functions have distinct requirements. The active site of an enzyme is of course responsible for ligand accommodation, but a sufficiently high conformational dynamics is needed to assist activation, chemical transformation, and release of the transformed ligand(s). For efficient catalysis, the ability of fast ligand binding and release is an absolute requirement; for example, in G-proteins, GTP hydrolysis is limited by slow dissociation of the GDP product, rendering these enzymes to be inefficient catalysts on their own.[27] We propose that the presence of charged or polar residues within the composite aromatic boxes of enzymes allow a less hydrophobic character for the quaternary ammonium binding cleft, leading to reduced desolvation of the bound ligand moiety. This in some cases may also contribute to increased local conformational dynamics, for instance, as shown in reference [28]. The increased conformational dynamics required for enzymatic function may also be provided by the pronounced flexibility of aromatic side chains with a partially polar character (e.g., tyrosine). Actually, for betaine aldehyde dehydrogenase,

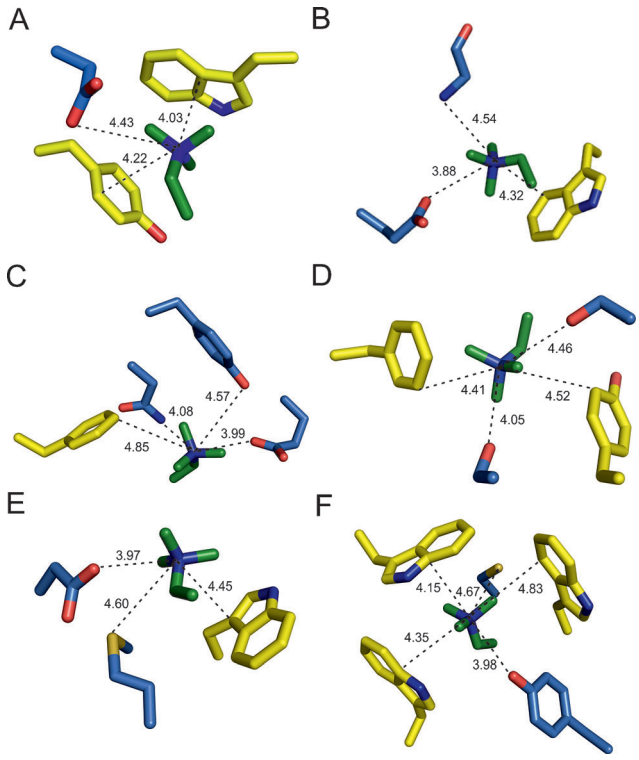

Figure 4. Quaternary ammonium recognition sites in enzymes (panels A–E) versus receptors (panel F). Selected examples show the characteristic composite aromatic box-type ligand binding site in enzymes. A) LicC bacterial CTP:phosphocholine cytidylyltransferase, PDB ID: 1JYL; B) Acetylcholinesterase (AchE), PDB ID: 2A3; C) Phospholipase C (PLC), PDB ID: 1P6D D) Carnitine *O*-acetyltransferase (1S5O); E) histone lysine *N*-methyltransferase, PDB ID: 4I58; F) Glycine betaine-binding protein (proX), PDB ID: 1R9L, is shown as illustration of the aromatic box structure present in receptors. Only the quaternary ammonium moiety is shown from the ligand structure as well as the side chain of residues. Charged and cation–π interactors are displayed within 5 Å and 6 Å of the quaternary nitrogen atom, respectively. Residues are shown as sticks, with atomic coloring based on the type of interaction in that they are involved (cation–π: yellow carbon; polar or charged: blue carbon; quaternary ammonium ligand, green carbon; O, red; N, blue; P, orange. For other examples of enzyme and receptor recognition, see the SI, Figures S9 and S10 and Tables S6 and S7.

computational studies proposed an accommodation of the quaternary ammonium ligand within the active site by four aromatic residues with significant static and dynamic disorder.[29] To gain in-depth insight in how residues of the composite aromatic box epitope site play their role in enzyme action, further thorough kinetic and structural analyses are clearly needed for each individual enzyme utilizing a quaternary ammonium.

In conclusion, we identified a potentially general architecture element termed as composite aromatic box within the active site of enzymes catalyzing the conversion of quaternary ammonium substrates. Harboring only one or two, instead of the three to four aromatic residues for cation–π interactions as seen in the aromatic box or cage, the composite aromatic box is proposed to be advantageous for assisting multiple steps of enzyme action. We hypothesize that the necessary conformational changes during the catalytic cycle may be poorly compatible with a fully hydrophobic rigid environment of an aromatic box. In a case study involving *Pf*CK and *Pf*CCT enzymes, we revealed the role of both charged/polar and aromatic residues within a composite aromatic box in ligand binding and catalysis. Together with literature data, our study points toward a general view of composite aromatic box sites in enzymes. This may lead to further pharmacological consequences, because many enzymes with quaternary ammonium ligands play important roles either in severe infectious diseases[30] or in diverse metabolic processes as lipid biosynthesis, epigenetics, or neurotransmitter metabolism. Their deficiencies lead to serious adverse phenotype effects in humans and therefore they themselves are well established drug targets.[31–34] The present study also contributes to a better understanding of the action of two malaria parasite enzymes, *Pf*CK and *Pf*CCT, that constitute potential antimalarial drug targets and may help in the ongoing structure-based pharmacophore design and validation.

Received: August 14, 2014
Published online: ■■ ■■, ■■■■

Keywords: cation–π interactions · enzyme catalysis · molecular recognition · quaternary ammonium · structural biology

[1] A. S. Mahadevi, G. N. Sastry, *Chem. Rev.* **2013**, *113*, 2100 – 2138.
[2] D. A. Dougherty, *Acc. Chem. Res.* **2013**, *46*, 885 – 893.
[3] L. M. Salonen, M. Ellermann, F. Diederich, *Angew. Chem. Int. Ed.* **2011**, *50*, 4808 – 4842; *Angew. Chem.* **2011**, *123*, 4908 – 4944.
[4] H. J. Vial, S. Wein, C. Farenc, C. Kocken, O. Nicolas, M. L. Ancelin, F. Bressolle, A. Thomas, M. Calas, *Proc. Natl. Acad. Sci. USA* **2004**, *101*, 15458 – 15463.
[5] S. Wein, M. Maynadier, Y. Bordat, J. Perez, S. Maheshwari, P. Bette-Bobillo, C. Tran Van Ba, D. Penarete-Vargas, L. Fraisse, R. Cerdan, et al., *Br. J. Pharmacol.* **2012**, *166*, 2263 – 2276.
[6] G. N. Nagy, L. Marton, B. Krámos, J. Oláh, Á. Révész, K. Vékey, F. Delsuc, É. Hunyadi-Gulyás, K. F. Medzihradszky, M. Lavigne, et al., *FEBS J.* **2013**, *280*, 3132 – 3148.
[7] M. Hendlich, A. Bergner, J. Günther, G. Klebe, *J. Mol. Biol.* **2003**, *326*, 607 – 620.
[8] J. Lee, J. Johnson, Z. Ding, M. Paetzel, R. B. Cornell, *J. Biol. Chem.* **2009**, *284*, 33535 – 33548.
[9] B.-Y. Kwak, Y.-M. Zhang, M. Yun, R. J. Heath, C. O. Rock, S. Jackowski, H.-W. Park, *J. Biol. Chem.* **2002**, *277*, 4343 – 4350.
[10] C. Yuan, C. Kent, *J. Biol. Chem.* **2004**, *279*, 17801 – 17809.
[11] A. Ordentlich, D. Barak, C. Kronman, N. Ariel, Y. Segall, B. Velan, A. Shafferman, *J. Biol. Chem.* **1995**, *270*, 2082 – 2091.
[12] S. F. Martin, B. C. Follows, P. J. Hergenrother, B. K. Trotter, *Biochemistry* **2000**, *39*, 3410 – 3415.
[13] G. Jogl, L. Tong, *Cell* **2003**, *112*, 113 – 122.
[14] K. D. Green, V. R. Porter, Y. Zhang, S. Garneau-Tsodikova, *Biochemistry* **2010**, *49*, 6219 – 6227.
[15] V. Campanacci, S. Mukherjee, C. R. Roy, J. Cherfils, *EMBO J.* **2013**, *32*, 1469 – 1477.
[16] D. A. Dougherty, D. A. Stauffer, *Science* **1990**, *250*, 1558 – 1560.
[17] J. L. Sussman, M. Harel, F. Frolow, C. Oefner, A. Goldman, L. Toker, I. Silman, *Science* **1991**, *253*, 872 – 879.
[18] N. Zacharias, D. A. Dougherty, *Trends Pharmacol. Sci.* **2002**, *23*, 281 – 287.
[19] K. Schärer, M. Morgenthaler, R. Paulini, U. Obst-Sander, D. W. Banner, D. Schlatter, J. Benz, M. Stihle, F. Diederich, *Angew.*

Chem. Int. Ed. **2005**, *44*, 4400 – 4404; *Angew. Chem.* **2005**, *117*, 4474 – 4479.
[20] H.-J. Schneider, *Angew. Chem. Int. Ed.* **2009**, *48*, 3924 – 3977; *Angew. Chem.* **2009**, *121*, 3982 – 4036.
[21] A. Schiefner, J. Breed, L. Bösser, S. Kneip, J. Gade, G. Holtmann, K. Diederichs, W. Welte, E. Bremer, *J. Biol. Chem.* **2004**, *279*, 5588 – 5596.
[22] S. Ressl, A. C. Terwisscha van Scheltinga, C. Vonrhein, V. Ott, C. Ziegler, *Nature* **2009**, *458*, 47 – 52.
[23] A. C. Kruse, J. Hu, A. C. Pan, D. H. Arlow, D. M. Rosenbaum, E. Rosemond, H. F. Green, T. Liu, P. S. Chae, R. O. Dror, et al., *Nature* **2012**, *482*, 552 – 556.
[24] J. A. Olsen, T. Balle, M. Gajhede, P. K. Ahring, J. S. Kastrup, *PLoS One* **2014**, *9*, e91232.
[25] M. Yun, J. Wu, J. L. Workman, B. Li, *Nat. Publ. Gr.* **2011**, *21*, 564 – 578.
[26] K. Haga, A. C. Kruse, H. Asada, T. Yurugi-Kobayashi, M. Shiroishi, C. Zhang, W. I. Weis, T. Okada, B. K. Kobilka, T. Haga, et al., *Nature* **2012**, *482*, 547 – 551.
[27] R. D. Vale, *J. Cell Biol.* **1996**, *135*, 291 – 302.
[28] B. Sanson, J.-P. Colletier, Y. Xu, P. T. Lang, H. Jiang, I. Silman, J. L. Sussman, M. Weik, *Protein Sci.* **2011**, *20*, 1114 – 1118.
[29] Á. G. Díaz-Sánchez, L. González-Segura, C. Mújica-Jiménez, E. Rudiño-Piñera, C. Montiel, L. P. Martínez-Castilla, R. A. Muñoz-Clares, *Plant Physiol.* **2012**, *158*, 1570 – 1582.
[30] J. A. Hermoso, L. Lagartera, A. González, M. Stelter, P. García, M. Martínez-Ripoll, J. L. García, M. Menéndez, *Nat. Struct. Mol. Biol.* **2005**, *12*, 533 – 538.
[31] T. A. Lagace, N. D. Ridgway, *Biochim. Biophys. Acta Mol. Cell Res.* **2013**, *1833*, 2499 – 2510.
[32] I. Anghelescu, I. Heuser, *MMW Fortschr. Med.* **2007**, *149 Suppl*, 76 – 78.
[33] D. Tousoulis, C. Bakogiannis, A. Briasoulis, N. Papageorgiou, E. Androulakis, G. Siasos, G. Latsios, A.-M. Kampoli, M. Charakida, K. Toutouzas, et al., *Curr. Pharm. Des.* **2013**, *19*, 1587 – 1592.
[34] C. Biancotto, G. Frigè, S. Minucci, *Adv. Genet.* **2010**, *70*, 341 – 386.

Communications

Enzyme Recognition

G. N. Nagy,* L. Marton, A. Contet, O. Ozohanics, L.-M. Ardelean, Á. Révész, K. Vékey, F. D. Irimie, H. Vial, R. Cerdan, B. G. Vértessy* _____ ■■■■–■■■■

Composite Aromatic Boxes for Enzymatic Transformations of Quaternary Ammonium Substrates

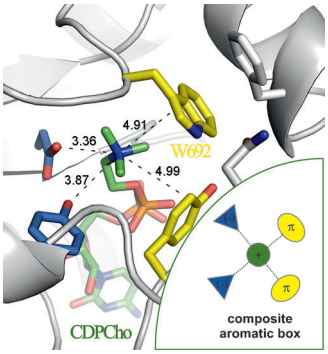

Composite aromatic box: The key functional role of both charged (blue) and cation–π (yellow in the picture) interactions within the choline-binding subsite of CTP:phosphocholine cytidylyltransferase and choline kinase from *Plasmodium falciparum* have been deciphered. The comparison of quaternary ammonium binding site structures revealed a general composite aromatic box pattern of enzyme recognition sites.

Angewandte Chemie
Eine Zeitschrift der Gesellschaft Deutscher Chemiker

Supporting Information

69451 Weinheim, Germany

Composite Aromatic Boxes for Enzymatic Transformations of Quaternary Ammonium Substrates**

Gergely N. Nagy, Lívia Marton, Alicia Contet, Olivér Ozohanics, Laura-Mihaela Ardelean, Ágnes Révész, Károly Vékey, Florin Dan Irimie, Henri Vial, Rachel Cerdan, and Beáta G. Vértessy**

anie_201408246_sm_miscellaneous_information.pdf

Table of Contents

Experimental Procedures

Materials

CTP, CDPCho (CDP-choline), inorganic pyrophosphatase, purine nucleoside phosphorylase, TCEP (Tris(2-carboxyethyl)phosphine) were purchased from Sigma-Aldrich (St. Luis, MO, USA). ATP and Choline (Cho) hydrochloride were purchased from Sigma-Aldrich Chimie (France). [methyl-^{14}C]Choline was from Perkin-Elmer SAS (France). ChoP (choline-phosphate) was from TCI Europe N.V. MESG (2-amino-6-mercapto-7-methylpurine riboside) was obtained from Berry and Associates (Dexter, MI). All other chemicals were of analytical grade of the highest purity available.

Mutagenesis, protein expression and purification

Site-directed mutagenesis to produce W692F, Y714F, D623N, Y741F and W692A mutant constructs of His-tagged *Pf*CCT MΔK[1] (PlasmoDB accession number: PF3D7_1316600)[2] were performed by the Quickchange method (Agilent). The following mutagenesis primers were used:

W692F 5'-3', catttctccgtgTCCgttcgtggtgacgccgg;
W692F 3'-5', ccggcgtcaccacGAAcggacacggagaaatg;
Y714F 5'-3', catgatgacatcccgTTTgctaacaatcagaaagaag;
Y714F 3'-5', cttctttctgattgttagcAAAcgggatgtcatcatg;
D623N 5'-3', cgtggtgatttacgccAATggtgtttacgacatgc;
D623N 3'-5',gcatgtcgtaaacaccATTggcgtaaatcaccacg;
Y741F 5'-3', caatcagaaagaagatattTTTgcttggctgaaac;
Y741F 3'-5'. gtttcagccaagcAAAaatatcttctttctgattg;
W692A 5'-3' catttctccgtgtccgGCGgtggtgacgccg;
W692A 3'-5' cggcgtcaccacCGCcggacacggagaaatg.

All constructs were verified by DNA sequencing. The constructs were expressed and purified as described previously.[1] Protein concentrations were determined by absorbance measurements carried out using a Nanodrop 2000 spectrophotometer (ThermoScientific).

Site-directed mutagenesis to produce E324A, Y329A, W392A, W395A and Y414A mutant constructs of His-tagged *Pf*CK (PlasmoDB accession number PF3D7_1401800)[2] were performed by the Quickchange method (Agilent). The following mutagenesis primers were used:

E324A 5'-3', gcaaacttctttataGCGacaacaatcgattattc;
E324A 3'-5', cgtttgaagaaatatCGCtgttgttagctaataag;
Y329A 5'-3', gaaacaacaatcgatGCGtcatataacgcatatcc;
Y329A 3'-5', ctttgttgttagctaCGCagtatattgcgtatagg;
W392A 5'-3', ggtttacatctaataGCGgcattctggtctatc;

W392A 3'-5', ccaaatgtagattatCGCcgtaagaccagatag;
W395A 5'-3', catctaatatgggcattcGCGtctatcataagagg;
W395A 3'-5', gtagattatacccgtaagCGCagatagtattctcc;
Y414A 5'-3', gttataatgaatttgatttcttcttaGCGgcaaaggaaagacttaaaatg;
Y414A 3'-5, caatattacttaaactaaagaagaatCGCcgtttcctttctgaattttac.

All constructs were verified by DNA sequencing. The constructs pET24b-*Pf*CK were expressed in BL21(DE3)-pRIL and purified as described previously.[3] Protein concentrations were determined by absorbance measurements carried out using a Nanodrop 2000 spectrophotometer (ThermoScientific).

Mass spectrometry

In the mass spectrometric study of protein complexes, a commercial Waters QTOF Premier instrument (Waters, Milford, MA, USA) equipped with electrospray ionization source (Waters, Milford, MA, USA) used in the positive ion mode. Mass spectra were obtained under native conditions: namely, the ions were generated from aqueous 10 mM NH_4HCO_3 buffer solution (pH 7.15) containing the gel filtered *Pf*CCT MΔK protein constructs at 0.4 μM monomer concentration. These conditions allow transfer of the native protein complex present in the solution into the gas phase. The capillary voltage was 3600 V, the sampling cone voltage was 125 V and the temperature of the source was kept at 80°C, collision cell pressure was $3.38*10^{-3}$ mbar and ion guide gas flow was 35.00 ml/min. Mass spectra were recorded using the software MassLynx 4.1 (Waters, Milford, MA, USA) in the mass range 1000–5000m/z as no signals could be detected above 5000 m/z.

Steady state activity

Steady-state activity measurements with *Pf*CCT were performed as described previously[1] in 20 mM HEPES, pH 7.5 buffer, containing 100 mM NaCl using a continuous coupled pyrophosphatase enzyme assay, which employs MESG substrate for colorimetric phosphate detection. In case of low activity point mutants, longer assay times up to five hours, as well as higher mutant enzyme concentrations (up to 300 μM) were employed. Data were fitted with Michaelis-Menten equation using Origin 7.5 (OriginLab Corp., Northampton, MA).

Steady-state activity measurements with *Pf*CK were performed as described previously[3] with some modifications, using a ^{14}C Choline assay in which enzymatic activity is measured by the formation of radiolabelled ChoP. Briefly, recombinant wild-type or mutants *Pf*CK were incubated with [methyl-^{14}C]Cho (specific activity of 55.2 μCi/μmol). For each assay, enzymatic reaction was carried out in a final volume of 100 μl with 125μM Tris/HCl pH 8.0

buffer, 10 mM ATP, 5 mM EGTA, 10 mM $MgCl_2$, 0.2 µCi of radiolabelled Cho and increasing concentrations of unlabeled Cho (from 50µM to 10 mM final Cho concentration). Reaction was initiated with the addition of 0.2 µg of *Pf*CK wild type or 0.5 µg of *Pf*CK alanine mutants followed by a 5 min incubation at 37°C. Reaction was stopped by heating at 99 °C for 5 min. Radiolabelled product and substrate were then separated on thin layer chromatography and product formation was quantified as previously described.[3] Data were fitted with Michaelis-Menten equation using GraphPad Prism 4 (GraphPad Software, Inc.). Experiments were done twice in triplicate.

Isothermal Titration Calorimetry measurements were performed as described previously.[1] Prior to titration, protein samples were dialized against buffer containing 20 mM Hepes, pH 7.5, 100 mM NaCl, 1 mM TCEP. Titration data were analyzed using MicroCal ORIGIN software following the directions of the manufacturer. Integrated heat data were corrected by subtracting heat data of ligand to buffer titration, performed under identical conditions.

PDB search

A full-range query of the Protein Data Bank (status 1st January 2014) was assessed for three dimensional structures (including NMR and crystal structures) containing tetraalkylammonium moiety compound up to 3.5Å resolution using Relibase.[4] The initial hitlist was refined by visual inspection. Only such cavities were taken into account in which the cognate quaternary ammonium ligand was coordinated by at least two residues. In order to define relative ligand- residue positions, distance between N atom as the geometric centre of the cationic ligand and the nearest non-hydrogen atom of the neighboring residue was shown. The respective W/Y/F residues were classified as cation-π interaction partners when their aromatic plane faced the quaternary ammonium moiety within the distance of 6 Å, based on [5] and in accordance with the results described in [6]. Distance criteria for polar or charged interaction partners was set to 5 Å, according to [7]. Structures obtained with quaternary ammonium crystallization agents were excluded. Enzyme: ligand recognition was assumed only when the quaternary ammonium ligand that corresponds to the cognate substrate, product or analogue was accommodated to active site of the enzyme. Otherwise, receptor: ligand interaction was assumed. The hits were classified based on ligand binding geometry. We defined the composite aromatic box interaction pattern with the joint coordination of the quaternary ammonium moiety with one or two aromatic residue(s), and polar or charged residues.

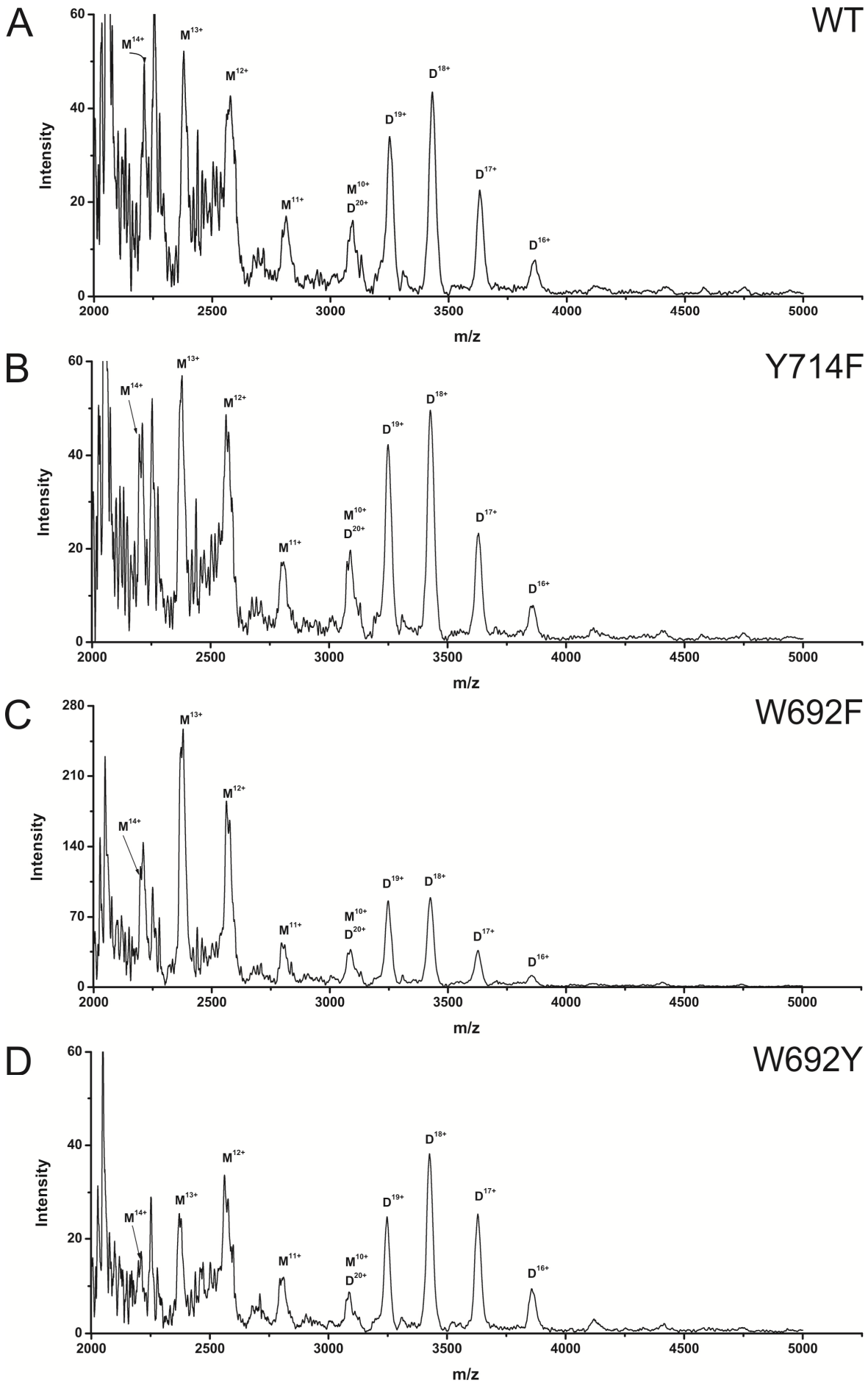
A
WT
B
Y714F
C
W692F
D
W692Y
Intensity
m/z
M14+
M13+
M12+
M11+
M10+
D20+
D19+
D18+
D17+
D16+

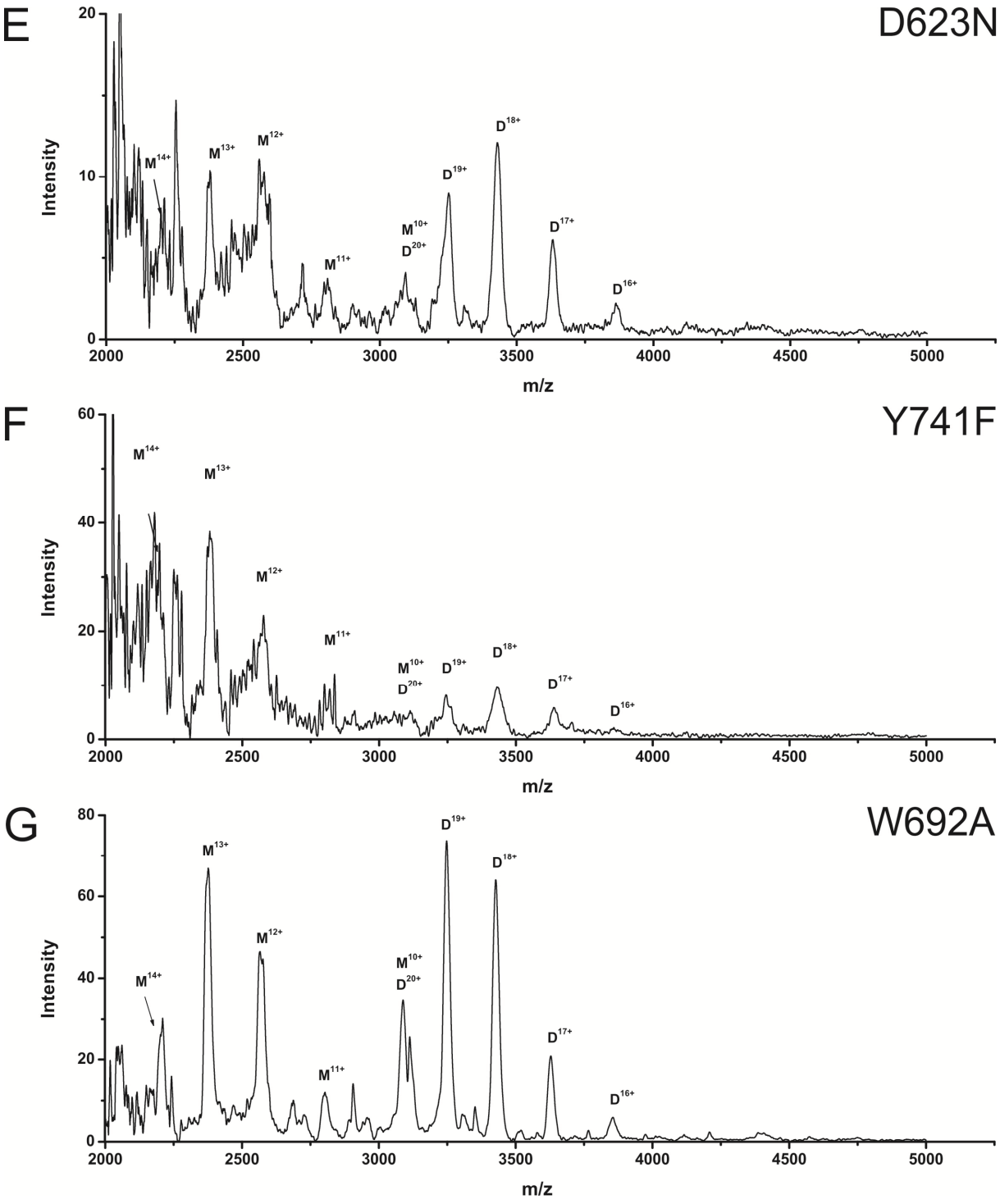

Figure 5 **Mass spectrum of *Pf*CCT MΔK mutant proteins under native electrospray conditions.**

Mass spectra of the *Pf*CCT MΔK protein and its point mutants under native electrospray conditions. M and D denote monomer and dimer signals, respectively; whereas numbers indicate the charge states. No signals were detected above 5000 m/z. Mass spectra for the mutants is analogous to that of the *Pf*CCT MΔK, i.e., a dimer:monomer ratio of ca. 1:1 was found, and no higher oligomeric forms can be observed. Thus, the mutants also specifically

form a dimer structure, which corroborates that these mutations do not induce major global conformational changes. In case of *Pf*CCT MΔK^{Y741F}, the low resolution of monomer and dimer m/z peaks might correlate with decreased stability of the construct under the conditions of ESI-MS experiment. **A)** Mass spectrum of *Pf*CCT MΔK^{WT} **B)** Mass spectrum of *Pf*CCT MΔK^{Y714F} **C)** Mass spectrum of *Pf*CCT MΔK^{W692F} **D)** Mass spectrum of *Pf*CCT MΔK^{W692Y} **E)** Mass spectrum of *Pf*CCT MΔK^{D623N} **F)** Mass spectrum of *Pf*CCT MΔK^{Y741F} **G)** Mass spectrum of *Pf*CCT MΔK^{W692A}.

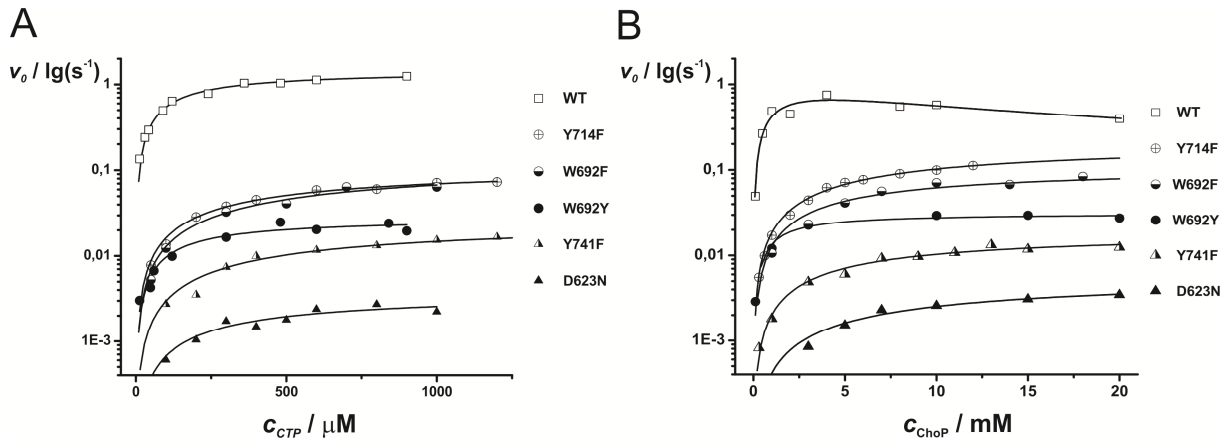

Figure 6 **Steady-state analysis of kinetics of *Pf*CCT MΔK point mutants.**

Michaelis-Menten kinetic curves of *Pf*CCT MΔK enzyme point mutants. **A)** Initial rates of reaction measured at fixed 5 mM concentration of ChoP and at varying concentration of CTP. **B)** Initial rates of reaction measured at fixed c_{CTP} of 1 mM and at varying concentration of ChoP. Titration data of *Pf*CCT MΔK from [1] is shown for comparison. Data points corresponding to mutants of charged interactors are depicted as triangles whereas mutants of cation-π interactors are depicted as circles. Note that for the WT *Pf*CCT MΔK, there is a slight inhibition exerted by the ChoP substrate, apparent at [ChoP] > 7 mM[1], considerably higher than the physiological ChoP concentration of 30 μM [8]. In the case of its mutants, this inhibition was not observed.

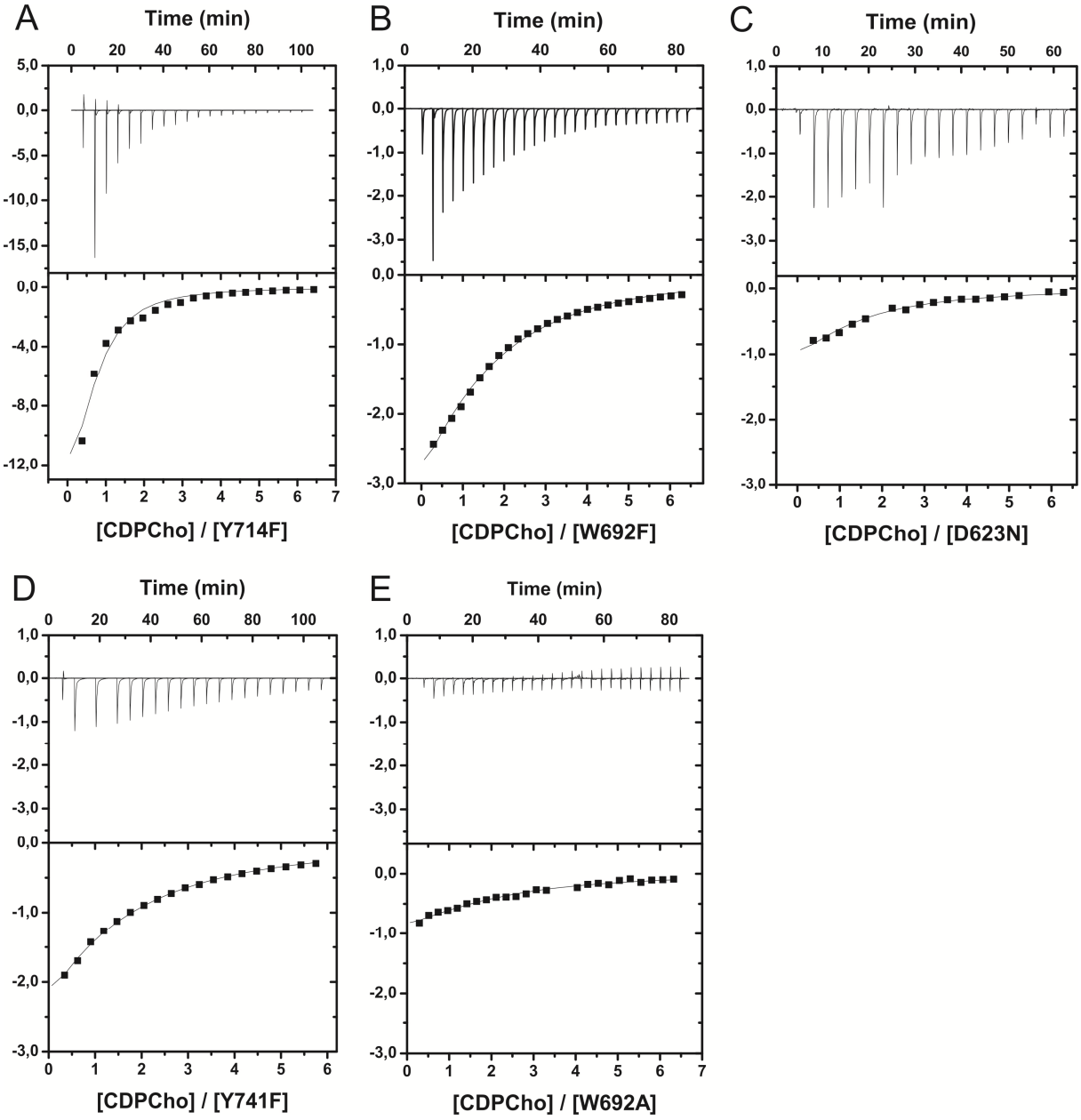

Figure 7 **Isothermal Titration Calorimetry analysis of CDPCho binding to *Pf*CCT MΔK mutant enzymes.**

Isothermal titration calorimetry curves of CDPCho binding to PfCCT MΔK mutants. Data gave best fit with the One set of binding sites model, as described by the manufacturer.

A). Titration of 319 μM *Pf*CCT MΔK^{Y714F} (monomer concentration) with 10 mM CDPCho

B) Titration of 369 μM *Pf*CCT MΔK^{W692F} (monomer concentration) with 11 mM CDPCho.

C) Titration of 430 μM *Pf*CCT MΔK^{D623N} (monomer concentration) with 13 mM CDPCho

D) Titration of 357 μM *Pf*CCT MΔK^{Y741F} (monomer concentration) with 10 mM CDPCho

E) Titration of 250 μM *Pf*CCT MΔK^{W692A} (monomer concentration) with 7.5 mM CDPCho.

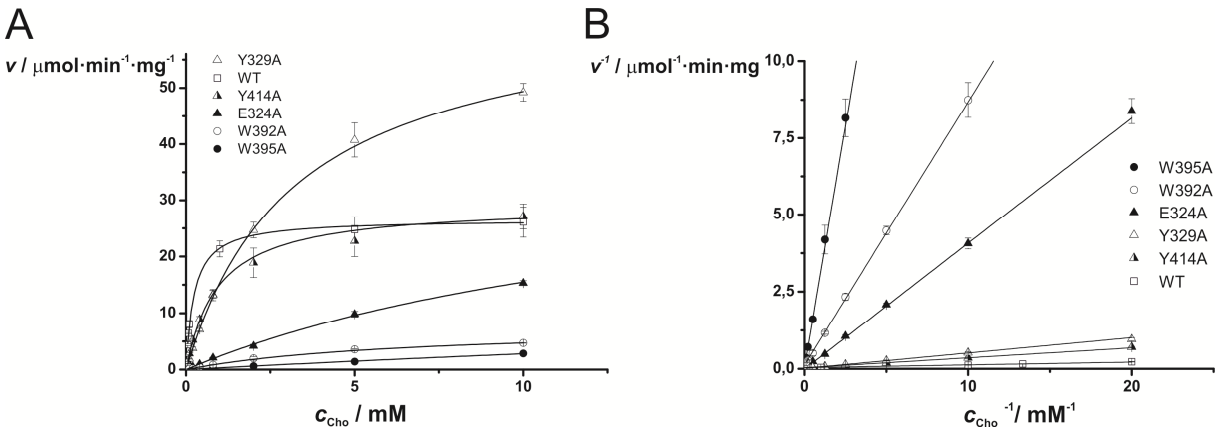

Figure 8 **Steady-state kinetic analysis of *Pf*CK point mutants.**

A) Michaelis-Menten kinetic curves of mutant *Pf*CK. Initial rates of reaction measured at fixed concentrations of 10 mM ATP and at varying concentration of choline (Cho). **B)** Lineweaver-Burk plots. Results are presented as the mean ±SD from three parallel measurements from one representative experiment.

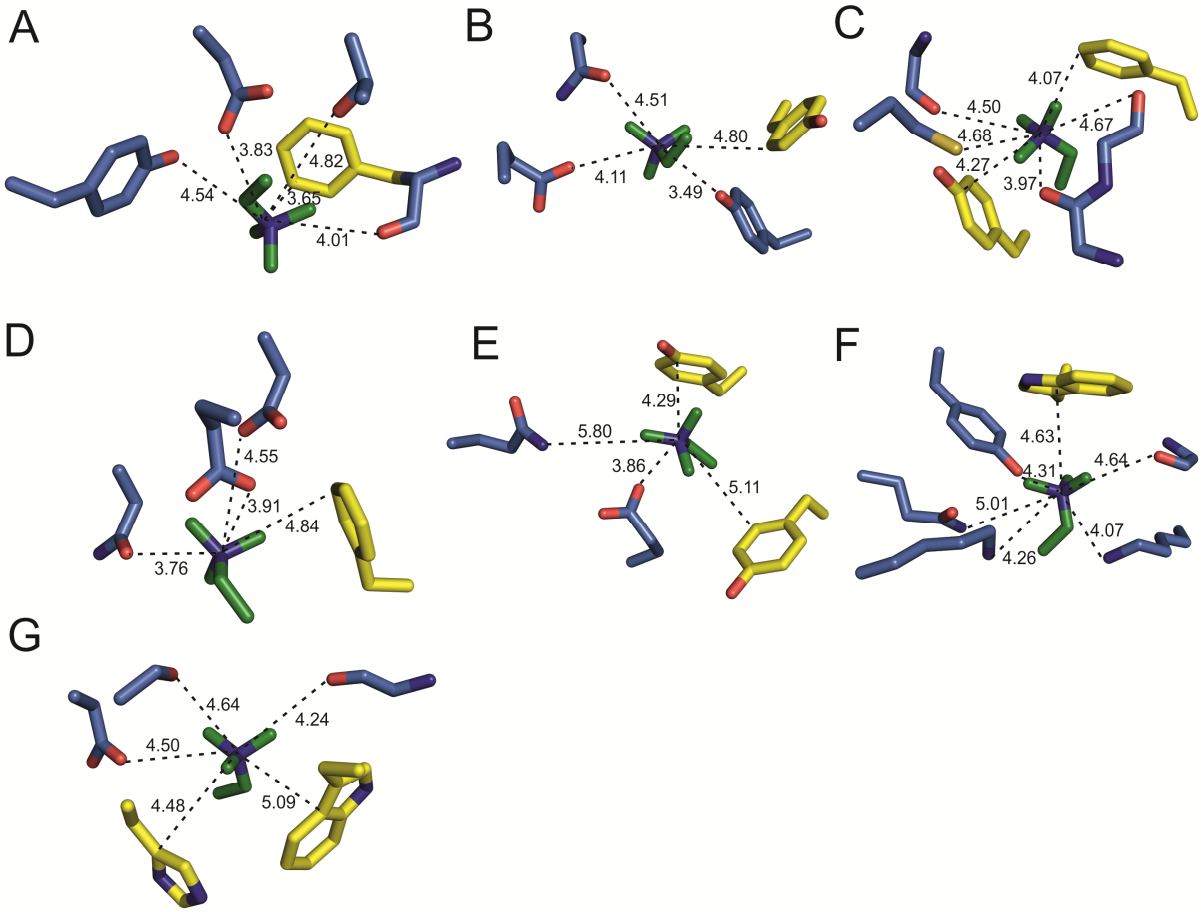

Figure 9 **Enzyme active sites displaying composite aromatic box character**.

Additional examples show the widespread structural solution evolved for accommodation of quaternary ammonium enzyme ligands. A single representative was chosen from all protein family clans, based on Pfam annotations[9], where a protein three dimensional structural hit was deposited in the Protein Data Bank with bound quaternary ammonium substrate or product. The structure with optimal resolution available was selected. Active site close-up of enzyme structures are shown with quaternary ammonium moiety of the bound ligand. For the sake of clarity, only the quaternary ammonium moiety of the respective ligand is displayed (stick model, atomic coloring with green carbon, blue nitrogen). Stick models of interacting residue side chains or main chains are in atomic coloring where carbon is either yellow or blue for cation-π or charged interactions, respectively. For visualization of proximity, the distance of the closest residue atom from the quaternary ammonium N is displayed (even though the nitrogen atom itself is negatively charged [10]). **A)** Betaine aldehyde dehydrogenase, PDB ID: 1WNB; **B)** JMJD2D lysine demethylase, PDB ID: 4HON; **C)** RuBisCO LSMT PDB ID: 2H23; **D)** Phosphocholine transferase (AnkX), PDB ID: 4BES; **E)** Cronobetainyl-CoA:carnitine CoA transferase (CaiB), PDB ID: 1XVV; **F)** 4-hydroxyproline

betaine 2-epimerase, PDB ID: 4J1O; **G)** Teichoic acid phosphorylcholine esterase (CbpE), PDB ID: 2BIB.

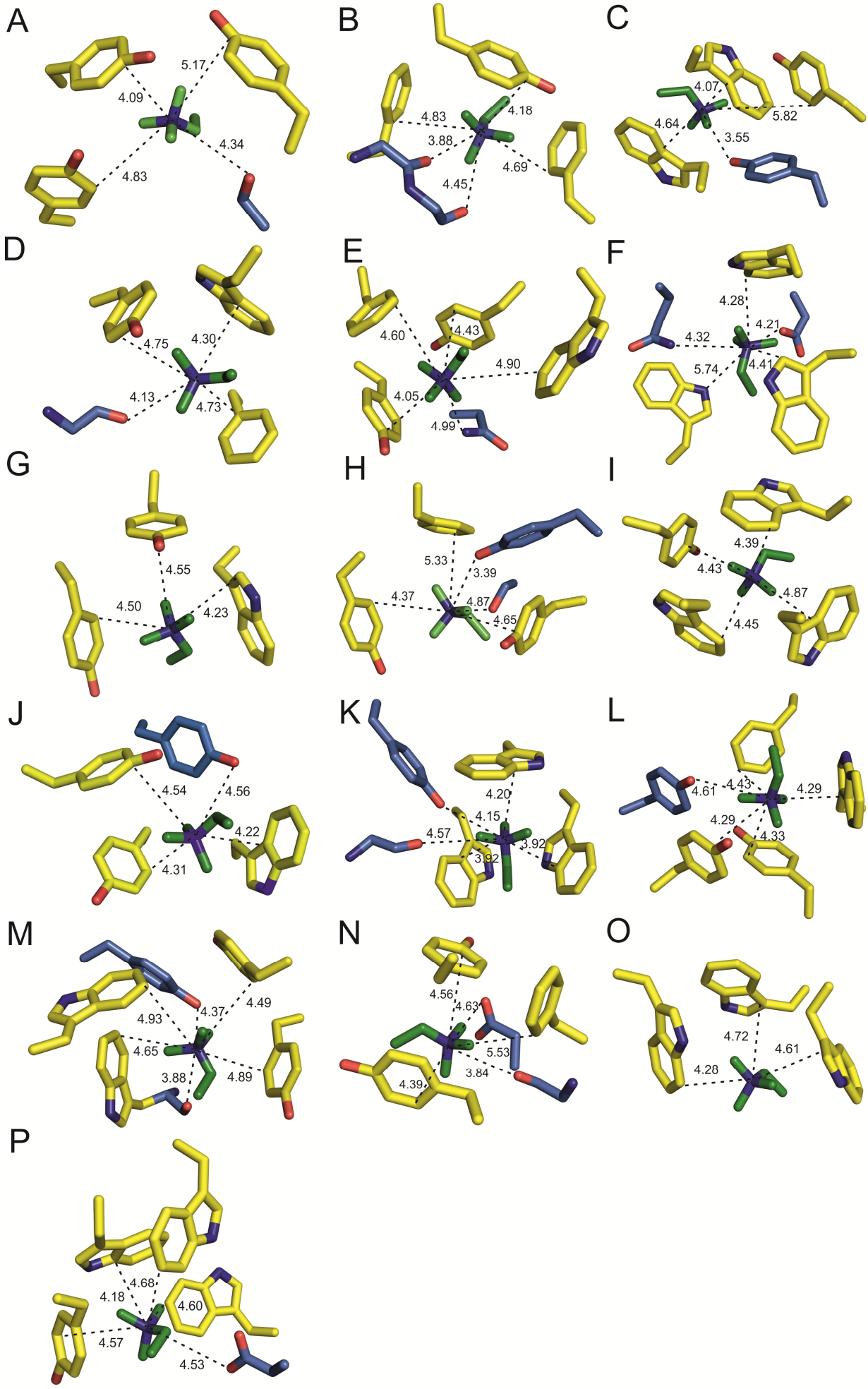
A
5.17
4.09
4.34
4.83
B
4.83
4.18
3.88
4.69
4.45
C
4.07
5.82
4.64
3.55
D
4.75
4.30
4.13
4.73
E
4.60
4.43
4.90
4.05
4.99
F
4.28
4.21
4.32
4.41
5.74
G
4.55
4.50
4.23
H
5.33
3.39
4.37
4.87
4.65
I
4.39
4.43
4.87
4.45
J
4.54
4.56
4.22
4.31
K
4.20
4.15
4.57
3.92
3.92
L
4.61
4.43
4.29
4.29
4.33
M
4.93
4.37
4.49
4.65
3.88
4.89
N
4.56
4.63
5.53
3.84
4.39
O
4.72
4.61
4.28
P
4.68
4.18
4.60
4.57
4.53

Figure 10 **Ligand recognition sites of receptors displaying aromatic box character.**
Additional examples verify that the aromatic box is the widespread structural solution evolved for efficient accommodation of quaternary ammonium receptor ligands (Panels A-P). Each receptor is represented here by one of its ligand complex structure. Here we assign receptor function to such enzymes as well that binds cognate quaternary ammonium ligand allosterically. Ligand binding site close-up of the respective structures is depicted. For the sake of clarity, only the quaternary ammonium moiety of the respective ligand is shown (stick model, atomic coloring with green carbon, blue nitrogen). Residue side chains located at ca. 5 Å from the quaternary nitrogen atom are shown (stick models, atomic coloring where carbon is either yellow or blue for cation-π or charged interactions, respectively; nitrogen is colored blue, oxygen, red).. Tyrosines are depicted with orange carbon atomic coloring when both their aromatic ring and OH group is exposed to the quaternary ammonium moiety. Hydrophobic contacts of quaternary ammonium moiety, present in Panel T, are shown sticks, grey atomic coloring. **A)** M3 muscarinic acetylcholine receptor, PDB ID: 4DAJ; **B)** Cytochrome b-c1, PDB ID: 1SQP; **C)** Seminal plasma protein (PDC-109), PDB ID: 1H8P; **D)** Coagulation factor X (Factor X) PDB ID: 2JKH; **E)** Polycomb protein EED, PDB ID: 3K26; **F)** Transcriptional regulator, C7MT25, PDB ID: 4KWA; **G)** Nucleosome-remodeling factor subunit (BPTF), PDB ID: 2F6J; **H)** CRAL-TRIO domain-containing protein, PDB ID: 3B7Z; **I)** Choline-binding protein F (CbpF), PDB ID: 2V05; **J)** Phosphatidylcholine transfer protein (PC-TP), PDB ID: 1LN1; **K)** Glycine betaine transporter (BetP), PDB ID: 4AIN; **L)** Spindlin-1 (SPIN1), PDB ID: 4H75; **M)** Acetylcholine-binding protein (AchBP), PDB ID: 1UV6; **N)** SAGA-associated factor 29 homolog, (SGF-29), PDB ID: 3MEA; **O)** Zinc finger CW-type PWWP domain protein 1, PDB ID: 2RR4; **P)** Ig λ1 chain V, PDB ID:1DL7.

Table 4 **Relative molecular mass (M_r) of *Pf*CCT construct monomers determined by native ESI-MS**

Protein construct	**M_r, by ESI-MS (Da)**	**Mw, theoretical[a] (Da)**
*Pf*CCT MΔK^{WT}	30906 ± 50	30898
*Pf*CCT MΔK^{Y714F}	30840 ± 50	30882
*Pf*CCT MΔK^{W692F}	30808 ± 50	30859
*Pf*CCT MΔK^{W692Y}	30846 ± 50	30875
*Pf*CCT MΔK^{D623N}	30856 ± 50	30897
*Pf*CCT MΔK^{Y741F}	30956 ± 50	30882
*Pf*CCT MΔK^{W692A}	30786 ± 50	30783

[a] Theoretical molecular masses are calculated based on the His-tagged protein sequence.

Table 5 **Results of PDB search for structures with quaternary ammonium ligands**

Total # of enzyme hits with quaternary ammonium ligands[a]	**150**	
composite aromatic box	**86**	93%
not composite aromatic box	**6**	7%
not relevant (solvent exposed, non-specific) [b]	**64**	

Total # of receptor hits with quaternary ammonium ligands [a]	**313**	
aromatic box	**107**	78%
composite aromatic box-like	**30**	22%
not relevant (solvent exposed or non-specific) [b]	**176**	

[a] To avoid redundancy, only a single hit was considered for each enzyme and receptor for the statictical analysis. Enzyme: ligand recognition was assumed only when the quaternary ammonium ligand that corresponds to the cognate substrate, product or analogue was accommodated to active site of the enzyme. Otherwise, receptor: ligand interaction was assumed, provided that the quaternary ammonium moiety of the ligand is accommodated within the ligand binding pocket of the enzyme.
[b] Ligands found absorbed on protein surface (i.e. not within the active site or ligand binding pocket) were catergorized as ‘non-specific’.

Table 6 **Architecture of choline binding sites in enzymes**

Enzyme name	E.C. #	Protein family	Pfam CLAN	Ligand	PDB ID	Resolution (Å)
Betaine aldehylde dehydrogenase, putative (BALDH)	1.2.1.8	**Aldedh** (PF00171)	**ALDH-like** (CL0099)	betaine aldehyde	1WNB	2.20
JMJD2D lysine demethylase	1.14.11	**JmjC** (PF02373), **JmjN** (PF02375),	**Cupin** (CL0029)	trimethyllysine	4HON	1.80
Histone-lysine N-methyltransferase MLL5	2.1.1.43	**MORN** (PF02493), **SET** (PF00856)	**MORN** (CL0251)	trimethyllysine	4L58	1.48
RuBisCO LSMT	2.1.1.127	**Rubis-subs-bind** (PF09273)	n/a	trimethyllysine	2H23	2.45
CTP:phosphocholine Cytidylyltransferase (LicC)[a]	2.7.7.15	**NTP_transferase** (PF00483)	**GT-A** (CL0110)	CDP-choline	1JYL	2.40
CTP:phosphocholine Cytidylyltransferase (CCT)[a]	2.7.7.15	**CTP_transf_2** (PF01467)	**HUP** (CL0039)	CDP-choline	3HL4	2.20
Carnitine *O*-Acetyltransferase (CrAT)	2.3.1.7	**Carn_acyltransf** (PF00755)	**CoA-acyltrans** (CL0149)	carnitine	1S5O	1.80
Phosphocholine transferase, AnkX	2.7.1.-	**Fic** (PF02661), **Ank_2** (PF12796)	**Ank** (CL0465)	choline-phosphate	4BES	2.54
Choline kinase (Ck)	2.7.1.32	**Choline_kinase** (PF01633)	**PKinase** (CL0016)	choline	3C5I	2.20
Cronobetainyl-CoA:carnitine CoA transferase (CaiB)	2.8.3.-	**CoA_transf_3** (PF02515)	n/a	carnitinyl-CoA	1XVV	2.40
Acetylcholinesterase (AchE)	3.1.1.7	**COesterase** (PF00135)	**AB_hydrolase** (CL0028)	choline	2HA3	2.25
Phospholipase C (PLC)	3.1.4.3	**Zn_dep_PLPC** (PF00882)	**PhosC-NucP1** (CL0368)	phosphatidyl-choline	1P6D	2.00
4-hydroxyproline betaine 2-epimerase (Hyp-B 2-epimerase)	5.1.1.-	**MR_MLE** (PF0118) **MR_MLE_N** (PF02746)	**Enolase_TIM** (CL0256), **Enolase_N** (CL0227)	l-proline betaine	4J1O	1.60
Teichoic acid phosphorylcholine esterase/ choline binding protein E (CbpE)	n/a	**Lactamase_B** (PF00753)	**Metallo-HOrase** (CL0381)	choline-phosphate	2BIB	1.92

[a] These are analogous enzymes, i.e. they catalyze the same reaction but possess no detectable sequence similarity.

Enzyme active sites possessing composite aromatic box quaternary ammonium binding pattern. One representative is shown for each protein family clan.

Table 7 **Architecture of quaternary ammonium binding sites in receptors**

Receptors[a]	Protein family	Clan	Ligand	PDB code	Resolution (Å)
M3 muscarinic acetylcholine receptor (M_3 mAChR)	**7_tm** (PF00001)	GPCR_A (CL0192)	tiotropium	4DAJ	3.40
Cytochrome b-c1	**Cytochrome b N_2** (PF00032)	**2heme_cytochrom** (CL0328)	phosphatidylcholine	1SQP	2.70
Seminal plasma protein (PDC-109)	**fn_2** (PF00040)	n/a	choline-phosphate	1H8P	1.82
Coagulation factor X (Factor X)	**Trypsin** (PF00089)	**Peptidase_PA** (CL0124)	quaternary inhibitor	2JKH	1.25
Polycomb protein EED (EED)	**WD40** (PF00400)	**Beta_propeller** (CL0186)	trimethyllisine	3K26	1.58
Transcriptional regulator, C7MT25	**tetR** (PF00440)	**HTH** (CL0123)	choline	4KWA	1.80
Nucleosome-remodeling factor subunit (BPTF)	**PHD** (PF00628)	**zf_FYVE_PHD** (CL0390)	trimethyllisine	2F6J	2.00
CRAL-TRIO domain-containing protein (YKL091C)	**CRAL_TRIO** (PF00650)	**CRAL_TRIO** (CL0512)	phosphatidylcholine	3B7Z	2,03
Choline-binding protein F (CbpF)	**CW_binding_1** (PF01473)	n/a	choline	2V05	1.67
Phosphatidylcholine transfer protein (PC-TP)	**START** (PF01852)	**Bet_V_1_like** (CL0209)	phosphatidylcholine	1LN1	2,40
Glycine betaine transporter (BetP)	**BCCT** (PF02028)	n/a	betaine	4AIN	3,10
Spindlin-1 (SPIN1)	**Spin-Ssty (**PF02513)	n/a	trimethyllisine	4H75	2,1
Acetylcholine-binding protein (AchBP)	**Neur_chan_LBD** (PF02931)	n/a	carbamyl-choline	1UV6	2,50
Glycine betaine-binding periplasmic protein (proX)	**OpuAC** (PF04069)	**PBP** (CL0177)	betaine	1R9L	1,59
SAGA-associated factor 29 homolog, (SGF-29)	**DUF1325** (PF07039)	**Tudor** (CL0049)	trimethyllisine	3MEA	1,26
Zinc finger CW-type PWWP domain protein 1 (ZCWPW1)	**zf-CW** (PF07496)	n/a	trimethyllisine	2RR4	(NMR)
Ig λ1 chain V	**V-set** (PF07686)	**Ig** (CL0011)	choline-phosphate	1DL7	2,35

[a] Receptor function is assigned to an enzyme, too, when the respective quaternary ammonium ligand was bound allosterically.

Receptor binding sites possessing aromatic box quaternary ammonium binding pattern. One representative is shown for each protein family (Pfam) clan.

References for the Supporting Information

[1] G. N. Nagy, L. Marton, B. Krámos, J. Oláh, Á. Révész, K. Vékey, F. Delsuc, É. Hunyadi-Gulyás, K. F. Medzihradszky, M. Lavigne, et al., *FEBS J.* **2013**, *280*, 3132–48.

[2] C. Aurrecoechea, J. Brestelli, B. P. Brunk, J. Dommer, S. Fischer, B. Gajria, X. Gao, A. Gingle, G. Grant, O. S. Harb, et al., *Nucleic Acids Res.* **2009**, *37*, D539–43.

[3] B. Alberge, L. Gannoun-zaki, C. T. V. A. N. Ba, H. Vial, **2010**, *158*, 149–158.

[4] M. Hendlich, A. Bergner, J. Günther, G. Klebe, *J. Mol. Biol.* **2003**, *326*, 607–20.

[5] J. P. Gallivan, D. A. Dougherty, *Proc. Natl. Acad. Sci. U. S. A.* **1999**, *96*, 9459–64.

[6] C. Rapp, E. Goldberger, N. Tishbi, R. Kirshenbaum, *Proteins* **2014**, DOI 10.1002/prot.24519.

[7] S. Kumar, R. Nussinov, *Biophys. J.* **2002**, *83*, 1595–612.

[8] M. L. Ancelin, H. J. Vial, *Biochim. Biophys. Acta* **1989**, *1001*, 82–9.

[9] M. Punta, P. C. Coggill, R. Y. Eberhardt, J. Mistry, J. Tate, C. Boursnell, N. Pang, K. Forslund, G. Ceric, J. Clements, et al., *Nucleic Acids Res.* **2012**, *40*, D290–301.

[10] D. A. Dougherty, *Acc. Chem. Res.* **2013**, *46*, 885–93.

II.

PLOS ONE

RESEARCH ARTICLE

Molecular Mechanism for the Thermo-Sensitive Phenotype of CHO-MT58 Cell Line Harbouring a Mutant CTP:Phosphocholine Cytidylyltransferase

Lívia Marton[1,2]*, Gergely N. Nagy[1,3], Olivér Ozohanics[4], Anikó Lábas[5], Balázs Krámos[5], Julianna Oláh[5], Károly Vékey[4], Beáta G. Vértessy[1,3]*

1 Institute of Enzymology, Research Centre for National Sciences, HAS, Budapest Hungary, **2** Doctoral School of Multidisciplinary Medical Science, University of Szeged, Szeged, Hungary, **3** Department of Applied Biotechnology and Food Science, Budapest University of Technology and Economics, Budapest, Hungary, **4** Institute of Organic Chemistry, Research Centre for National Sciences, HAS, Budapest, Hungary, **5** Department of Inorganic and Analytical Chemistry, Budapest University of Technology and Economics, Budapest, Hungary

* marton.livia@ttk.mta.hu (LM); vertessy@mail.bme.hu (BGV)

Citation: Marton L, Nagy GN, Ozohanics O, Lábas A, Krámos B, Oláh J, et al. (2015) Molecular Mechanism for the Thermo-Sensitive Phenotype of CHO-MT58 Cell Line Harbouring a Mutant CTP: Phosphocholine Cytidylyltransferase. PLoS ONE 10(6): e0129632. doi:10.1371/journal.pone.0129632

Academic Editor: Manuela Helmer-Citterich, University of Rome Tor Vergata, ITALY

Received: February 5, 2015

Accepted: May 10, 2015

Published: June 17, 2015

Data Availability Statement: All relevant data are within the paper and its Supporting Information files.

Funding: Hungarian Scientific Research Fund (OTKA NK 84008, OTKA K109486), the Intramural Grant Support, ICGEB CRP/HUN14-01, European Commission FP7 Biostruct X-project (Contract No 283570), and Hungarian Academy of Sciences TTKIF-28/2012 for BGV. GNN was supported by the Pro Progressio Foundation. This research was supported by the European Union and the State of Hungary, co-financed by the European Social Fund in the framework of TÁMOP 4.2.4. A/2-11-1-2012-0001

Abstract

Control and elimination of malaria still represents a major public health challenge. Emerging parasite resistance to current therapies urges development of antimalarials with novel mechanism of action. Phospholipid biosynthesis of the Plasmodium parasite has been validated as promising candidate antimalarial target. The most prevalent *de novo* pathway for synthesis of phosphatidylcholine is the Kennedy pathway. Its regulatory and often also rate limiting step is catalyzed by CTP:phosphocholine cytidylyltransferase (CCT). The CHO-MT58 cell line expresses a mutant variant of CCT, and displays a thermo-sensitive phenotype. At non-permissive temperature (40°C), the endogenous CCT activity decreases dramatically, blocking membrane synthesis and ultimately leading to apoptosis. In the present study we investigated the impact of the analogous mutation in a catalytic domain construct of *Plasmodium falciparum* CCT in order to explore the underlying molecular mechanism that explains this phenotype. We used temperature dependent enzyme activity measurements and modeling to investigate the functionality of the mutant enzyme. Furthermore, MS measurements were performed to determine the oligomerization state of the protein, and MD simulations to assess the inter-subunit interactions in the dimer. Our results demonstrate that the R681H mutation does not directly influence enzyme catalytic activity. Instead, it provokes increased heat-sensitivity by destabilizing the CCT dimer. This can possibly explain the significance of the *Pf*CCT pseudoheterodimer organization in ensuring proper enzymatic function. This also provide an explanation for the observed thermo-sensitive phenotype of CHO-MT58 cell line.

'National Excellence Program' for LM. JO acknowledges the financial support of a Bolyai János Research Fellowship. AL acknowledges the financial support of Richter Gedeon Talentum Foundation.

Competing Interests: The authors have declared that no competing interests exist.

Introduction

With 1.2 billion people being at high risk of infection, malaria still presents a major health challenge [1]. Development of antimalarials with novel mechanism of action is essential to keep pace with the emerging antimalarial drug resistance [2]. Targeting the lipid biosynthesis of the causative agent Plasmodium parasites is among the promising candidate antimalarial strategies [3]. It relies on almost exclusive use of phospholipids (PL) acquired by *de novo* biosynthesis as membrane constituents during the intraerythrocytic life stage of the parasite [4]. The choline analogue lead compound Albitiazolium was shown to block the carrier mediated choline entry into the parasite, besides, inhibition of further metabolic steps of the Kennedy phospholipid *de novo* phosphatidylcholine (PC) biosynthesis pathway were also confirmed [5].

Among the enzymes that assist PC biosynthesis in the parasite, CTP:phosphocholine cytidylyltransferase (CCT) is of particular interest. It catalyzes one of the rate limiting steps of the metabolic pathway by converting CTP and choline-phosphate (ChoP) to CDP-choline (CDPCho) and pyrophosphate (PP_i). Besides, this enzyme is regulated by a reversible membrane interaction mechanism that involves structural rearrangement of two putative amphipathic α-helices in the membrane binding domain [6,7]. The lipid composition dependent membrane interaction results in 5.5–fold enzyme activity stimulation [8]. Truncated constructs of CCT from Plasmodium and rat consisting only the catalytic domain were shown to be constitutively active [9–11]. Essential role of CCT was demonstrated by gene disruption or knock-out experiments in Plasmodium [12] as well as several eukaryotic organisms [13–15] or cell lines [16–19].

A chemically mutated Chinese Hamster Ovary (CHO) cell-line with an inducible CCT-deficient phenotype was described as a tool for the functional investigation of CCT [19]. At a permissive temperature of 33°C, CHO-MT58 cells grow at a rate of about 80% of the parental line while maintaining 80–90% PC levels of the parental CHO-K1 strain [19]. At a non-permissive temperature of 40°C, the PC content of the mutant cells decrease by 40% in the first 8 h and by a total of 80% in 24 h [20] as a result of dramatically decreased CCT enzyme activity and CDPCho metabolite levels [19], eventually leading to apoptosis [21]. Noteworthy, mutant cells possess 20-fold less CCT activity than CHO-K1 cells even at 33°C. Western blot analysis demonstrated that the CCT content of CHO-MT58 cells is less than 5% of the amount in parental cells, while the respective steady-state mRNA levels are similar in the two cell types [22]. These results may suggest that the mutant CCT enzyme possesses impaired thermal stability, however this suggestion has not yet been experimentally verified. The temperature-sensitive phenotype of CHO-MT58 cells is conveyed by a single point mutation of the CCTα isoform [19,23,24]. The guanine to adenine nucleotide change at the position 419 corresponds to the point mutation R140H in the catalytic domain of the endogenous CCT.

High conservation of CCT catalytic domains enables the investigation of the role of R140 residue in the rat CCT crystal structure [25]. Similarly to the majority of CCT enzymes, rat CCTα functions as a homodimer [26,27]. R140 is part of ^{140}RYVD^{143} sequence motif that has key importance in dimer stabilization in case of rat CCT [25]. Crystal structures show that this segment, buried at the dimer interface, anchors the two monomers with the arginine forging multiple inter-chain polar interactions [25,28].

Although the point mutation in the *cct* gene was already described in 1994 and the cell line CHO-MT58 is well characterized and frequently used in studying apoptosis and lipid metabolism (for example [29–32]), still there are no direct *in vitro* enzyme studies to describe the molecular mechanism causing this thermo-sensitive phenotype.

In the present study we investigated the *in vitro* effects of the mutation corresponding to R140H in the catalytic domain construct of *Plasmodium falciparum* CCT. *In silico* and *in vitro*

R/H mutagenesis in the *Pf*CCT catalytic domain enabled the investigation of the consequences of the mutation on enzyme structure, function and stability. Our results highlight the significance of *Pf*CCT catalytic domain dimer formation and reveal that the quaternary structure has critical role in ensuring enzyme function. This contributes to the molecular characterization of this important antimalarial drug target enzyme. Besides our *in vitro* study provides a probable explanation for the thermo-sensitive phenotype observed in CHO-MT58.

Materials and Methods

Materials

Restriction enzymes and DNA polymerases were obtained from New England Biolabs (Ipswich, MA, USA). Isopropyl β-D-1-thiogalactopyranoside (IPTG) was obtained from Fisher Scientific GmbH (Schwerte, Germany). Nickel-nitrilotriacetic acid (Ni-NTA) was from Qiagen (Düsseldorf, Germany), protease inhibitor cocktail tablets were purchased from Roche (Basel, Switzerland). CTP, CDPCho, Sypro Orange, inorganic pyrophosphatase, purine nucleoside phosphorylase, DNA purification kit and antibiotics were purchased from Sigma-Aldrich (St Louis, MO, USA). Phosphocholine chloride sodium salt hydrate (further termed as ChoP) was from TCI Europe N.V. (Antwerp, Belgium). MESG (7-methyl-6-thioguanosine) was obtained from Berry and Associates (Dexter, MI, USA). All other chemicals were of analytical grade of the highest purity available.

Alignment of CCT sequences

Conservation of the RYVD motif was investigated using the PipeAlign webserver [33]. The PipeAlign is a protein family analysis method using a five step process beginning with the search for homologous sequences in protein and 3D structure databases and ending up in the definition of subfamilies (clusters). The server performs multiple alignment of 200 complete sequences originating from different clusters. Blast search for homologous sequences of rat CCTα, (Uniprot code: P19836) was performed using Ballast with filter for BlastP search, then Blast gapped alignment was done on 200 sequences from sampled Blast/Ballast results with fragments removal, then adjusted manually. Selected sequences were chosen from different clusters using the most appropriate clustering method suggested by the server. The extent of conservation of selected amino acids was visualized by Weblogo [34].

Homology modelling and molecular dynamics simulations

The catalytic domain of the rat CCT (PDB ID: 4MVC) [35] was used to construct the homodimer homology models of *Pf*CCT MΔK^{WT} containing the second catalytic domain of *Pf*CCT (528–795, Δ720–737) and its point mutant *Pf*CCT MΔK^{R681H}. The aligned sequences were 44.56% and 44.02% identical in the case of wild type and R681H mutant CCT, respectively [36] (Fig 1A). MODELLER 9.14 [37] software was used to create 80 homology models in both cases using the same alignment. The models with the lowest value of the MODELLER objective function were selected and visually inspected using VMD program [38]. The selected models were evaluated using PROCHECK [39], WHAT_CHECK [40] and ERRAT [41] programs (for further details see S1 File). Model data are available in the Protein Model DataBase (PMDB) under the accession number PM0079950 (*Pf*CCT MΔK^{WT}) and PM0079951 (*Pf*CCT MΔK^{R681H}).

Molecular dynamics (MD) simulations were carried out for both enzyme variant models using the same computational protocol. The protonation state of the ionisable amino acid side chains was verified by H++ webserver version 3.1 [42] and PROPKA [43]. Based on the

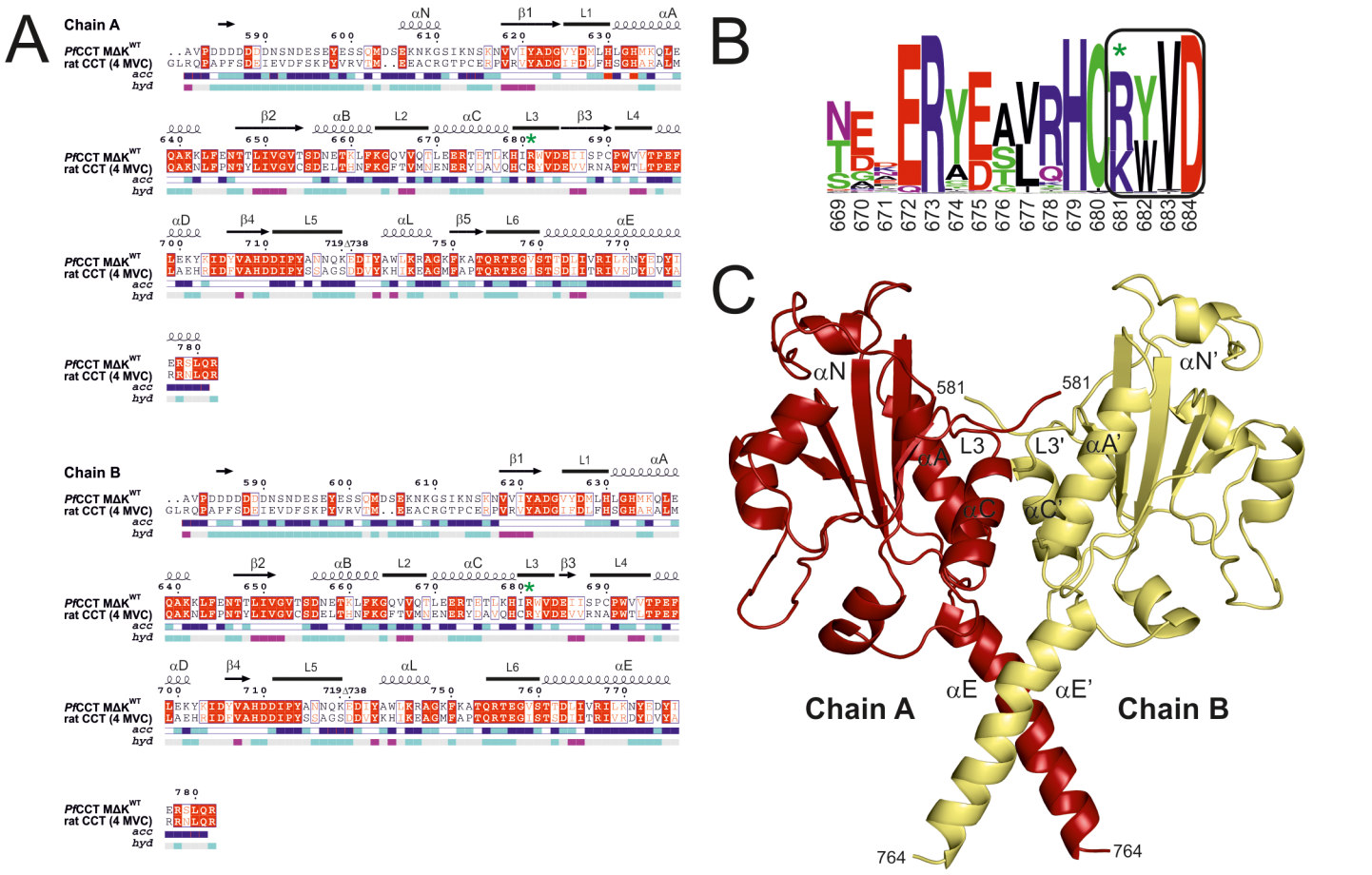

Fig 1. Protein structure prediction of *Pf*CCT MΔK^{WT} and *Pf*CCT MΔK^{R681H}. A) Alignment of rat CCT (PDB ID: 4MVC) and *Pf*CCT MΔK^{WT} sequences used for modeling and MD stimulations. Numbering is according to *Pf*CCT MΔK^{WT}. Secondary structure elements are represented by squiggles (α-helices), arrows (β-strands) and lines (turns). In the aligned sequences, red box with white character indicates strict identity and red character means similarity in groups. R681 corresponding to R140 in rat CCT is indicated by a green star. Hydropathy (pink—hydrophobic, grey—intermediate, cyan—hydrophilic) and accessibility (blue—accessible, cyan—intermediate, white—buried) are also presented below the sequences. The layout with secondary structure elements was generated with ESPript 3.0 [66], supplemented with visual inspection of structures. B) Conservation of the RYVD signature sequence in CCTs, shown by Weblogo. Numbering is according to the *Plasmodium falciparum* sequence, where the ^{681}RWVD^{684} corresponds to the ^{140}RYVD^{143} in the rat sequence. C) Dimer structure of MΔK^{WT} homology model. Chain A is coloured in red and chain B is coloured in yellow. Important secondary structure elements are indicated.

doi:10.1371/journal.pone.0129632.g001

estimated pKa values residues D584, D585, E685 of chain A and D584, E685 of chain B were protonated in both enzyme variants. In addition, D589 and D590 were also protonated in chain B of *Pf*CCT MΔK^{R681H}. Based on the pKa predictions H709 and H681 at the mutated position were protonated both on the δ and ε positions, having a +1 charge. The surrounding of neutral histidine residues was visually inspected to decide their most likely protonation state, and all histidine residues were protonated in the ε position in both enzyme variants with the exception of H679 which was as protonated on the δ position. CHARMM program [44] and CHARMM27 force field [45] was applied using the self-consistent GBSW implicit solvent model [46] to carry out the MD simulations. The calculations were carried out with the optimized PB radii [47], and the CMAP correction optimized for GBSW [48]. The nonpolar surface tension coefficient was 0.005 kcal/(mol Å^2), the number of angular integration points was 50 and the grid spacing for lookup table was 1.5 Å. Structures were heated up from 10 K to 310 K over 60 ps. At this temperature MD equilibration was carried out over 100 ps, which was

followed by the final 5 ns long productive MD simulation. Interaction energies between the two chains of enzyme variants were calculated over the whole trajectory for all frames (i) defined as Eq (1):

$$W(R^M)^i_{\text{int}} = W(R^M)^i_{\text{dim}\,er} - W(R^M)^i_{chainA} - W(R^M)^i_{chainB} \quad (1)$$

where $W(R^M)$ is the effective energy of the protein with coordinates R^M in solution (Eq (2))

$$W(R^M) = H_{\text{int}\,ra}(R^M) + \Delta G_{solv}(R^M) \quad (2)$$

where H_{intra} is the intramacromolecular energy, consisting of bonded and non-bonded energy terms, and ΔG_{solv} is the solvation free energy [49].

The volume and the surface of the proteins were calculated by 3v website [50] using a high resolution grid and 1.4 Å probe radius. The number of hydrogen bonds were measured by CHARMM using the default 2.4 Å distance and 999.0 angle cut-offs.

Mutagenesis, protein expression and purification

The R681H mutant construct of His-tagged *Pf*CCT MΔK (528–795, Δ720–737) was produced by site-directed mutagenesis [10] (PlasmoDB accession number: PF3D7_1316600) [51] using the QuikChange method (Agilent) (for more details about sequence of the protein used for *in vitro* studies see Fig. A in S2 File). Primers used for mutagenesis (R681H 5'-3', `gaaacacatc CATtgggttgac`; R681H 3'-5', `gtcaacccaATGgatgtgtttc`) were synthesized by Eurofins MWG GmbH. Constructs were verified by DNA sequencing at Eurofins MWG GmbH. *Pf*CCT $M\Delta K^{WT}$ and *Pf*CCT $M\Delta K^{R681H}$ were expressed and purified as described previously [10] with minor modifications. Briefly, the His-tagged fusion proteins were expressed using the BL21 (DE3) Rosetta *E. coli* expression system. Expression was induced with 0.6 mM IPTG for 20 h at 16°C. In case of *Pf*CCT $M\Delta K^{R681H}$ Ni-NTA affinity chromatography was performed at 18°C to maintain protein stability. Protein eluted from Ni-NTA column was dialyzed into 20 mM HEPES, pH 7.5 buffer, containing 100 mM NaCl (buffer A). Samples for MS analysis were further purified by size-exclusion chromatography (gel filtration) using a GE Healthcare ÄKTA system with a Superose12 column.

Protein concentrations were determined spectrophotometrically from the absorbance at 280 nm using a Nanodrop 2000c spectrophotometer (Thermo Scientific). Extinction coefficient 31400 $M^{-1}cm^{-1}$ as calculated on the basis of amino acid composition by using ProtParam server was used [52].

Steady-state activity

Steady-state activity measurements were performed as described previously [10] in buffer A using a continuous coupled pyrophosphatase enzyme assay, which employs MESG (7-methyl-6-thioguanosine) substrate for colorimetric phosphate detection [53]. For heat inactivation, protein samples were incubated for 15 min in buffer A at various temperatures (10-60°C); enzyme activity was immediately measured at 20°C.

Kinetic titrations

For CTP substrate titrations, CTP concentration was varied between 12 μM and 1.2 mM while ChoP concentration was kept at 5 mM. For ChoP substrate titrations, ChoP concentration was varied between 0.1 and 20 mM while CTP concentration was kept at 1 mM. Kinetic data were fitted with Eqs (3) and (4) (Michaelis–Menten equation and competitive substrate inhibition

equation, respectively) using OriginPro 8 (OriginLab Corp., Northampton, MA, USA):

$$v = \frac{v_{\max}[S]}{K_M + [S]} \quad (3)$$

$$v = \frac{v_{\max}}{\left(1 + \frac{K_M}{[S]} + \frac{[S]}{K_i}\right)} \quad (4)$$

in these equations, v is the reaction rate, v_{max} is the maximum velocity of the reaction, [S] is the concentration of the substrate and K_i describes the binding of a substrate molecule to the enzyme resulting in a decrease of the maximal reaction rate by half.

Mass spectrometry

In the mass spectrometric study of protein complexes, a commercial Waters QTOF Premier instrument (Waters, Milford, MA, USA) equipped with electrospray ionization source (Waters, Milford, MA, USA) was used in the positive ion mode. Mass spectra were obtained under native conditions; namely, the ions were generated from aqueous 5 mM NH_4HCO_3 buffer solution (pH 7.2) containing the gel filtered *Pf*CCT MΔK protein constructs at 0.4 μM monomer concentration. These conditions allow transfer of the native protein complex present in the solution into the gas phase. The capillary voltage was 3600 V, the sampling cone voltage was 125 V and the temperature of the source was kept at 80°C, collision cell pressure was $3.38 \cdot 10^{-3}$ mbar and ion guide gas flow was 15.00 ml/min. Mass spectra were recorded using the software MassLynx 4.1 (Waters, Milford, MA, USA) in the mass range 1000-5000 m/z as no signals could be detected above 5000 m/z. To ensure reproducible results, 3 samples originating from different expressions were measured for both *Pf*CCT $M\Delta K^{WT}$ and *Pf*CCT $M\Delta K^{R681H}$.

Results

R681 is highly conserved and serves dimer stabilization roles

As the ^{140}RYVD^{143} segment is of prime importance in dimer stabilization in case of rat CCT, we decided to analyze the overall conservation pattern of this motif in CCT enzymes. By performing a Blast search with PipeAlign webserver [33] we compared 200 CCT sequences from different evolutionary clusters. Our results confirmed the previously proposed high degree of conservation [28] for this sequence motif (cf. boxed residues on Fig 1B). While the first and second position of the motif is characterized with conserved basic (R/K) and aromatic (Y/W) residues, the last two positions are exclusively occupied by V and D. RYVD is the most frequently occurring motif, apparent in ca. 50% of investigated sequences. We also found conserved histidine and cysteine residues directly adjacent to this motif, which were also shown to participate in the interaction network stabilizing the dimer of rat CCT [25]. Remarkably, none of the investigated sequences contained a histidine at the arginine position (noted by a star on Fig 1B), despite its potentially basic character.

Additionally, we performed a dbSNP database search for human pcyt1a corresponding CCTα to see whether this mutation is present as an amino acid variation. From the 183 single nucleotide variations denoted up to November 2014, 48 caused missense mutations and 2 nonsense mutations, but none of them concerned either the RYVD or HxGH motif, another signature sequence of cytidylyltransferases, that plays key role in catalysis [54]. Nevertheless, Payne et al. described the mutation of V142 in human CCT causing congenital lipodystrophy and fatty liver disease [55]. This residue is the main interaction partner of R140, therefore its

Table 1. Polar inter-chain interactions between L3, αA and N-terminal regions in homology models of both enzyme variants.

*Pf*CCT MΔK^{WT}			*Pf*CCT MΔK^{R681H}		
L3	**L3'**	**d (Å)**	**L3**	**L3'**	**d (Å)**
H679-O	R681-N	2.98	H679-O	H681-N	3.00
R681-NH2	I680-O	2.96	H681-ND1	I680-O	3.50
R681-NH1	I680-O	3.54			
R681- NH2	R681-O	2.79	H681- ND1	H681-O	3.40
R681- NH2	V683-O	2.65			
R681-N	H679-O	2.96	H681-N	H679-O	2.81
L3	**αA'**	**d [Å]**	**L3**	**αA'**	**d [Å]**
H679- NE2	K635-NZ	3.31			
L3	**Nterm'**	**d [Å]**	**L3**	**Nterm'**	**d [Å]**
R681- NH2	D584-OD1	2.69			
R681- NH1	D584-OD1	3.28			
R681- NH2	D584-OD2	3.53			
W682-NE1	A581-O	2.58	W682-NE1	A581-O	2.58
Nterm	**L3'**	**d [Å]**	**Nterm**	**L3'**	**d [Å]**
A581-O	W682-NE1	2.77	A581-O	W682-NE1	2.69
V582-O	R681- NH2	2.98			

N-terminal region consists of residues 581–620 (cf. Fig 1A).

doi:10.1371/journal.pone.0129632.t001

exchange to methionine may adversely affect dimer interaction. These observations underline the importance of the integrity of RYVD motif.

Our *Plasmodium falciparum* CCT construct (*Pf*CCT MΔK) encompasses the second catalytic domain (Cat2) of the full length enzyme including ^{681}RWVD^{684} as the analogue for the cognate motif (of ^{140}RYVD^{143} in the rat sequence). CCT evolved in Plasmodia by a lineage-specific gene duplication event, resulting in duplicated catalytic and membrane binding domains [10]. Construct of the second catalytic domain of *Pf*CCT, termed as MΔK, was shown to exist in a dimer oligomerization state *in vitro* that is highly similar to the assembly of Cat1Cat2 catalytic domains from the full length enzyme [10]. To visualize inter-subunit interactions of MΔK dimers, a homology model was built using the rat CCT catalytic domain structure as a template [35] (Fig 1A and 1C). Due to the considerable sequence identity between target and template, the *Pf*CCT model displayed similar fold as the rat CCT. As in the case of rat CCT [25], R681 provides two direct inter-subunit polar interactions to the main chain atom of V683' and one polar main chain interaction through I680 to V683' (Table 1). There is also a polar main chain interaction present between the main chain atoms of I680 and R681' bringing the two chains to a distance of 3.7 Å at this specific point (d(R/H681, CA - H679', O)) (Fig 2A and 2B). Polar interactions of H679 and W682 (corresponding the H138 and Y141 in rat) are missing (Fig 2A). Overall, eight polar interactions can be identified that contribute to dimer stability in the Plasmodium CCT structural model. *In silico* modelling of the R681H mutation showed that the two direct interactions between V683 and R681 are lost (Table 1 and Fig 2B), which indicates a possibility for decreased inter-domain stability [56]. N-terminal segment contributes also to dimer stabilization by forging contacts with helix αA and loop L3, which is also effected by R681H mutation (Table 1).

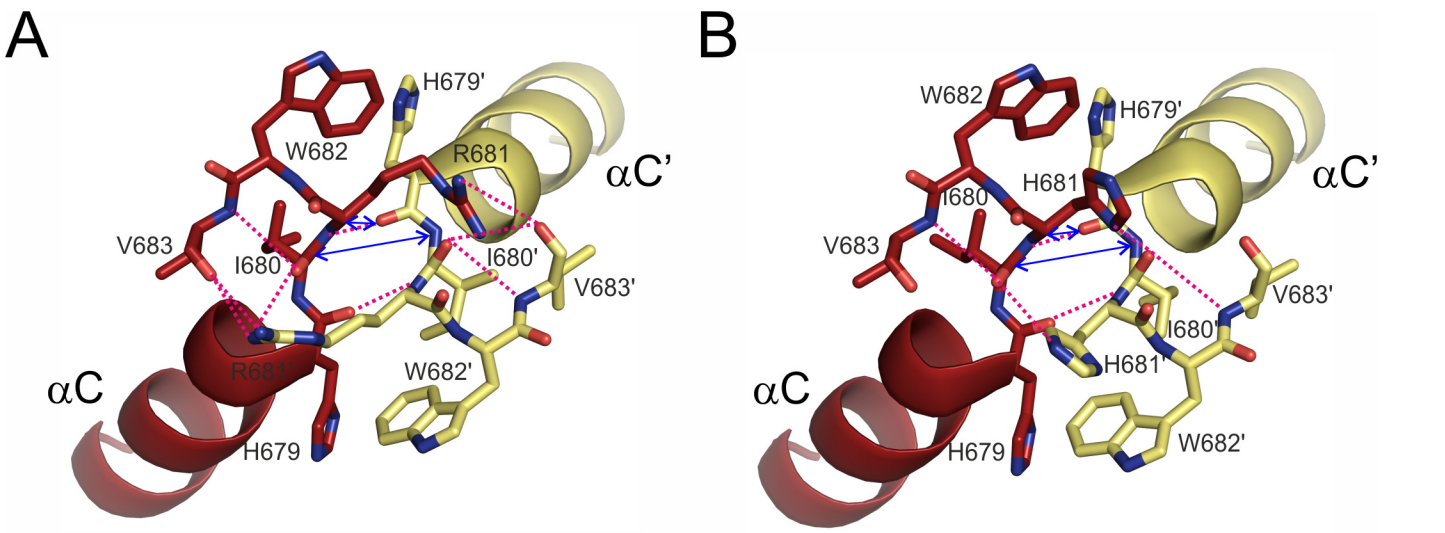

Fig 2. Polar interactions at the dimer interface of *Pf*CCT MΔK^{WT} and *Pf*CCT MΔK^{R681H} involving ^{681}RWVD^{684}. A) Direct interactions harbouring ^{681}RWVD^{684} signature sequence motif in *Pf*CCT MΔK^{WT}. The residues involved in the inter-chain interaction are shown in stick representation, and interactions are indicated by pink dashed lines. Characteristic dimer interface distances d(R681, CA - H679', O) and d(I680, CA - I680', N) are denoted by blue double-headed arrows. Residues in chain B are marked with apostrophes. B) Direct interactions harbouring the ^{681}HWVD^{684} mutated signature sequence motif *Pf*CCT MΔK^{R681H}. The residues involved in the inter-chain interaction are shown in stick representation, and interactions are indicated by pink dashed lines. Characteristic dimer interface distances d(H681, CA - H679', O) and d(I680, CA - I680', N) are denoted by blue double-headed arrows. Residues in chain B are marked with apostrophes.

doi:10.1371/journal.pone.0129632.g002

Unaltered enzyme function with impaired heat stability due to R681H mutation

For *in vitro* studies we generated the R681H variant of the *Pf*CCT MΔK construct. Already upon expression of this variant performed at 16°C, we observed lower yield of expression as compared to the *Pf*CCT MΔK^{WT} (cf. Fig. A in S2 File). First, we investigated the functionality of *Pf*CCT MΔK^{R681H} at 20°C using a continuous spectrophotometric enzyme activity assay, and compared its kinetic properties to that of *Pf*CCT MΔK^{WT} [10]. Data shown in Fig 3 and Table 2 indicate that in the case of the mutant CCT enzyme the substitution to histidine attenuates k_{cat} by 60% when analyzed by [CTP] variation, but has little effect when analyzed by [ChoP] variation assayed at the permissive temperature of 20°C. In addition, substrate inhibition observed at millimolar ChoP concentration range is also apparent with the mutant enzyme. Therefore the mutation does not alter the enzymatic function heavily under the experimental conditions. These results are in good agreement with findings on the CHO-MT58 cell line, which was shown to possess a wild-type phenotype at permissive temperatures (33°C) despite reduced overall CCT levels [24].

To elucidate the mechanism of temperature-induced inactivation of CCT, we characterized the thermal stability of *Pf*CCT MΔK^{R681H}. We adopted the experiment described by Belužić et al. [57] to assess temperature dependence of protein stability and functionality. Protein samples were incubated at different temperatures for 15 minutes then their enzyme activity was measured immediately at 20°C. The mutant enzyme lost half of its activity at circa 25°C and was completely inactivated at 30°C, while similar relative thermal inactivation states of the wild type enzyme occurred at 55°C and 60°C, respectively (Fig 4). Importantly, the wild-type and mutant enzymes display a marked difference in kinetic stability at the physiological temperature range, which is in agreement with the temperature sensitivity of the CHO-MT58 strain.

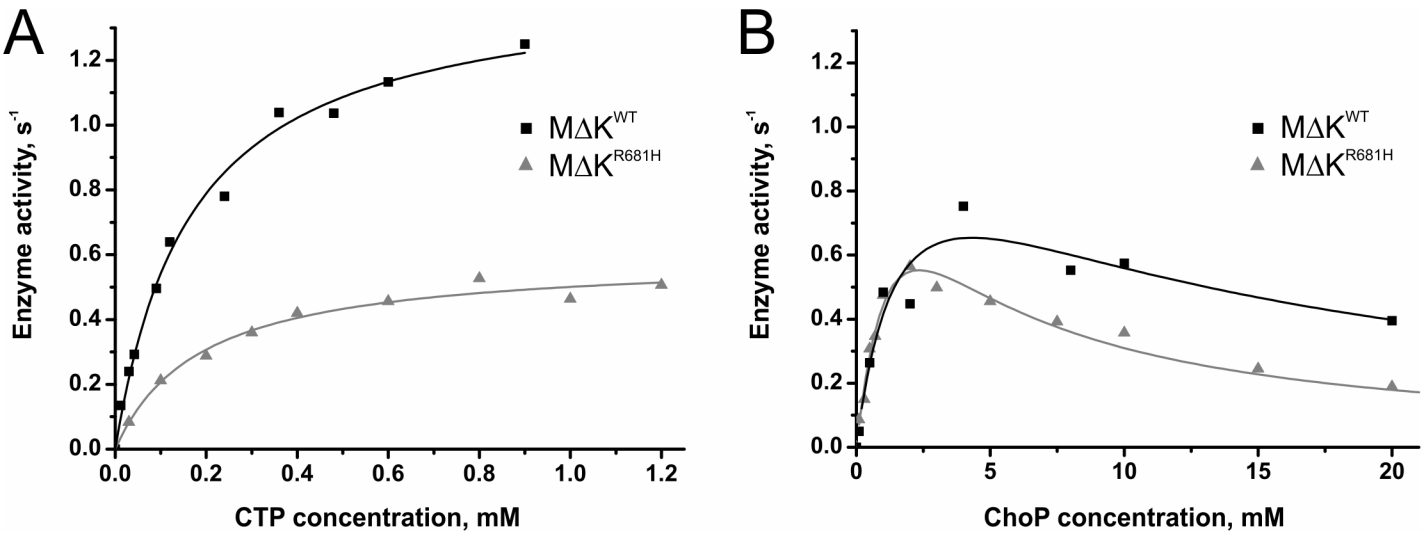

Fig 3. Steady-state kinetic analysis of *Pf*CCT MΔK^{WT} and *Pf*CCT MΔK^{R681H}. A) CTP titration of the activity of the CCTs at a fixed ChoP concentration of 5 mM. The plot shows one representative experiment. Titration data are fitted with the Michaelis–Menten kinetic model assuming no cooperativity. B) ChoP titration of the activity of the CCTs at a fixed CTP concentration of 1 mM. The plot shows one representative experiment. Titration data are fitted with a kinetic model assuming substrate inhibition without cooperativity. Note the substrate inhibition effect of ChoP as an initial rate decrease is observed at higher substrate concentrations.

doi:10.1371/journal.pone.0129632.g003

Perturbed oligomerization state and dynamic properties of *Pf*CCT MΔK^{R681H}

Having demonstrated the drastically impaired thermal stability of the *Pf*CCT MΔK^{R681H} mutant (cf. Fig 4), we wished to investigate the underlying molecular mechanism of this phenomenon. Based on our results and the fact that the mutation affects a key motif of the dimer interface, we hypothesized that the mutation might perturb oligomerization of *Pf*CCT MΔK^{R681H}. To reveal the potential alterations in dimer formation, mass spectrometric analysis was performed under native electrospray conditions, as an appropriate method for determining protein oligomerization state [58].

Mass spectra provided well reproducible (within 20%) dimer:monomer abundance ratios from *Pf*CCT MΔK^{WT} and *Pf*CCT MΔK^{R681H}. Importantly, while reasonable amount of dimer was present in the wild type enzyme (Fig 5A), the dimer:monomer abundance ratios were approximately 20 times lower in the mutant (Fig 5B), indicating attenuated dimer cohesion. These findings were also confirmed by native gel electrophoresis and glutaraldehyde crosslinking experiments (data not shown).

To further analyse the effect of the mutation on binding energetics and dimer stability, molecular dynamics simulations were performed on the homology models of *Pf*CCT MΔK^{WT}

Table 2. Kinetic parameters of *Pf*CCT MΔK^{WT} and *Pf*CCT MΔK^{R681H} catalysis.

	CTP titration		ChoP titration		
	k_{cat} (s^{-1})	$K_{M,\ CTP}$ (mM)	k_{cat} (s^{-1})	$K_{M,\ ChoP}$ (mM)	$K_{i,\ ChoP}$ (mM)
Pf*CCT MΔK^{WT}	1.45 ± 0.05	0.17 ± 0.02	1.2 ± 0.4	1.8 ± 1.1	10.5 ± 7.5
***Pf*CCT MΔK^{R681H}**	0.59 ± 0.02	0.19 ± 0.03	1.2 ± 0.2	1.6 ± 0.4	3.8 ± 1.0

*data obtained from [10]

doi:10.1371/journal.pone.0129632.t002

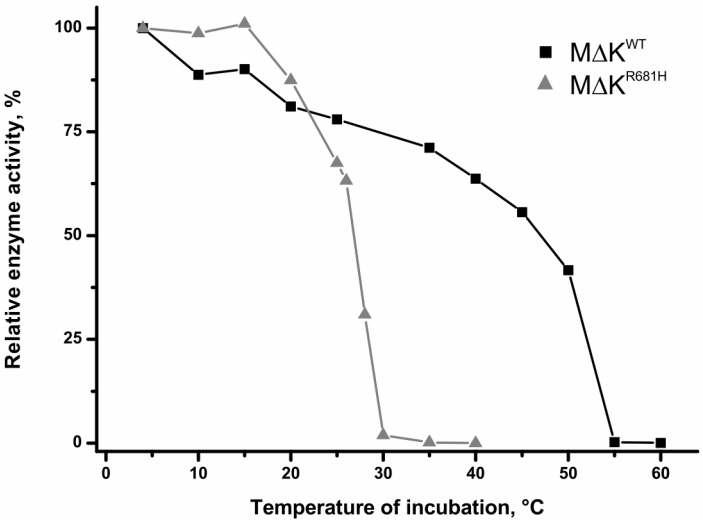

Fig 4. Kinetics of thermal inactivation of *Pf*CCT MΔK^{WT} and *Pf*CCT MΔK^{R681H}. Protein samples were incubated for 15 min in buffer A at different temperatures prior to the measurement performed at 20°C. Inactivation is shown as the fraction of remaining CCT activity. One representative is shown for each temperature and each protein.

doi:10.1371/journal.pone.0129632.g004

and *Pf*CCT MΔK^{R681H}. Productive MD simulations were carried out using an implicit solvent model at 310 K for 5 ns after a 100 ps long equilibration. Interaction energies were equilibrated at 3.25 ns resulting in a 25 percent decrease in the average inter-chain interaction energy in case of the mutant enzyme (Fig 6 and Table 3). The observed tendencies of interaction analysis reveal multiple causes possibly leading to this phenomenon. These involve much favourable solvation energy (ΔG^{eq}_{solv}) of *Pf*CCT MΔK^{WT}, while the van der Waals-type hydrophobic interactions (E^{eq}_{vdW}) also give better contributions to the effective energies of the *Pf*CCT MΔK^{WT} dimers. Thus, the interacting surface area (A^{lf}_{int}) of the homodimers containing mainly hydrophobic amino acid side chains is much larger in case of *Pf*CCT MΔK^{WT} leading to a more compact volume (V^{lf}) (Table 3). Impaired interaction of *Pf*CCT MΔK^{R681H} monomers is particularly apparent at the ^{681}RWVD^{684} conserved dimer interaction motifs. To illustrate this, we followed the distance variation of two representative inter-chain distances (R/H681, CA - H679', O and I680, CA - I680', N) in the course of the MD simulations (cf. Fig 2). Importantly, the former interaction constitutes the proximal inter-monomer contact within the *Pf*CCT homology model as well as in the rat CCT structure [25]. The characteristic deviation of cognate distances between *Pf*CCT MΔK^{R681H} and *Pf*CCT MΔK^{WT} shown on Fig 7 argues for a major perturbation of local contacts that could contribute to observed reduction of dimer interaction surface.

It should be kept in mind that the entropy loss due to decrease of translational and rotational degrees of freedom opposes the formation of the dimer and this become more pronounced with increase in the temperature. This taken together with the reduced interaction energy in the mutant may explain the temperature dependence of the dimerization state of the mutant [59]. *In silico* results thus indicate the adverse effect of R681H mutation on dimer stability. Regarding the considerable extent of intersubunit interface located between dimer pair of catalytic domains, we suppose that the mutation might affect overall structural stability of the full length *Pf*CCT protein as well through perturbed interdomain interactions.

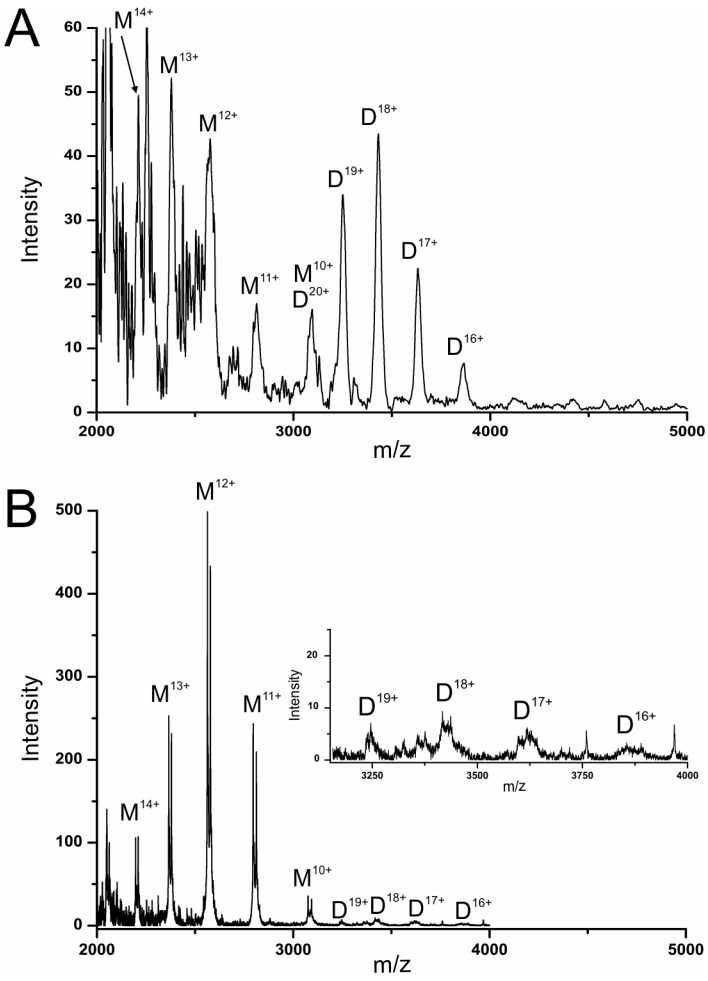

Fig 5. Mass spectra of *Pf*CCT MΔK^{WT} and *Pf*CCT MΔK^{R681H} proteins under native electrospray conditions. M and D indicate signals contributing monomers and dimers, respectively, while numbers denote the charge states. A) Mass spectrum of *Pf*CCT MΔK^{WT} measured in the present study for direct comparison (cf. also [10]). B) Mass spectrum of *Pf*CCT MΔK^{R681H}. In the inset the 10-times enlarged graph of dimer regions (3150–4000 m/z) is shown.

doi:10.1371/journal.pone.0129632.g005

Discussion

Our results suggest that an intact dimer form of the catalytic domains of *Pf*CCT is critical for its enzymatic function. This is in agreement with preferential dimer functional assembly of evolutionarily related cytidylyltransferases: CCT, GCT (CTP:glycerol-3-phosphate cytidylyltransferase), ECT (CTP:ethanolamine phosphate cytidylyltransferase) [60], demonstrated by multiple observations. Gene disruption experiment of *Plasmodium berghei cct* gene, a close homologue of the *pfcct* gene evolved by gene duplication revealed that the truncated protein devoid of second catalytic domain could not restore the function of the wild type form [12]. This effect is possibly mediated by the disruption of the pseudo-heterodimer interface. Analyses of crystal structures have shown that the well-studied bacterial representative of the cytidylyltransferase enzyme family *Bacillus subtilis* GCT and the mammalian representative rat CCT, which are structurally related cytidylyltransferases but only possess one CT domain each, form homodimers [25,28,61]. Cross-linking studies of the rat CCT indicated that domains N and C of rat CCT, approximately corresponding to the construct PfCCT MΔK, have a predominant

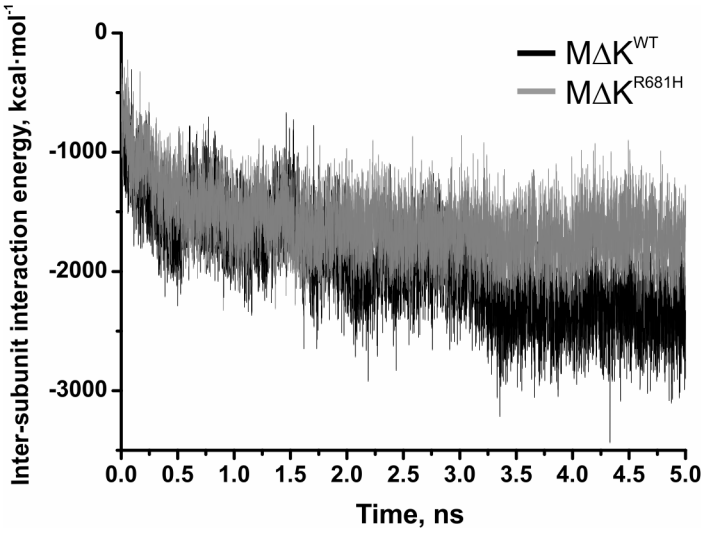

Fig 6. Inter-subunit interaction energies during molecular dynamics simulations. Interaction energies are calculated as Eq 1 and represented by black line in case of *Pf*CCT MΔK^{WT} and by grey line in case of *Pf*CCT MΔK^{R681H}, respectively.

doi:10.1371/journal.pone.0129632.g006

contribution to dimerization. It was also shown that membrane binding, which induces enzyme activation, perturbs the dimer interface, yet it does not cause dimer dissociation [27].

The equivalent of RYVD motif, (R/K)(Y/W)VD is a general signature sequence in cytidylyltransferases [54,62] found at dimer interface of crystal structures (PDB ID: 1COZ, 3HL4 and 3ELB for *Bs*GCT, rat CCT and human ECT, respectively) [25,28]. The functional role of this conserved arginine at the dimer interface was also assessed in *Bs*GCT by alanine mutagenesis of the corresponding residue R63 resulting in a 10-fold decrease in k_{cat} values, but $K_{M,\ CTP}$ was not altered considerably [62]. These results also indicate that this conserved residue does not interfere with substrate/ligand binding at the active site. Contribution of the C-terminal CT domain to the structural stability in the two tandem catalytic domain containing ECT was also suggested [63]. Identification of a novel splice variant (Pcyt2γ) lacking the C-terminal CT domain and being completely devoid of enzyme activity proved also that both cytidylyltransferase domains are required for activity [64]. The effect of a single point mutation on structural stability and protein functionality is also not without precedent in other enzyme families, as an R/H exchange in crystallins was shown to be responsible for congenital cataract through disrupted interactions at the inter-subunit interface [65].

Table 3. Overall effective interaction energy (W_{int}^{eq}) and the contribution of non-bonded van der Waals (E_{vdW}^{eq}) and Coulomb (E_{Cou}^{eq}) interaction energy terms and of the solvation free energy change upon dimerization (ΔG_{solv}^{eq}) averaged over all frames of the equilibrated phase of the productive MD simulations.

	W_{int}^{eq}(kcal·mol^{-1})	ΔG_{solv}^{eq} (kcal·mol^{-1})	E_{vdW}^{eq}(kcal·mol^{-1})	E_{Cou}^{eq} (kcal·mol^{-1})	N_{H-b}^{eq}	V^{lf} (Å^3)	A^{lf} (Å^2)	A_{int}^{lf} (Å^2)
***Pf*CCT MΔK^{WT}**	-2315 ± 266	-2777 ± 275	-188 ± 8	654 ± 54	4.0	61064	17057	1814
***Pf*CCT MΔK^{R681H}**	-1729 ± 233	-1973 ± 244	-141 ± 7	383 ± 58	3.0	61428	17339	1383

The superscript 'eq' denotes the equilibrated phase (final 1.75 ns) of the productive MD simulations. Data from the last frame of the simulations are denoted as 'lf'. Important geometric data such as volume ((V^{lf}) and surface area (A^{lf}), interaction surface area (A_{int}^{lf}) and the average number of inter-subunit hydrogen bonds during the simulations (N_{H-b}^{eq}) are also indicated.

doi:10.1371/journal.pone.0129632.t003

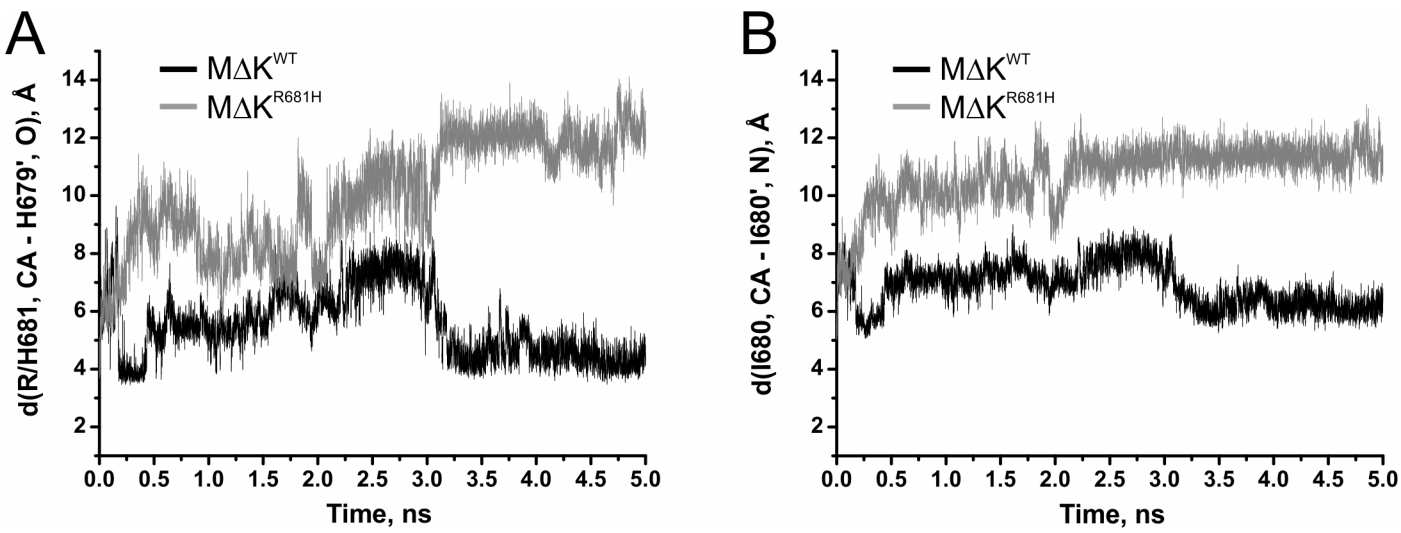

Fig 7. Inter-subunit interaction distances during molecular dynamics simulations. A) Variation of the atomic distance d(R/H681, CA - H679', O) as a characteristic proximal inter-subunit contact of the catalytic domains (cf. Fig 2A and 2B). Distances are represented by black line in case of *Pf*CCT MΔK^{WT} and by grey line in case of *Pf*CCT MΔK^{R681H}, respectively. B) Variation of the atomic distance d(I680, CA - I680', N) as a characteristic proximal inter-subunit distance of the catalytic domains (cf. Fig 2A and 2B). Distances are represented by black line in case of *Pf*CCT MΔK^{WT} and by grey line in case of *Pf*CCT MΔK^{R681H}.

doi:10.1371/journal.pone.0129632.g007

Conclusions

Our results reveal that R/H mutation of a conserved residue at the dimer interface does not directly compromise the enzyme activity of *Pf*CCT. Instead, it induces decreased thermal stability which in turn results in the inactivation of the enzyme. The structural model, molecular dynamics simulations as well as oligomerization results together reveal attenuation of dimer interactions induced by the point mutation. We conclude that maintaining intact dimer interactions is critical for enzyme activity of *Pf*CCT. These consequences also provide an explanation for the observed thermo-sensitive phenotype of CHO MT58 cell line, where an accelerated degradation of CCT was observed at higher temperatures.

Supporting Information

S1 File. Validation of the homology models.
(PDF)

S2 File. *In vivo* evaluation of protein stability.
(PDF)

Acknowledgments

We would like to thank Gergely Szakács for fruitful discussions.

Author Contributions

Conceived and designed the experiments: LM GNN OO AL BK JO KV BGV. Performed the experiments: LM GNN OO AL BK. Analyzed the data: LM GNN OO AL BK JO KV BGV. Contributed reagents/materials/analysis tools: JO KV BGV. Wrote the paper: LM GNN OO AL JO BGV.

References

1. World Health Organization (2014) Malaria. 165–176 p. doi: 10.1007/s00108-013-3390-9
2. Ashley EA, Dhorda M, Fairhurst RM, Amaratunga C, Lim P, et al. (2014) Spread of Artemisinin Resistance in Plasmodium falciparum Malaria. N Engl J Med 371: 411–423. Available: http://www.pubmedcentral.nih.gov/articlerender.fcgi?artid=4143591&tool = pmcentrez&rendertype = abstract. Accessed 31 July 2014. doi: 10.1056/NEJMoa1314981 PMID: 25075834
3. Visser BJ, van Vugt M, Grobusch MP (2014) Malaria: an update on current chemotherapy. Expert Opin Pharmacother 15: 2219–2254. Available: http://www.ncbi.nlm.nih.gov/pubmed/25110058. Accessed 31 March 2015. doi: 10.1517/14656566.2014.944499 PMID: 25110058
4. Vial HJ, Wein S, Farenc C, Kocken C, Nicolas O, et al. (2004) Prodrugs of bisthiazolium salts are orally potent antimalarials. Proc Natl Acad Sci U S A 101: 15458–15463. Available: http://www.pubmedcentral.nih.gov/articlerender.fcgi?artid=523447&tool = pmcentrez&rendertype = abstract. PMID: 15492221
5. Wein S, Maynadier M, Bordat Y, Perez J, Maheshwari S, et al. (2012) Transport and pharmacodynamics of albitiazolium, an antimalarial drug candidate. Br J Pharmacol 166: 2263–2276. Available: http://www.ncbi.nlm.nih.gov/pubmed/22471905. Accessed 23 April 2013. doi: 10.1111/j.1476-5381.2012.01966.x PMID: 22471905
6. Larvor M, Cerdan R, Gumila C, Maurin L, Seta P, et al. (2003) Characterization of the lipid-binding domain of the Plasmodium falciparum CTP: phosphocholine cytidylyltransferase through synthetic-peptide studies. 661: 653–661. PMID: 12901716
7. Ding Z, Taneva SG, Huang HKH, Campbell S a, Semenec L, et al. (2012) A 22-mer segment in the structurally pliable regulatory domain of metazoan CTP: phosphocholine cytidylyltransferase facilitates both silencing and activating functions. J Biol Chem 287: 38980–38991. Available: http://www.pubmedcentral.nih.gov/articlerender.fcgi?artid=3493939&tool = pmcentrez&rendertype = abstract. Accessed 26 November 2014. doi: 10.1074/jbc.M112.402081 PMID: 22988242
8. Yeo H, Larvor M, Ancelin M, Vial HJ (1997) Plasmodium falciparum CTP:phosphocholine cytidylyltransferase expressed in Escherichia coli: purification, characterization and lipid regulation. Biochem J 910: 903–910.
9. Friesen J a, Campbell H a, Kent C (1999) Enzymatic and cellular characterization of a catalytic fragment of CTP:phosphocholine cytidylyltransferase alpha. J Biol Chem 274: 13384–13389. Available: http://www.ncbi.nlm.nih.gov/pubmed/10224101. PMID: 10224101
10. Nagy GN, Marton L, Krámos B, Oláh J, Révész Á, et al. (2013) Evolutionary and mechanistic insights into substrate and product accommodation of CTP:phosphocholine cytidylyltransferase from Plasmodium falciparum. FEBS J 280: 3132–3148. Available: http://www.ncbi.nlm.nih.gov/pubmed/23578277. Accessed 4 February 2015. doi: 10.1111/febs.12282 PMID: 23578277
11. Nagy GN, Marton L, Contet A, Ozohanics O, Ardelean L-M, et al. (2014) Composite Aromatic Boxes for Enzymatic Transformations of Quaternary Ammonium Substrates. Angew Chemie Int Ed 53: 13471–13476. Available: http://www.ncbi.nlm.nih.gov/pubmed/25283789. Accessed 28 November 2014. doi: 10.1002/anie.201408246 PMID: 25283789
12. Déchamps S, Wengelnik K, Berry-Sterkers L, Cerdan R, Vial HJ, et al. (2010) The Kennedy phospholipid biosynthesis pathways are refractory to genetic disruption in Plasmodium berghei and therefore appear essential in blood stages. Mol Biochem Parasitol 173: 69–80. Available: http://www.ncbi.nlm.nih.gov/pubmed/20478340. Accessed 5 November 2013. doi: 10.1016/j.molbiopara.2010.05.006 PMID: 20478340
13. Wang L, Magdaleno S, Tabas I, Jackowski S (2005) Early embryonic lethality in mice with targeted deletion of the CTP:phosphocholine cytidylyltransferase alpha gene (Pcyt1a). Mol Cell Biol 25: 3357–3363. Available: http://www.pubmedcentral.nih.gov/articlerender.fcgi?artid=1069620&tool = pmcentrez&rendertype = abstract. Accessed 9 December 2014. PMID: 15798219
14. Weber U, Eroglu C, Mlodzik M (2003) Phospholipid membrane composition affects EGF receptor and Notch signaling through effects on endocytosis during Drosophila development. Dev Cell 5: 559–570. Available: http://www.ncbi.nlm.nih.gov/pubmed/14536058. Accessed 30 January 2015. PMID: 14536058
15. TSUKAGOSHI Y, NIKAWA J, YAMASHITA S (1987) Molecular cloning and characterization of the gene encoding cholinephosphate cytidylyltransferase in Saccharomyces cerevisiae. Eur J Biochem 169: 477–486. Available: http://doi.wiley.com/10.1111/j.1432-1033.1987.tb13635.x. Accessed 10 December 2014. PMID: 2826147
16. Zhang D, Tang W, Yao PM, Yang C, Xie B, et al. (2000) Macrophages deficient in CTP:Phosphocholine cytidylyltransferase-alpha are viable under normal culture conditions but are highly susceptible to free cholesterol-induced death. Molecular genetic evidence that the induction of phosphatidylcholine

biosynthes. J Biol Chem 275: 35368–35376. Available: http://www.ncbi.nlm.nih.gov/pubmed/10944538. Accessed 27 November 2014. PMID: 10944538

17. Tian Y, Zhou R, Rehg JE, Jackowski S (2007) Role of phosphocholine cytidylyltransferase alpha in lung development. Mol Cell Biol 27: 975–982. Available: http://www.pubmedcentral.nih.gov/articlerender.fcgi?artid=1800673&tool = pmcentrez&rendertype = abstract. Accessed 10 December 2014. PMID: 17130238
18. Marijani R, O. Abonyo B (2011) CTP: Phosphocholine Cytidyltransferase Alpha (CCTα) siRNA Induce Cell Death of Lung Cancer Cells. Pharm Anal Acta 02. Available: http://www.omicsonline.org/2153-2435/2153-2435-2-121.digital/2153-2435-2-121.html. Accessed 20 June 2013.
19. Esko, Jeffrey D, Raetz CRH (1980) Autoradiographic detection of animal cell membrane mutants altered in phosphatidylcholine synthesis. Proc Natl Acad Sci U S A 77: 5192–5196. PMID: 6254065
20. Van der Sanden MHM, Houweling M, van Golde LMG, Vaandrager AB (2003) Inhibition of phosphatidylcholine synthesis induces expression of the endoplasmic reticulum stress and apoptosis-related protein CCAAT/enhancer-binding protein-homologous protein (CHOP/GADD153). Biochem J 369: 643–650. Available: http://www.pubmedcentral.nih.gov/articlerender.fcgi?artid=1223098&tool = pmcentrez&rendertype = abstract. PMID: 12370080
21. Cui Z, Houweling M (1996) A Genetic Defect in Phosphatidylcholine Biosynthesis Triggers Apoptosis in Chinese Hamster Ovary Cells. J Biol Chem 271: 14668–14671. Available: http://www.jbc.org/cgi/doi/10.1074/jbc.271.25.14668. Accessed 13 June 2013. PMID: 8663247
22. Wang Y, Sweitzer TD, Weinhold P a., Kent C (1993) Nuclear localization of soluble CTP:phosphocholine cytidylyltransferase. J Biol Chem 268: 5899–5904. PMID: 8383679
23. Esko JD, Wermuth MM, Raetz CR (1981) Thermolabile CDP-choline synthetase in an animal cell mutant defective in lecithin formation. J Biol Chem 256: 7388–7393. Available: http://www.ncbi.nlm.nih.gov/pubmed/6265447. PMID: 6265447
24. Sweitzer TD, Kent C (1994) Expression of Wild-Type and Mutant Rat Liver CTP:Phosphocholine Cytidylyltransferase in a Cytidylyltransferase-Deficient Chinese Hamster Ovary Cell Line. Arch Biochem Biophys 311: 107–116. PMID: 8185307
25. Lee J, Johnson J, Ding Z, Paetzel M, Cornell RB (2009) Crystal Structure of a Mammalian CTP : Phosphocholine Cytidylyltransferase Catalytic Domain Reveals Novel Active Site Residues within a Highly Conserved Nucleotidyltransferase Fold. J Biol Chem 284: 33535–33548. doi: 10.1074/jbc.M109.053363 PMID: 19783652
26. Cornell R (1989) Chemical cross-linking reveals a dimeric structure for CTP:phosphocholine cytidylyltransferase. J Biol Chem 264: 9077–9082. Available: http://www.ncbi.nlm.nih.gov/pubmed/2542297. Accessed 3 December 2014. PMID: 2542297
27. Xie M, Smith JL, Ding Z, Zhang D, Cornell RB (2004) Membrane binding modulates the quaternary structure of CTP:phosphocholine cytidylyltransferase. J Biol Chem 279: 28817–28825. Available: http://www.ncbi.nlm.nih.gov/pubmed/15069071. Accessed 30 January 2013. PMID: 15069071
28. Weber CH, Park YS, Sanker S, Kent C, Ludwig ML (1999) A prototypical cytidylyltransferase: CTP:glycerol-3-phosphate cytidylyltransferase from bacillus subtilis. Structure 7: 1113–1124. Available: http://www.ncbi.nlm.nih.gov/pubmed/10508782. PMID: 10508782
29. Gehrig K, Cornell RB, Ridgway ND (2008) Expansion of the Nucleoplasmic Reticulum Requires the Coordinated Activity of Lamins and CTP: Phosphocholine Cytidylyltransferase. 19: 237–247. doi: 10.1091/mbc.E07 PMID: 17959832
30. Sarri E, Sicart A, Lázaro-Diéguez F, Egea G (2011) Phospholipid synthesis participates in the regulation of diacylglycerol required for membrane trafficking at the Golgi complex. J Biol Chem 286: 28632–28643. Available: http://www.pubmedcentral.nih.gov/articlerender.fcgi?artid=3151104&tool = pmcentrez&rendertype = abstract. Accessed 5 November 2013. doi: 10.1074/jbc.M111.267534 PMID: 21700701
31. Niebergall LJ, Vance DE (2012) The ratio of phosphatidylcholine to phosphatidylethanolamine does not predict integrity of growing MT58 Chinese hamster ovary cells. Biochim Biophys Acta 1821: 324–334. Available: http://www.ncbi.nlm.nih.gov/pubmed/22079326. Accessed 5 November 2013. doi: 10.1016/j.bbalip.2011.10.018 PMID: 22079326
32. Morton CC, Aitchison AJ, Gehrig K, Ridgway ND (2013) A mechanism for suppression of the CDP-choline pathway during apoptosis. J Lipid Res 54: 3373–3384. Available: http://www.pubmedcentral.nih.gov/articlerender.fcgi?artid=3826684&tool = pmcentrez&rendertype = abstract. Accessed 9 December 2014. doi: 10.1194/jlr.M041434 PMID: 24136823
33. Plewniak F (2003) PipeAlign: a new toolkit for protein family analysis. Nucleic Acids Res 31: 3829–3832. Available: http://nar.oxfordjournals.org/lookup/doi/10.1093/nar/gkg518. Accessed 26 November 2014. PMID: 12824430

34. Crooks GE, Hon G, Chandonia J-M, Brenner SE (2004) WebLogo: a sequence logo generator. Genome Res 14: 1188–1190. Available: http://www.pubmedcentral.nih.gov/articlerender.fcgi?artid=419797&tool = pmcentrez&rendertype = abstract. Accessed 23 October 2014. PMID: 15173120

35. Lee J, Taneva SG, Holland BW, Tieleman DP, Cornell RB (2014) Structural basis for autoinhibition of CTP:phosphocholine cytidylyltransferase (CCT), the regulatory enzyme in phosphatidylcholine synthesis, by its membrane-binding amphipathic helix. J Biol Chem 289: 1742–1755. Available: http://www.ncbi.nlm.nih.gov/pubmed/24275660. Accessed 2 June 2014. doi: 10.1074/jbc.M113.526970 PMID: 24275660

36. SIAS: Sequence Identity and Similarity (2008). Available: http://imed.med.ucm.es/Tools/sias.html.

37. Eswar N, Webb B, Marti-Renom MA, Madhusudhan MS, Eramian D, et al. (2006) Comparative protein structure modeling using Modeller. Curr Protoc Bioinformatics Chapter 5: Unit 5.6. Available: http://www.pubmedcentral.nih.gov/articlerender.fcgi?artid=4186674&tool = pmcentrez&rendertype = abstract. Accessed 28 November 2014.

38. Humphrey W, Dalke A, Schulten K (1996) VMD: visual molecular dynamics. J Mol Graph 14: 33–38, 27–28. Available: http://www.ncbi.nlm.nih.gov/pubmed/8744570. Accessed 7 January 2015. PMID: 8744570

39. Laskowski RA, Rullmannn JA, MacArthur MW, Kaptein R, Thornton JM (1996) AQUA and PROCHECK-NMR: programs for checking the quality of protein structures solved by NMR. J Biomol NMR 8: 477–486. Available: http://www.ncbi.nlm.nih.gov/pubmed/9008363. Accessed 3 December 2014. PMID: 9008363

40. Hooft RW, Vriend G, Sander C, Abola EE (1996) Errors in protein structures. Nature 381: 272. Available: doi: 10.1038/381272a0 Accessed 3 December 2014. PMID: 8692262

41. Colovos C, Yeates TO (1993) Verification of protein structures: patterns of nonbonded atomic interactions. Protein Sci 2: 1511–1519. Available: http://www.pubmedcentral.nih.gov/articlerender.fcgi?artid=2142462&tool = pmcentrez&rendertype = abstract. Accessed 3 December 2014. PMID: 8401235

42. Anandakrishnan R, Aguilar B, Onufriev A V (2012) H++ 3.0: automating pK prediction and the preparation of biomolecular structures for atomistic molecular modeling and simulations. Nucleic Acids Res 40: W537–W541. Available: http://nar.oxfordjournals.org/content/40/W1/W537.short. Accessed 12 December 2014. doi: 10.1093/nar/gks375 PMID: 22570416

43. Olsson MHM, Søndergaard CR, Rostkowski M, Jensen JH (2011) PROPKA3: Consistent Treatment of Internal and Surface Residues in Empirical p K a Predictions: 525–537.

44. Brooks BR, Brooks CL, Mackerell AD, Nilsson L, Petrella RJ, et al. (2009) CHARMM: the biomolecular simulation program. J Comput Chem 30: 1545–1614. Available: http://www.pubmedcentral.nih.gov/articlerender.fcgi?artid=2810661&tool = pmcentrez&rendertype = abstract. Accessed 14 July 2014. doi: 10.1002/jcc.21287 PMID: 19444816

45. MacKerell AD, Banavali N, Foloppe N (2001) Development and current status of the CHARMM force field for nucleic acids. Biopolymers 56: 257–265. Available: http://www.ncbi.nlm.nih.gov/pubmed/11754339. Accessed 3 December 2014.

46. Im W, Lee MS, Brooks CL (2003) Generalized born model with a simple smoothing function. J Comput Chem 24: 1691–1702. Available: http://www.ncbi.nlm.nih.gov/pubmed/12964188. PMID: 12964188

47. Nina M, Beglov D, Roux B (1997) Atomic Radii for Continuum Electrostatics Calculations Based on Molecular Dynamics Free Energy Simulations. J Phys Chem B 101: 5239–5248. Available: doi: 10.1021/jp970736r Accessed 16 April 2015.

48. Chen J, Im W, Brooks CL (2006) Balancing solvation and intramolecular interactions: toward a consistent generalized Born force field. J Am Chem Soc 128: 3728–3736. Available: http://www.pubmedcentral.nih.gov/articlerender.fcgi?artid=2596729&tool = pmcentrez&rendertype = abstract. Accessed 16 April 2015. PMID: 16536547

49. Lazaridis T, Karplus M (1999) Effective Energy Function for Proteins in Solution. Proteins 35: 133–152. Available: http://www.ncbi.nlm.nih.gov/pubmed/10223287. Accessed 23 January 2015. PMID: 10223287

50. Voss NR, Gerstein M (2010) 3V: cavity, channel and cleft volume calculator and extractor. Nucleic Acids Res 38: W555–W562. Available: http://www.pubmedcentral.nih.gov/articlerender.fcgi?artid=2896178&tool = pmcentrez&rendertype = abstract. Accessed 23 January 2015. doi: 10.1093/nar/gkq395 PMID: 20478824

51. Llinás M, Bozdech Z, Wong ED, Adai AT, DeRisi JL (2006) Comparative whole genome transcriptome analysis of three Plasmodium falciparum strains. Nucleic Acids Res 34: 1166–1173. Available: http://www.pubmedcentral.nih.gov/articlerender.fcgi?artid=1380255&tool = pmcentrez&rendertype = abstract. Accessed 30 January 2013. PMID: 16493140

52. Artimo P, Jonnalagedda M, Arnold K, Baratin D, Csardi G, et al. (2012) ExPASy: SIB bioinformatics resource portal. Nucleic Acids Res 40: W597–W603. Available: http://www.pubmedcentral.nih.gov/

articlerender.fcgi?artid=3394269&tool = pmcentrez&rendertype = abstract. Accessed 26 August 2014. doi: 10.1093/nar/gks400 PMID: 22661580

53. Webb MR (1992) A continuous spectrophotometric assay for inorganic phosphate and for measuring phosphate release kinetics in biological systems. Proc Natl Acad Sci U S A 89: 4884–4887. PMID: 1534409

54. Veitch DP, Gilham D, Cornell RB (1998) The role of histidine residues in the HXGH site of CTP:phosphocholine cytidylyltransferase in CTP binding and catalysis. Eur J Biochem 255: 227–234. Available: http://www.ncbi.nlm.nih.gov/pubmed/9692923. PMID: 9692923

55. Payne F, Lim K, Girousse A, Brown RJ, Kory N, et al. (2014) Mutations disrupting the Kennedy phosphatidylcholine pathway in humans with congenital lipodystrophy and fatty liver disease. Proc Natl Acad Sci U S A 111: 8901–8906. Available: http://www.ncbi.nlm.nih.gov/pubmed/24889630. Accessed 26 November 2014. doi: 10.1073/pnas.1408523111 PMID: 24889630

56. Takács E, Grolmusz VK, Vértessy BG (2004) A tradeoff between protein stability and conformational mobility in homotrimeric dUTPases. FEBS Lett 566: 48–54. doi: 10.1016/j.febslet.2004.04.039 PMID: 15147867

57. Beluzić R, Cuk M, Pavkov T, Fumić K, Barić I, et al. (2006) A single mutation at Tyr143 of human S-adenosylhomocysteine hydrolase renders the enzyme thermosensitive and affects the oxidation state of bound cofactor nicotinamide-adenine dinucleotide. Biochem J 400: 245–253. Available: http://www.pubmedcentral.nih.gov/articlerender.fcgi?artid=1652816&tool = pmcentrez&rendertype = abstract. Accessed 26 November 2014. PMID: 16872278

58. Loo JA (2000) Electrospray ionization mass spectrometry: a technology for studying noncovalent macromolecular complexes. Int J Mass Spectrom 200: 175–186. Available: http://www.sciencedirect.com/science/article/pii/S1387380600002980. Accessed 2 December 2014.

59. Tamura A, Privalov PL (1997) The entropy cost of protein association. J Mol Biol 273: 1048–1060. Available: http://www.ncbi.nlm.nih.gov/pubmed/9367790. Accessed 4 February 2015. PMID: 9367790

60. Aravind L, Anantharaman V, Koonin E V (2002) Monophyly of class I aminoacyl tRNA synthetase, USPA, ETFP, photolyase, and PP-ATPase nucleotide-binding domains: implications for protein evolution in the RNA. Proteins 48: 1–14. Available: http://www.ncbi.nlm.nih.gov/pubmed/12012333. Accessed 26 November 2014. PMID: 12012333

61. Taneva S, Dennis MK, Ding Z, Smith JL, Cornell RB (2008) Contribution of each membrane binding domain of the CTP:phosphocholine cytidylyltransferase-alpha dimer to its activation, membrane binding, and membrane cross-bridging. J Biol Chem 283: 28137–28148. Available: http://www.pubmedcentral.nih.gov/articlerender.fcgi?artid=2661385&tool = pmcentrez&rendertype = abstract. Accessed 29 August 2012. doi: 10.1074/jbc.M802595200 PMID: 18694933

62. Park YS, Gee P, Sanker S, Schurter EJ, Zuiderweg ERP, et al. (1997) Identification of Functional Conserved Residues of CTP: glycerol-3-phosphate Cytidylyltransferase. 272: 15161–15166. PMID: 9182537

63. Tian S, Ohtsuka J, Wang S, Nagata K, Tanokura M, et al. (2014) Human CTP:phosphoethanolamine cytidylyltransferase: enzymatic properties and unequal catalytic roles of CTP-binding motifs in two cytidylyltransferase domains. Biochem Biophys Res Commun 449: 26–31. Available: http://www.ncbi.nlm.nih.gov/pubmed/24802409. Accessed 27 January 2015. doi: 10.1016/j.bbrc.2014.04.131 PMID: 24802409

64. Pavlovic Z, Singh RK, Bakovic M (2014) A novel murine CTP:phosphoethanolamine cytidylyltransferase splice variant is a post-translational repressor and an indicator that both cytidylyltransferase domains are required for activity. Gene 543: 58–68. Available: http://www.ncbi.nlm.nih.gov/pubmed/24703999. Accessed 27 January 2015. doi: 10.1016/j.gene.2014.04.005 PMID: 24703999

65. Basak A, Bateman O, Slingsby C, Pande A, Asherie N, et al. (2003) High-resolution X-ray Crystal Structures of Human γD Crystallin (1.25Å) and the R58H Mutant (1.15Å) Associated with Aculeiform Cataract. J Mol Biol 328: 1137–1147. Available: http://www.sciencedirect.com/science/article/pii/S0022283603003759. Accessed 4 December 2014. PMID: 12729747

66. Robert X, Gouet P (2014) Deciphering key features in protein structures with the new ENDscript server. Nucleic Acids Res 42: W320–W324. Available: http://www.pubmedcentral.nih.gov/articlerender.fcgi?artid=4086106&tool = pmcentrez&rendertype = abstract. Accessed 30 September 2014. doi: 10.1093/nar/gku316 PMID: 24753421